

Research & Development of Triboelectric Energy Generation for Military Applications

April 28, 2022

Peter Fagerholm

Kaleigh Hess

Caitlin Kean

Kyle Postans

Joshua Woodruff

Prof. Pratap Rao, Primary Advisor

Prof. Gregory Noetscher, Advisor

Justin Silvia, Project Co-Sponsor

US Army DEVCOM Soldier Center



WPI



DEVCOM
SOLDIER
CENTER



Abstract

In collaboration with the U.S. Army Combat Capabilities Development Command (DEVCOM), this MQP team aimed to modify equipment worn by a soldier to be capable of providing power to external electronic components. Our prototype designs implemented triboelectric nanogenerators (TENGs) into the military footwear to capitalize on unused energy generated when walking. TENGs behave based on the triboelectric effect, which produces electrical power through the dynamic interaction of two triboelectric materials. This project's multiple areas of focus were consolidated to produce an optimized final prototype. Researched rectification circuits were printed onto flexible substrates to output a linearized direct current from TENG input. An automated tester was constructed to provide consistent force for testing. Separate TENG iterations were constructed and tested to analyze the effect of spacing and surface contact between triboelectric materials. These areas of research and development allowed our team to improve prototypes and design our final prototype.



Acknowledgments

This project would not have been possible without the contribution of others. These individuals donated their time, expertise, advice, and generosity to this project.

- Our Advisors Professor Pratap Rao and Professor Gregory Noetscher for their support and guidance that helped us create this Major Qualifying Project. We would also like to thank them for the use of the lab space in the NanoEnergy Laboratory in Gateway Park II and the lab space in the ECE lab in Atwater Kent. We would also like to thank Joseph Adegite who lent his time and expertise to the team.
 - Our Sponsor, the US Army Combat Capabilities Development Command Soldier Center (DEVCOM), for providing this team with the challenge of triboelectric energy generation. We especially want to thank Justin Silvia for his insight and help during this project.
 - Last year's MQP team: Aaron McCutchenson, Naancy Nguyen, Eric Scholz, Rebecca Serven, and Spencer Tess. For all their hard work last year on this project and this year answering any questions we had.
 - The Mechanical Engineering Department's Administrative Assistant, Barbara Furman, for making sure that we were able to obtain all the necessary materials to make this project successful.
 - Worcester Polytechnic Institute for allowing this team to complete the Major Qualifying Project and providing us with the necessary space and time to successfully complete the project.
-

Table of Contents

Abstract	i
Acknowledgments.....	ii
Table of Figures	vii
List of Tables.....	xii
Authorship	xiii
Chapter 1: Introduction	1
Chapter 2: Background	2
2.1 Fundamental Physics.....	2
2.2 Circuitry Fundamentals	5
2.3 Circuitry in TENGs.....	6
2.3.1 Common Circuit Components	6
2.3.2 Resistors	6
2.3.3 Capacitors	7
2.3.4 Diodes	8
2.3.5 Power Supply	8
2.4 U.S. Army Portable Energy Sources & Methods	9
2.5 Previous Team's Work	10
2.5.1 Material Matrix.....	10
2.5.2 TENG Mode and Design Discussion.....	11
2.5.3 TENG Selections for Design and Fabrication	14
2.5.4 TENG Performance Evaluations	16
2.6 Fabrication Techniques	18
2.6.1 Bonding	18
2.6.2 Surface Modifications	18
2.6.3 Methods of Assembly	19
2.6.4 Previous Triboelectric Team's Fabrication Techniques	20
2.7 TENG Design.....	23

2.7.1	Reducing Power Decay.....	23
2.7.2	Stacking.....	24
2.7.3	Improving Applications through Materials.....	25
2.8	TENG Applications	26
2.8.1	Experimental Applications	26
2.9	Flexible Printed Circuit Boards	29
2.9.1	Common Materials Found in FPCBs.....	29
2.9.2	Fabrication Processes for FPCBs	30
2.9.3	Voltera V-One PCB Printer.....	32
2.9.4	Multilayer FPCBs	33
2.9.5	Disadvantages of FPCBs.....	33
2.10	Power Management Module (PMM).....	34
Chapter 3:	Project Scope and Objectives.....	40
Chapter 4:	Rectification Circuit Design and Evaluation	41
4.1	Circuit Schematics and Simulation Results	42
4.1.1	Bennet’s Doubler Rectification Circuit Schematic and Simulation	42
4.1.2	Fractal Switch Capacitor Converter Schematic and Simulation	43
4.1.3	Full Wave Rectification Circuit Schematic and Simulation.....	44
4.1.4	Half Wave Rectification Circuit Schematic and Simulation	45
4.1.5	Parallel Switch Circuit Schematic and Simulation	46
4.1.6	Series Switch Circuit Schematic and Simulation.....	47
4.1.7	Self Doubled Rectification Circuit Schematic and Simulation.....	48
4.2	Simulated Circuit Changes and Improvements	49
4.3	Simulating Change in Capacitance.....	53
4.4	Breadboard Rectification Circuits Testing and Evaluation	60
4.4.1	Half Wave Rectification Circuit Breadboard Evaluation.....	60
4.4.2	Bennet’s Doubler Rectification Circuit Evaluation	61
4.4.3	Self Doubled Rectification Circuit Breadboard Evaluation	62

4.5	Flexible Printed Rectification Circuit Fabrication and Performances	64
4.5.1	Rectification FPCB Schematics	64
4.5.2	FPCB Components and Fabrication	65
4.5.3	FPCB Evaluation and Conclusions.....	68
Chapter 5:	Automated Tester	70
5.1	Design Parameters	70
5.2	Summary of Designs	71
5.3	Pneumatic Gait Design	71
5.4	Weight-Based Design.....	72
5.5	Final Design - Pneumatic Straight Tester.....	72
Chapter 6:	TENG Iterations	76
6.1	Research for Criteria of Voltage Increase	76
6.2	TENG Iteration Composition	78
6.2.1	Influence of Wire Geometry.....	78
6.2.2	Folded Iterations	79
6.2.3	Inducing Spacing Between TENG Layers.....	82
6.3	Results for TENG Iterations.....	83
6.3.1	Influence of Wire Geometry.....	85
6.3.2	Folded Iterations Results.....	86
6.3.3	Inducing Spacing Between TENG Layers.....	87
Chapter 7:	Prototyping Stage One	90
7.1	Initial Design Concepts	90
7.2	Stage One Prototype Construction	92
7.2.1	Midsole I	92
7.2.2	Sock I.....	93
7.2.3	Sock-Insole I	94
7.2.4	Insole I	95
7.3	Stage One Prototype Tests and Results.....	95
7.3.1	Midsole I	96

7.3.2	Sock I	97
7.3.3	Sock-Insole I	99
7.3.4	Insole I	100
7.4	Stage One Prototype Conclusions	101
Chapter 8: Prototyping Stage II		103
8.1	Stage Two Prototype Construction	103
8.2	Stage Two Prototype Tests and Results	105
8.2.1	Midsole II	106
8.2.2	Insole II	107
8.3	Stage Two Prototype Conclusions	108
Chapter 9: Final Prototyping Stage		109
9.1	Final Prototype Construction	109
9.2	Final Prototype Tests and Results	113
9.3	Final Prototype Stage Conclusions	116
Chapter 10: Conclusion and Broader Impact		117
10.1	Automated Tester Modifications	117
10.2	Bending Effects	117
10.3	Improved Midsole III TENG Accessibility	117
10.4	Improved Rectification Circuit Schematic	118
10.5	Prototype Design Based on Biomechanics	118
10.6	TENG Current Output Measurements	118
10.7	Triboelectric Material Spacing Improvements	118
10.8	Broader Impacts	119
10.8.1	Engineering Ethics	119
10.8.2	Societal and Global Impacts	119
10.8.3	Environmental Impacts	119
10.8.4	Economic Impacts	119
10.9	Final Remarks	119
Bibliography		121
Appendix		126

Table of Figures

Figure 1: Four Configurations of TENGs [7]	5
Figure 2: Carbon Composition Resistor	7
Figure 3: Standard 50k Ω Adjustable Potentiometer	7
Figure 4: Non-Polarized Capacitor	8
Figure 5: 60S4 Diode	8
Figure 6: The Short Circuit vs. Open Circuit Voltage for TENG Modes	12
Figure 7: Surface Power Density vs Open Circuit Voltage for the TENG Modes	13
Figure 8: TENG Modes Compatibility Table	13
Figure 9: TENG Mode and Design Matrix	14
Figure 10: Impact and Wind Testing Fabrication Setup	15
Figure 11: DEVCOM Fabric Samples	15
Figure 12: Impact Testing Apparatus	17
Figure 13: Wind Testing Apparatus	18
Figure 14: Nanofiber Membrane Attached at an Electrode using Kapton Tape	20
Figure 15: DEVCOM Fabric Samples	20
Figure 16: Impact TENG Layers	21
Figure 17: Photo of Fabricated TENGs	21
Figure 18: Wind TENG Fabrication Graphic	22
Figure 19: Photo of Wind TENGs	22
Figure 20: Step Layers	23
Figure 21: Photo of STEP	23
Figure 22: Various Designs using Rigid Metal are Proposed [40]	24
Figure 23: Ultra-thin Stacked Wind Design using A Polymer Membrane	24
Figure 24: Individual vs Woven Threads using Silicon-Coated Silver Thread [41]	25
Figure 25: Leaf Spring-Type Design Used in TENG Designs and Studies [45]	26
Figure 26: Diagram of the Working Model for the Thin Electrode Wind Application	27
Figure 27: Micro-Scale Diagram of Water Droplet Interaction	27
Figure 28: Duck Wave Harvester Design using Nylon Balls as a Dielectric	28
Figure 29: Ratcheting Wheel Design for a Rotational TENG	28

Figure 30: Water-Based Rotary Design using Typical Dielectric Materials	28
Figure 31: Rotating TENG Design	29
Figure 32: Polyimide Dielectric Film FPCB	30
Figure 33: Laser Direct Imaging a Copper Circuit Path	31
Figure 34: Direct Ink Writing for Electronic Circuits Process	31
Figure 35: Voltera V-One PCB Printer.....	32
Figure 36: Example Multilayer Flexible Printed Circuit Board	33
Figure 37: Steps for Charging TENGs.....	34
Figure 38: TENG with Parallel Switch.....	35
Figure 39: TENG with Series Switch	36
Figure 40: Comparison of Full-Wave Rectifier (Left) to Rectifier with Parallel Switch (Right).....	36
Figure 41: Charge Density PMM.....	37
Figure 42: Bennet's Doubler Conditioning Circuit	38
Figure 43: Inductive Transformers	38
Figure 44: Two-stage PMM.....	39
Figure 45: Fractal Switch Capacitor Converter	39
Figure 46: Bennet's Double Conditioning Circuit on Breadboard	43
Figure 47: Multisim Circuit and Results of Bennet's Doubler	43
Figure 48: The Multisim Circuit and Results of the Bennet's Doubler	44
Figure 49: Full Wave Rectifier on a Breadboard.....	44
Figure 50: Multisim Model and Results of the Full Wave Rectifier	45
Figure 51: The Half Wave Rectifier on a Breadboard.....	45
Figure 52: Multisim Model and Results of the Half Wave Rectifier.....	46
Figure 53: The Parallel Switch Circuit on a Breadboard	46
Figure 54: Multisim Model and Results of Parallel Switch Circuit	47
Figure 55: The Series Switch Circuit on a Breadboard	47
Figure 56: Multisim Model and Results of the Series Switch Circuit	48
Figure 57: The Self Double Rectification Circuit on the Breadboard	48
Figure 58: Multisim Model and Resulta of the Self Double Rectification Circuit	49
Figure 59: Benet's Doubler Rectification Circuit with PWM Power Source	50
Figure 60: Bennet's Doubler Rectification Circuit with PWN Power Supply Voltage Supply	50

Figure 61: Full Wave Rectification Circuit with PWN Power Source	50
Figure 62: Full Wave Rectification Circuit Voltage Reading	51
Figure 63: Half Wave Rectification Circuit with PWM Power Source	51
Figure 64: Half Wave Rectification Circuit (R4) Voltage Reading	52
Figure 65: Self Doubled Rectification Circuit with PMW Power Source	52
Figure 66: Self Doubled Rectification Circuit Voltage Output	53
Figure 67: Graph of Average Voltage vs Capacitance	55
Figure 69: Graphs of Average Voltage vs Difference in Capacitance.....	57
Figure 71: Smoothing Capacitance vs Voltage for No Internal Resistance.....	60
Figure 72: Half Wave Circuit Breadboard Voltage Output	61
Figure 73: Bennet's Doubler Breadboard Circuit Voltage Output	62
Figure 74: Self Doubled Rectification Breadboard Circuit Voltage Output.....	63
Figure 75: Full Wave Rectification Breadboard Circuit Voltage Output	63
Figure 76: Self Doubled Rectification Circuit KiCAD Schematic	64
Figure 77: Full Wave Rectification Circuit KiCAD Schematic	65
Figure 78: Surface Mount Capacitor Component	65
Figure 79: Surface Mount Diode Component as Seen Under Microscope	66
Figure 80: Self Doubled Rectification Circuit Mounted onto Voltera V-One Printer.....	66
Figure 81: Self Doubled Rectification Circuit with Soldered Components	67
Figure 82: Full Wave Rectification Circuit with Soldered Components	67
Figure 83: Self Doubled Rectification Circuit with Soldered Lead Wires Connected to Oscilloscope ...	68
Figure 84: Graph of Rectification FPCB Test Voltage Output.....	68
Figure 85: Gait cycle for average humans. ^[70]	70
Figure 86: Pneumatic gait design.....	71
Figure 87: Weight-based Design	72
Figure 88: Pneumatic Straight Design	74
Figure 89: Pneumatic system for the final design.....	75
Figure 90: Final flowchart diagram for Arduino code and decision-making process	75
Figure 91: Folded TENG from Literature.....	77
Figure 92: Spacing for TENG from Literature	78
Figure 93: Image of Wire Through.....	79

Figure 94: Image of Wire at the End of the TENG.....	79
Figure 95: CAD of Single-Folded TENG.....	79
Figure 96: Image of TENG Single-Folded	80
Figure 97: CAD of Double-Fold TENG	80
Figure 98: Image of Double Fold TENG.....	81
Figure 99: CAD of Triple-Fold.....	81
Figure 100: Image of Triple-Fold	81
Figure 101: Image of Sponge Four Corners	82
Figure 102: Image of Sponge Four Corners Half Height	82
Figure 103: Image of Sponge in Center	83
Figure 104: Image of Foam Four Corners	83
Figure 105: Filtering Out Noise from Data.....	84
Figure 106: Average Peak-to-Peak for Iterations	85
Figure 107: Graph Comparison of Original Sample to Wire Through.....	86
Figure 108: Comparison Once Folded to Unfolded Iteration	86
Figure 109: Graph Comparison of Double-Folded to Unfolded.....	87
Figure 110: Graph Comparisons of Triple-Folded to Unfolded	87
Figure 111: Comparison Graphs of Sponge Layers.....	88
Figure 112: Comparison Graphs Foam vs Sponge	88
Figure 113: The Basic Midsole Design Idea.....	90
Figure 114: The Basic Sock Design Idea.....	91
Figure 115: The Sole to Sock Design Idea	91
Figure 116: The Basic Sole Design Idea.....	92
Figure 117: Midsole I Prototype	93
Figure 118: Sock I Prototype	94
Figure 119: Sock to Insole I Prototype	95
Figure 120: Insole I Prototype	95
Figure 121: Midsole I Prototype Automated Testing	96
Figure 122: Midsole I Prototype Test Results	97
Figure 123: Sock I Prototype Automated Testing	98
Figure 124: Sock I Prototype Test Results	98

Figure 125: Sock to Insole I Prototype Automated Testing	99
Figure 126: Sock to Insole I Prototype Test Results.....	100
Figure 127: Insole I Prototype Automated Testing.....	100
Figure 128: Insole I Prototype Test Results.....	101
Figure 129: Camouflage Fabric Layer Prototype II.....	103
Figure 130: PTFE Layer Prototype II	104
Figure 131: Prototype II TENG Layers	104
Figure 132: Midsole II Prototype Automated Testing	105
Figure 133: Insole II Prototype Automated Testing	106
Figure 134: Midsole II Prototype Test Results	107
Figure 135: Insole II Prototype Test Results	107
Figure 136: Final TENG Prototype.....	110
Figure 137: CAD Drawing of Final Prototype TENG.....	110
Figure 138: Final Prototype TENG Placement.....	111
Figure 139: Force Exerted by Foot During Walking [74]	111
Figure 140: Final Prototype Midsole Measurements.....	112
Figure 141: Screw Placement on Final Prototype.....	113
Figure 142: Final Prototype Test Results Automated Tester.....	114
Figure 143: Walking Test Performed on Final Prototype.....	115
Figure 144: Final Prototype Walking Test Results.....	115



List of Tables

Table 1: Triboelectric Table.....	3
Table 2: The Material Matrix.....	11
Table 3: Simulated Circuit Results Summary.....	42
Table 4: Capacitances and their Output Value Across Resistors.....	54
Table 5: Weight of Item in Average Loadout.....	70
Table 6: Variable Definitions for Voltage Equation.....	76
Table 7: Results from All Iterations.....	85



Authorship

Peter Fagerholm



Mechanical
Engineering

Newtown, CT

Kaleigh Hess



Mechanical
Engineering

Berea, KY

Caitlin Kean



Mechanical
Engineering

Shrewsbury, MA

Kyle Postans



Mechanical
Engineering

Hartland, VT

Joshua Woodruff



Mechanical
Engineering

Littleton, NY



Section	Author(s)
Abstract	PF, KH, CK, KP
Acknowledgments	KH
Chapter 1: Introduction	PF, KH, CK, KP
Chapter 2: Background Literature	All
2.1 Fundamental Physics	JW
2.2 Circuitry Fundamentals	JW
2.3 Circuitry in TENGs	PF
2.3.1 Common Circuit Components	PF
2.4 U.S. Army Portable Energy Sources & Methods	JW
2.5 Previous Team's Work	KH
2.5.1 Material Matrix	KH
2.5.2 TENG Mode and Design Discussion	KH
2.5.3 TENG Selections for Design and Fabrication	KH
2.5.4 TENG Performance Evaluations	KH
2.6 Fabrication Techniques	KH
2.6.1 Bonding	KH
2.6.2 Surface Modifications	KH
2.6.3 Methods of Assembly	KH
2.6.4 Previous Triboelectric Team's Fabrication Techniques	KH
2.7 TENG Design	KP
2.7.1 Reducing Power Decay	KP
2.7.2 Stacking	KP
2.7.3 Improving Application Through Materials	KP
2.8 TENG Applications	KP
2.8.1 Experimental Applications	KP
2.9 Flexible Printed Circuit Boards	PF
2.9.1 Common Materials Found in FPCBs	PF
2.9.2 Fabrication Process for FPCBs	PF
2.9.3 Voltera V-One PCB Printer	PF

2.9.4 Multilayer FPCBs	PF
2.9.5 Disadvantages of FPCBs	PF
2.10 Power Management Modules (PMM)	CK
Chapter 3: Project Scope and Objectives	PF, KP
Chapter 4: Circuitry	PF, KH, CK
4.1 Circuit Schematics and Simulation Results	PF, KH, CK
4.1.1 Bennet's Doubler Rectification Circuit Schematic and Simulation	CK
4.1.2 Fractal Switch Capacitor Converter Schematic and Simulation	CK
4.1.3 Full Wave Rectification Circuit Schematic and Simulation	PF
4.1.4 Half Wave Rectification Circuit Schematic and Simulation	CK
4.1.5 Parallel Switch Circuit Schematic and Simulation	KH
4.1.6 Series Switch Circuit Schematic and Simulation	KH
4.1.7 Self Doubled Rectification Circuit Schematic and Simulation	PF
4.2 Simulation Circuit Changes and Improvements	CK
4.3 Breadboard Rectification Circuits Testing and Evaluation	PF
4.3.1 Half Wave Rectification Circuit Breadboard Evaluation	PF
4.3.2 Bennet's Doubler Rectification Circuit Evaluation	PF
4.3.3 Self Doubled Rectification Circuit Breadboard Evaluation	PF
4.4 Flexible Printed Rectification Circuit Fabrication and Performances	PF
4.4.1 Rectification FPCB Schematics	PF
4.4.2 FPCB Components and Fabrication	PF
4.4.3 FPCB Evaluation and Conclusions	PF
Chapter 5: Automated Tester	KP
5.1 Design Parameters	KP
5.2 Summary of Designs	KP
5.3 Pneumatic Gait Design	KP
5.4 Weight Based Design	KP
5.5 Final Design – Pneumatic Straight Tester	KP
Chapter 6: TENG Iterations	CK
6.1 Research	CK
6.2 TENG Iteration Composition	CK
6.2.1 Wire Iteration	CK

6.2.2 Folded Iterations	CK
6.2.3 Spacing	CK
6.3 Results	CK
6.3.1 Wire	CK
6.3.2 Folded Iteration Results	CK
6.3.3 Spacing	CK
Chapter 7: Prototyping Stage One	PF, KH
7.1 Initial Design Concepts	KH
7.2 Stage One Prototype Construction	KH
7.2.1 Midsole I	KH
7.2.2 Sock I	KH
7.2.3 Sock-Insole I	KH
7.2.4 Insole I	KH
7.3 Stage One Prototype Tests and Results	PF, KH
7.3.1 Midsole I	PF, KH
7.3.2 Sock I	PF, KH
7.3.3 Sock-Insole I	PF, KH
7.3.4 Insole I	PF, KH
7.4 Conclusions	PF
Chapter 8: Prototype Stage II	PF, KH
8.1 Stage Two Prototype Construction	KH
8.2 Stage Two Prototype Tests and Results	PF
8.2.1 Midsole II	PF
8.2.2 Insole II	PF
8.3 Stage Two Prototype Conclusions	PF
Chapter 9: Final Prototyping Stage	PF, KH
9.1 Final Prototype Construction	KH
9.2 Final Prototype Tests and Results	PF
9.3 Final Prototype Stage Conclusions	PF
Chapter 10: Conclusion and Broader Impact	PF, KH, CK, KP
10.1 Automated Testing Modification	KP
10.2 Bending Affects	KP

10.3 Improved Midsole III TENG Accessibility	KH
10.4 Improved Rectification Circuit Schematic	PF
10.5 Prototype Design Based on Biomechanics	PF
10.6 TENG Current Output Measurements	CK
10.7 Triboelectric Material Spacing Improvements	CK
10.8 Broader Impacts	PF, KH, CK, KP
10.8.1 Engineering Ethics	KP
10.8.2 Societal and Global Impacts	PF
10.8.3 Environmental Impacts	KH
10.8.4 Economic Impacts	CK
10.9 Final Remarks	PF
Appendices	PF, KH, CK, KP
Appendix A: Pneumatic Gait Tester Design BOM	KP
Appendix B: Weight-Based Tester Design BOM	KP
Appendix C: Final Straight Pneumatic Tester Design BOM	KP
Appendix D: Additional Detail Drawing of A.T. Support	KP
Appendix E: Structural Analysis of A.T. Support	KP
Appendix F: Structural Analysis of Vertical Frame	KP
Appendix G: Structural Analysis of Horizontal Frame	KP
Appendix H: Automated Tester Code	KP
Appendix I: Procedure for Creating 2x2 Samples	CK
Appendix J: Procedure for Creating Folded TENGs	CK
Appendix K: Procedures for Oscilloscope Tests	KH
Appendix L: Voltera V-One Circuit Printer Procedure	PF

Chapter 1: Introduction

As modern technology advances, the demand for efficient power sources increases. What used to be driven through physical labor is now mechanically or electromechanically driven. In order to actuate these machines and devices, reliable and powerful energy sources are needed. Coal, gas, or nuclear energy production has been used to power our technology for centuries. However, we have begun to move away from these traditional methods, as they are wasteful and harmful to our environment. Demand for clean energy solutions has grown over recent decades. This need has increased to a point where it has become an area of research/implementation across all industries, which has allowed for scientific breakthroughs in clean energy. Energy sources such as solar, wind, and hydroelectric power have started to compete with traditional energy solutions. Beyond these commonly known clean energy sources, new discoveries have been made in this area of power. Though these are only small breakthroughs now, these newly discovered options have potential. These include recently discovered power sources such as triboelectric nanogenerators (TENGs), which could be used for advanced technology.

TENGs first came to fruition in 2012 “first proposed by [Professor] Wang’s group” to harness ambient mechanical energy. TENGs combine the ideas of both the triboelectric effect and electrostatic charges. The triboelectric effect refers to the electric charge created when two different materials come into contact with each other. Usually, the triboelectric effect is an undesirable effect because the electrostatic charges can lead to dielectric breakdown and electronic damage. However, the electrical charges can power capacitive energy devices when the two surfaces are separated. Electrostatic induction, also known as an electrostatic influence, is an object's redistribution of electric charges. When the triboelectric effect and electrostatic influence work together, triboelectrification creates polarized charges on the material surfaces in contact, while electrostatic induction drives the transformation of mechanical energy to electricity ^[1]. TENG has started to gain popularity and expanded to different working modes. TENGs are popular due to their versatile operation modes, broad material availability lightweight, low cost, and high efficiency (with most methods approaching 100%). There are broad applications to the TENGs, such as harnessing the energy of mechanical vibrations, human motion, wind, and water waves. Our project will focus on harnessing energy from human motion, specifically forces from walking.

Our project is the continuation of a previous MQP. Within their project, the team previously proved the concepts of TENGs by fabricating several prototypes. We will continue to collaborate with the US Army Combat Capabilities Development Command (DEVCOM) Soldier Center to further develop these TENGs. This MQP aims to continue to design and iterate plausible TENG applications for military footwear.

Chapter 2: Background

This chapter will provide insight into triboelectric energy generation, resources available to make such generation possible, and potential applications of TENGs. The basic background physics and mechanics are explained in detail. Electrical solutions utilized to create TENG applications are explored. Theorized and tested TENG designs are introduced and analyzed for potential applications towards this project. Along with these areas, the milestones accomplished by last year's MQP team are summarized and explained.

2.1 Fundamental Physics

The triboelectric effect occurs when electrons transfer from one surface to another as a result of two materials making contact and separating. This effect can be amplified by using materials that are more prone to giving up or accepting electrons by their large relative difference in electron affinity. It is also amplified by increasing the amount of friction between the two materials ^[2]. The result of this effect is the build-up of equal and opposite charges on the two material faces, effectively forming a capacitor ^[3].

The triboelectric series is a qualitative list, which compares the relative electron affinity of a set of materials. An example is shown in Table 1. The affinity for these materials is quantified as an amount of charge transferred per a controlled variable that is dependent on the method of testing ^[3]. It is typically Coulombs per a specific variable such as surface area or the energy gained from friction; in this table, nanoCoulombs per Joule is used.

Table 1: Triboelectric Material Qualities ^[4]

Column 1 (this col.): Insulator name. Col.2: Charge affinity in nC/J (nano ampsec/wattsec of friction). Col.3: Charge acquired if rubbed with metal (W=weak, N=normal, or consistent with the affinity). Col.4: Notes.

Triboelectric Table

Tests were performed by Bill Lee (Ph.D., physics). ©2009 by AlphaLab, Inc. (TriField.com), which also manufactured the test equipment used. This table may be reproduced only if reproduced in whole.

	Affinity nC/J	Metal effect	Notes
Polyurethane foam	+60	+N	All materials are good insulators (>1000 T ohm cm) unless noted.
Sorbothane	+58	-W	Slightly conductive. (120 G ohm cm).
Box sealing tape (BOPP)	+55	+W	Non-sticky side. Becomes more negative if sanded down to the BOPP film.
Hair, oily skin	+45	+N	Skin is conductive. Cannot be charged by metal rubbing.
Solid polyurethane, filled	+40	+N	Slightly conductive. (8 T ohm cm).
Magnesium fluoride (MgF2)	+35	+N	Anti-reflective optical coating.
Nylon, dry skin	+30	+N	Skin is conductive. Cannot be charged by metal rubbing.
Machine oil	+29	+N	
Nylatron (nylon filled with MoS ₂)	+28	+N	
Glass (soda)	+25	+N	Slightly conductive. (Depends on humidity).
Paper (uncoated copy)	+10	-W	Most papers & cardboard have similar affinity. Slightly conductive.
Wood (pine)	+7	-W	
GE brand Silicone II (hardens in air)	+6	+N	More positive than the other silicone chemistry (see below).
Cotton	+5	+N	Slightly conductive. (Depends on humidity).
Nitrile rubber	+3	-W	
Wool	0	-W	
Polycarbonate	-5	-W	
ABS	-5	-N	
Acrylic (polymethyl methacrylate) and adhesive side of clear carton-sealing and office tape	-10	-N	Several clear tape adhesives are have an affinity almost identical to acrylic, even though various compositions are listed.
Epoxy (circuit board)	-32	-N	
Styrene-butadiene rubber (SBR, Buna S)	-35	-N	Sometimes inaccurately called "neoprene" (see below).
Solvent-based spray paints	-38	-N	May vary.
PET (mylar) cloth	-40	-W	
PET (mylar) solid	-40	+W	
EVA rubber for gaskets, filled	-55	-N	Slightly conductive. (10 T ohm cm). Filled rubber will usually conduct.
Gum rubber	-60	-N	Barely conductive. (500 T ohm cm).
Hot melt glue	-62	-N	
Polystyrene	-70	-N	
Polyimide	-70	-N	
Silicones (air harden & thermoset, but not GE)	-72	-N	
Vinyl: flexible (clear tubing)	-75	-N	
Carton-sealing tape (BOPP), sanded down	-85	-N	Raw surface is very + (see above), but close to PP when sanded.
Olefins (alkenes): LDPE, HDPE, PP	-90	-N	UHMWPE is below. Against metals, PP is more neg than PE.
Cellulose nitrate	-93	-N	
Office tape backing (vinyl copolymer ?)	-95	-N	
UHMWPE	-95	-N	
Neoprene (polychloroprene, not SBR)	-98	-N	Slightly conductive if filled (1.5 T ohm cm).
PVC (rigid vinyl)	-100	-N	
Latex (natural) rubber	-105	-N	
Viton, filled	-117	-N	Slightly conductive. (40 T ohm cm).
Epichlorohydrin rubber, filled	-118	-N	Slightly conductive. (250 G ohm cm).
Santoprene rubber	-120	-N	
Hypalon rubber, filled	-130	-N	Slightly conductive. (30 T ohm cm).
Butyl rubber, filled	-135	-N	Conductive. (900 M ohm cm). Test was done fast.
EDPM rubber, filled	-140	-N	Slightly conductive. (40 T ohm cm).
Teflon	-190	-N	Surface is fluorine atoms-- very electronegative.

Table 1: Triboelectric Table

As the triboelectric materials are two oppositely charged materials separated by a gap, they can be modeled as a capacitor. Therefore, the capacitance equations listed below apply to TENGs^[5].

$$C = \frac{q}{V}, C = \frac{\epsilon_0 A}{d}$$

Taking these two expressions we can set:

$$\frac{q}{V} = \frac{\epsilon_0 A}{d}$$

And then solve for voltage:

$$V = \frac{qd}{\epsilon_0 A}$$

From this we find two physically alterable variables which can be used to increase voltage, an increase in gap distance (d) and a decrease in the area overlap between electrodes (A).

Normally, a fixed geometry capacitor will not produce a current in an electrical system unless said capacitor is discharged. However, for a TENG, the dimensional properties change while the charge and dielectric material remain constant. Thus, the voltage across the two electrodes must change per Ohm's law, creating a current (I) given by the equation below in which we also assume the resistance (R) is constant.

$$I = \frac{\Delta V}{R}$$

Our independent variables in the model then become the charge differential (q) and permittivity (ϵ) for any individual TENG design. The charge differential is determined by the selected triboelectric materials and can only be increased by choosing more effective materials. As permittivity decreases, the potential difference increases. The lowest permittivity achievable occurs in a vacuum. As the contact area or distance is modulated cyclically, it creates an oscillation in voltage that in turn generates an AC current. Varying the gap distance has a secondary effect due to electric field, which is given as follows [6].

$$E = \frac{q}{4\pi\epsilon_0 r^2}$$

Where (q) is the charge source and (r) is the distance from the charge. The electric field directly affects the voltage differential which in turn affects the current and power of the system. The distance has an inverse squared relationship to field strength therefore, it also has an inverse squared relationship with the power output.

2.2 Circuitry Fundamentals

There are four main configurations to change the gap distance or contact area in order to Produce potential difference across the TENGs. The configurations are Vertical Contact-Separation, In-Plane Contact Sliding Mode, Single Electrode Mode, and Freestanding Layer Mode as shown in Figure 1.

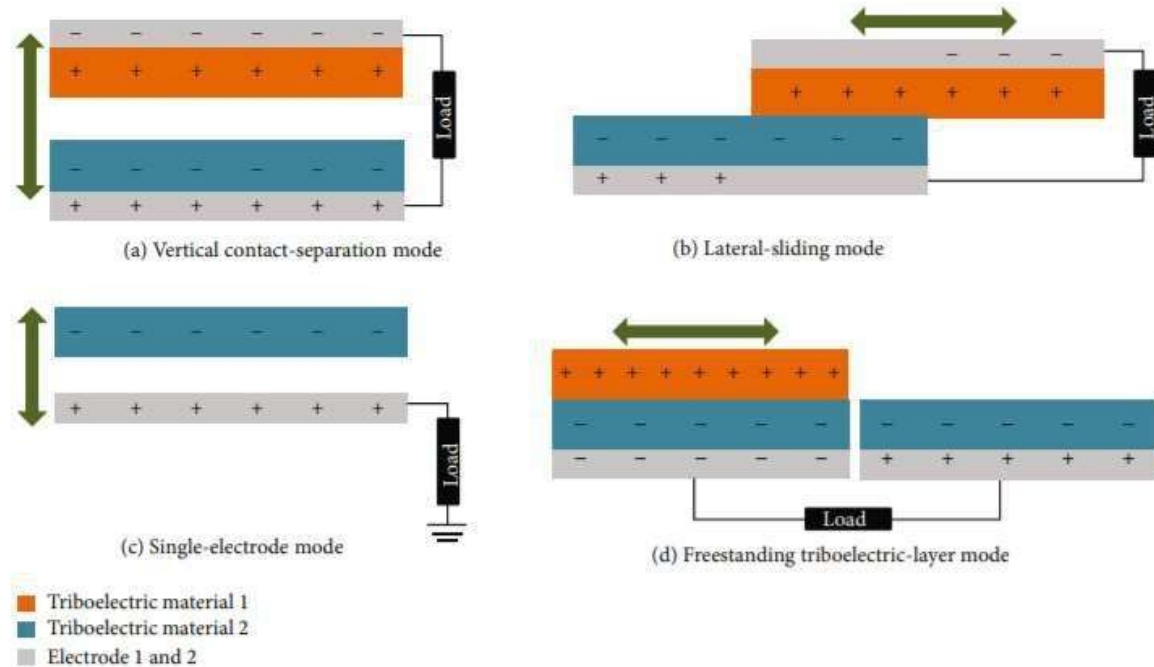


Figure 1: Four Configurations of TENGs [7]

All of these modes require the selected triboelectric materials to be connected to electrodes and have electrical insulation between layers and may include either dielectric-dielectric contact layers or metal-dielectric contact layers depending on the configuration. The repeated mechanical oscillation causes the triboelectric layers to generate forward and reverse potential between the electrodes, making the positive and negative peaks in the TENG output which generates an AC signal.

In Vertical Contact-Separation Mode, two conductive electrodes are connected to dielectric film placed on the top and the bottom of a stacked structure with a small air gap in between. When a force is applied perpendicular to the assembly, the upper electrode and dielectric film will come into physical contact with the lower electrode. Due to the triboelectric effect, the upper and lower layers will have the opposite charge of each other [8]. Potential difference is induced when the force is released and the layers separate, forcing electrons to move from one electrode to the other, which causes a current to flow through the circuit [8].

In-Plane Contact Sliding Mode, also known as Lateral Sliding Mode, differs mechanically as the electrodes move laterally without an increase in gap distance when an external force is applied. Initially, the electrodes are positioned fully overlapping, causing oppositely charged surfaces. Oscillation of the sliding contact surfaces creates a change in contact area which leads to a lateral separation in which areas of the electrodes which are not overlapping have a net charge and creates a potential difference [7].

Single Electrode Mode is configured so that one electrode is immobile while another material can move. The one electrode is connected to ground, while the top material will cause a charge via

triboelectric effect either donating or receiving electrons. The potential difference between the electrode and ground carries through the circuit as current output [9].

Freestanding Layer Mode utilizes a dielectric layer and two electrodes in the same plane with a lateral gap between the two symmetric electrodes that is smaller than the length of the dielectric layer. At the original position, the state of the dielectric layer and first electrode is similar to lateral-sliding mode. The dielectric layer and electrode become oppositely charged. When the dielectric layer oscillates between overlapping each electrode, there will be a potential difference between the two electrodes due to the change in distribution of overlapped area, which drives the electron exchanges between them [9]. The asymmetric charge distribution creates a voltage which results in a current.

Because TENGs generate alternating current (AC) signals and power storage devices such as batteries and capacitors require direct current (DC), the AC must be converted to DC to be useful. A common way to convert AC to DC is using a bridge rectifier, which employs diodes. Diodes only allow one-way current flow within a rated voltage. By using diodes, a setup can be achieved such that a direct current flow is the generated output of the circuit. In effect, the diodes implemented into the rectification circuit will direct positive and negative polarized current flow in a way to combine and produce a direct current of equal magnitude to the peak-to-peak voltages of the original AC signal [5]. To do this, bridge rectifiers use a configuration of four diodes, along with a smoothing capacitor which is added to smooth the voltage of the direct current. This effectively makes the TENG voltage output compatible with direct current devices [5].

2.3 Circuitry in TENGs

Proper circuitry must be implemented into TENG designs to achieve specialized energy outputs. Circuitry integrated into TENG designs for military applications needs to be lightweight, mobile, and durable as these devices will be utilized in a variety of environments. This implementation can provide a power source for several military devices. The schematics of such circuits need to be manufacturable and capable of housing all required circuit components. Recent circuit fabrication methods have opened the door for lightweight electronic applications such as TENG designs. Through modern manufacturing techniques, circuits can be 3D printed onto flexible circuit boards and covered in a protective insulative coating^[10]. These fabrication techniques ensure efficient and durable printed circuit boards that give the ability to mobilize TENG prototypes that were bound by traditional electronic hardware.

2.3.1 Common Circuit Components

Common circuit components such as resistors, capacitors, diodes, transistors, and power supplies are interconnected on circuit boards to create an electrical system's designed output. These components are used to direct, regulate, and amplify current flow along with harvesting a circuit's produced power for a system's designed outcome. This subsection will highlight the functions of these common circuit components.

2.3.2 Resistors

As described in its name, a resistor is a circuit element that has electrical resistance. Resistors are used for power dissipation and current regulation. Modern resistors are composed of a mixture of carbon, metal, and metal-oxide materials covering the interconnection between the inlet and outlet of the component [6]. Resistors can be used to protect other circuit components that are sensitive to high

voltage or current values. Besides having high electric resistivity, resistors also have high thermal conductivity. This is important to consider when designing a circuit, as the heat produced from the resistors can be disruptive or destructive to the circuit^[11]. Depending on the type of resistor being implemented it can have a set or variable resistance. Figure 2 below shows a carbon composition resistor.

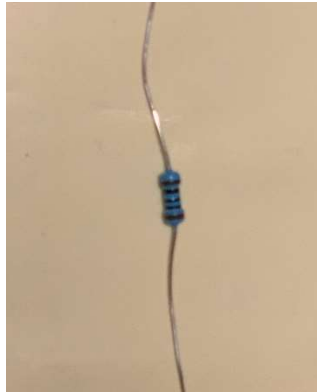


Figure 2: Carbon Composition Resistor

The colored bands found on the coating of the carbon on the resistor can be used to identify the resistor's fixed voltage value. Unlike fixed resistors, variable resistors can have their electrical resistance adjusted. A commonly used variable resistor is known as a potentiometer. A potentiometer's resistance can be adjusted via a rotating knob or a slider. It has three leads: an inlet, a drain (ground source), and the output pin. Figure 3 below shows a picture of a standard 50k Ω potentiometer.

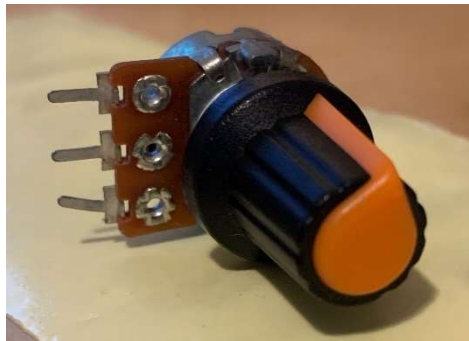


Figure 3: Standard 50k Ω Adjustable Potentiometer

For this specific potentiometer module, as the knob is rotated counterclockwise the power dissipated by this potentiometer increases^[12]. Variable resistors can be utilized when testing circuits to determine the required resistances in specific circuit paths.

2.3.3 Capacitors

Capacitors are used to store charge in a circuit. They consist of two conductive plates separated by a dielectric which acts as an insulator to minimize unwanted current flow. The two plates build up oppositely polarized charges^[13]. The charge build-up on both plates create a voltage stored within the capacitor. Once the capacitor's stored voltage is at the same value as the power supply it is identified as fully charged. If a new path in the circuit is created (examples include through a switch or short-circuiting the capacitor will then discharge and the built-up charges will be released into the current^[14].

Figure 4 below shows a 0.1 μ F capacitor. Inside the black coating seen in Figure 4 are two plates and a porcelain dielectric separator.



Figure 4: Non-Polarized Capacitor

Capacitors can be used for smoothing electrical signals in circuits. If the power supply in a circuit is erratic and unsteady a capacitor can be implemented into the circuitry to smooth the voltage supply across a circuit section. When a capacitor is used for this purpose, it is known as a smoothing capacitor ^[14]. Since the voltage output from TENG mechanical interactions is not linear, a smoothing capacitor could be utilized in a TENG energy harvesting circuit to help output a steady and controlled power supply.

2.3.4 Diodes

The key function of electrical diodes is to control the direction of current flow. Current can only flow in one direction through diodes ^[15]. Diodes have a positive end (the anode) and a negative end (the cathode) which are both oppositely polarized. They are composed of semiconductive materials such as silicon or germanium. Figure 5 below shows a 60S4 Diode.



Figure 5: 60S4 Diode

Diodes are also known as rectifiers as they can convert an AC voltage input into a pulsating DC voltage output. If interfaced together, multiple diodes can interconnect in a circuit to change an AC voltage input into a DC voltage output. This concept is known as bridge rectification.

2.3.5 Power Supply

Power supply devices provide the voltage for an electrical circuit, and they can come in many forms. Examples of voltage supplies are batteries, alternators, and TENGs. The current output by these supplies can be categorized as either an alternating current (AC supply) or a direct current (DC supply) ^[16]. An AC supply will output a voltage supply that continuously changes its magnitude and periodically changes its polarity. Most power supplies will have an output terminal and a ground terminal which can

be hooked up to create a closed circuit. Multiple power supplies can be implemented in a circuit. Depending on the direction of the current flow in a circuit, these devices can be charged or activated to power other interconnected circuits and devices. This principle is why TENG research has gained more attention recently. The discovery of TENG has opened the doors of possibilities for possible circuits used for military applications. An efficient interconnection between these circuit components is not a simple creation. The fabrication of these energy harvesting circuits needs to produce a durable, reliable, and flexible circuit.

2.4 U.S. Army Portable Energy Sources & Methods

The US Army currently has several power solutions in place and under development. It has options for both power storage, delivery, and generation. The main limitation of power generation options is the lack of choices for portability. Many powers storage and generation options are still under development or yet to be put into use in significant quantities.

For man-portable power storage currently fielded, the US Army is moving away from disposable batteries with varying form factors and the logistical challenge of procuring and transporting large quantities and varieties of single-use batteries. Current developments in rechargeable batteries focus on body-mounted systems such as the Conformable Wearable Battery (CWB) and the Small Tactical Universal Battery (STUB). The CWB will be a lithium-ion rechargeable battery with a 10 Amp-hour capacity that mounts on the plate carrier vest of a soldier's body armor^[17]. The CWB is currently undergoing competition testing to determine the manufacturer^[18]. The STUB was designed to supplement equipment with smaller batteries while the CWB is disconnected. Electronics manufacturers are to design around the standardized sizes of the STUB batteries to reduce the need for unique batteries^[19]. The Army is also looking into portable fuel cells which bridge the gap between power generation and power storage. Though more energy-dense than traditional batteries, current fuel cells are comparatively bulky due to their more complex means of power generation^[20]. Though not yet fielded in man-portable scenarios, the US Army Operational Test Command has used methanol fuel cells to power test instrumentation in a vehicle setting. The US Army Operational Test Command estimated that "an almost ten-fold reduction in cost per operating hour can be achieved using fuel cells as battery replacements"^[21]. To address the power consumption demands of equipment each soldier has to carry, multiple CWBs would have to be carried for any operation lasting longer than 12 hours with each weighing multiple pounds. To address this, the Army is currently evaluating Direct Methanol Fuel Cells, Reformed Methanol Fuel Cells, and Alane-based Fuel Cells to determine their power generation and charging capabilities^[22].

Current portable power generation methods employed or explored by the Army include photovoltaic panels and man-portable generators. The man-portable photovoltaic solar panel system is known as the Rucksack Enhanced Portable Power System (REPPS). The system is a 10-pound, 62-watt solar panel that can be combined in series for larger power demands^[23]. The man-portable generators, known as Platoon Power Generation (PPG) are intended to be a series of commercial portable generators modified to run on JP-8, a standardized fuel widely used by the US military. As described in the name, this is intended to provide power and recharging at the platoon level and is not available to an individual if physically separated from the generator. Additionally, the generators are bulky, loud, and give off visible emissions when in use. The plan for developing this system may be defunct or inactive at the

time of writing ^[24]. There is some research into the application of piezoelectric material, which generates energy from compression of said material, in low-power military applications similar to our research into triboelectric power generation. A 2008 US army research study used a heel-strike design and was able to reach ~0.09 watts of their 0.5-watt goal per heel strike, further testing was recommended but no real-world development or substantial further research was done ^[25]. More recently in 2015, piezoelectric generators in a heel strike configuration were tested by the Indian military and were found to have the potential to power “ultra-low power microelectronic devices” ^[26].

2.5 Previous Team’s Work

As stated before, this project marks the continuation of the previous Triboelectric Energy MQP team’s work. The focus of their research was to determine pairs of materials with qualities preferable for TENG applications. Following this research, they fabricated and manufactured these TENG pairs and tested them. After extensive research and fabrication, they created two testing apparatuses and one final prototype with a TENG pair implemented. They had several iterations of each and successfully proved that using TENGs in a practical way is possible.

2.5.1 Material Matrix

The previous team used a material matrix to research and discover optimal materials for TENGs ^[27]. The matrix helped the team choose one electrode and two triboelectric materials to use for the project. Data was gathered from multiple sources about these materials to create more accurate assessments that considered variability in the testing environment. They graded these properties on a 1-10 scale (1 being least optimal and 10 being most ideal). After grading, the properties were then weighted on their overall importance. The only difference between the electrode and triboelectric grading process was how the properties were weighted at the end. The six TENG properties they reviewed were: use in studies, resistivity, affinity, density, yield strength, fatigue, and cost.

The first property they researched was how often the material appeared in research. The more these materials appear in research, the more likely they are to be compatible with TENGs ^[27]. The material with the lowest number of references was given a 1, while the one with the most was given a 10. This category was given a weight of 5% for the electrodes and 10% for the triboelectric materials. The next property reviewed was resistivity, which is the measure of a material’s ability to conduct electric current. A high resistivity designates a poor conductor while a low resistivity designates a good conductor. The material selected should have a lower resistivity in order to limit the power loss. Thus, the lowest resistivity value is given a 10 while the highest value is given a 1. This property was weighted at 5% because all the materials considered were conductive metals with low resistivity values. When building TENGs, the most important aspect is the relative affinity of one material to another. The group described and rated these materials for their tendency to gain or lose electrons. The materials were first listed from those most likely to lose electrons to the materials most likely to gain electrons. The lowest grades went to those within the middle of the list and the highest went to those on the opposite ends of the scale. This property was given a weight of 40% for the triboelectric materials, the highest percentage. Next, they ranked the density of the materials in order to produce a lightweight design. The densest material was given a 1 while the least dense was given a 10. For the electrode material, density was given a weight of 45%. Density was given a weight of 10% for triboelectric materials. Along with being lightweight, TENGs need to be flexible and resist deformation, both are illustrated in the yield

strength. The highest yield strength was given a 10 while the lowest was given a 1. The weight for both the electrode and triboelectric materials was between 15-20%. Another property evaluated was the durability of the TENG. Durability is the ability to withstand wear, pressure, and damage. In TENGs, the durability in cyclic motion must be considered [27]. A score of 10 was given to the most durable materials while 1 was given to the least durable. The group weighed this property 15-20%. The final consideration was cost. Expensive materials were given lower grades (near 1) and more affordable materials were given higher grades (near 10). The cost was given a weight of 5% because it was not considered a critical property. All these properties were then gathered into Table 2 which contains two tables, one for the electrodes and the other for the triboelectric materials. The column all the way to the right contains the material, the middle sections contain the individual categories, and all the way to the left are the final scores. The best performing electrodes were stainless steel, nickel, and case aluminum alloy. The best performing positive triboelectric materials were human skin and nylon-6 while the best performing negative materials were rayon, PTFE, and silicone-rubber. These charts were used by the team to analyze the pros and cons of potential TENG materials and aid in their fabrication choices.

ELECTRODE	Weighted Scores per Category						Final Weighted Score (1-10)
	Use in Studies (5%)	Resistivity (5%)	Density (45%)	Yield Strength (15%)	Fatigue (15%)	Cost (15%)	
Silver ->99.9%	0.22	0.50	2.60	0.31	0.36	1.48	5.48
Copper	0.33	0.50	2.98	0.18	0.18	1.50	5.67
Gold >99.5%	0.16	0.50	0.45	0.15	0.17	0.15	1.58
Cast Al Alloy	0.50	0.49	4.50	0.17	0.15	1.50	7.30
Nichrome	0.05	0.05	3.12	0.75	1.13	1.50	6.59
Nickel 99.8%Ni	0.16	0.47	3.00	1.06	1.15	1.50	7.34
Stainless steel	0.05	0.19	3.28	1.50	1.50	1.50	8.01

TRIBO MATERIALS	Weighted Scores per Category						Final Weight Score (1-10)
	Use in Studies (10%)	Affinity (40%)	Density (10%)	Yield Strength (15%)	Fatigue (20%)	Cost (5%)	
Human Skin	0.10	4.00	1.00	1.50	2.00	0.50	9.10
Nylon - 6	0.21	2.00	0.93	1.50	2.00	0.49	7.13
Aluminum Nitride	1.00	0.40	0.10	0.52	2.00	0.05	4.07
PMMA film	0.21	0.40	0.91	0.25	0.29	0.49	2.55
PET	0.21	0.80	0.85	0.23	0.36	0.50	2.96
EVA	0.10	1.20	1.00	0.17	0.26	0.50	3.22
Kapton	0.55	1.60	0.84	0.29	0.58	0.41	4.26
Natural Rubber	0.10	2.40	1.00	0.18	0.23	0.50	4.41
Rayon	0.10	2.80	0.98	0.83	2.00	0.49	7.21
Polyester	0.33	2.40	0.90	0.20	0.38	0.50	4.71
Acrylic Fiber (PAN)	0.10	1.60	0.91	0.65	2.00	0.49	5.76
PDMS	0.44	3.20	0.99	0.24	0.20	0.37	5.45
FEP	0.21	3.60	0.54	0.18	0.20	0.37	5.10
PVC	0.10	3.60	0.84	0.21	0.32	0.50	5.56
PTFE	0.78	4.00	0.53	0.18	0.20	0.46	6.15
Silicone-rubber	0.10	4.00	0.89	0.15	0.20	0.47	5.80

Table 2: The Material Matrix

2.5.2 TENG Mode and Design Discussion

Based on the constraints of the TENG design, the previous team discussed different design options and contact modes to discover the best configuration [27]. To start, they did an overview of the modes and their metrics to provide comparisons of their performance. Then, they identified the intersectionality between the modes and their design mechanism. Design mechanism is defined as the

way the TENG materials interact or are fabricated into the TENG. Lastly, the team created a TENG Mode and Mechanism Design Matrix to aid in the determination of the best overall configuration.

For the contact mode comparison, the research group reviewed the relevance in literature review, the current vs voltage, and the surface power density vs the voltage ^[27]. In their literature review, they found that the majority of the studies employed vertical contact separation with an emphasis in airdrop applications. They acknowledged that this may be because of the wind-based articles they were provided with and their initial direction toward parachute applications. The current versus voltage comparison is demonstrated in Figure 6 with the modes' short circuit current relative to their open circuit voltage. The open circuit voltage measures the maximum voltage while the short circuit current represents the electrical durability. The surface power density versus voltage comparison is charted in Figure 7 with surface power density relative to the open circuit voltage.

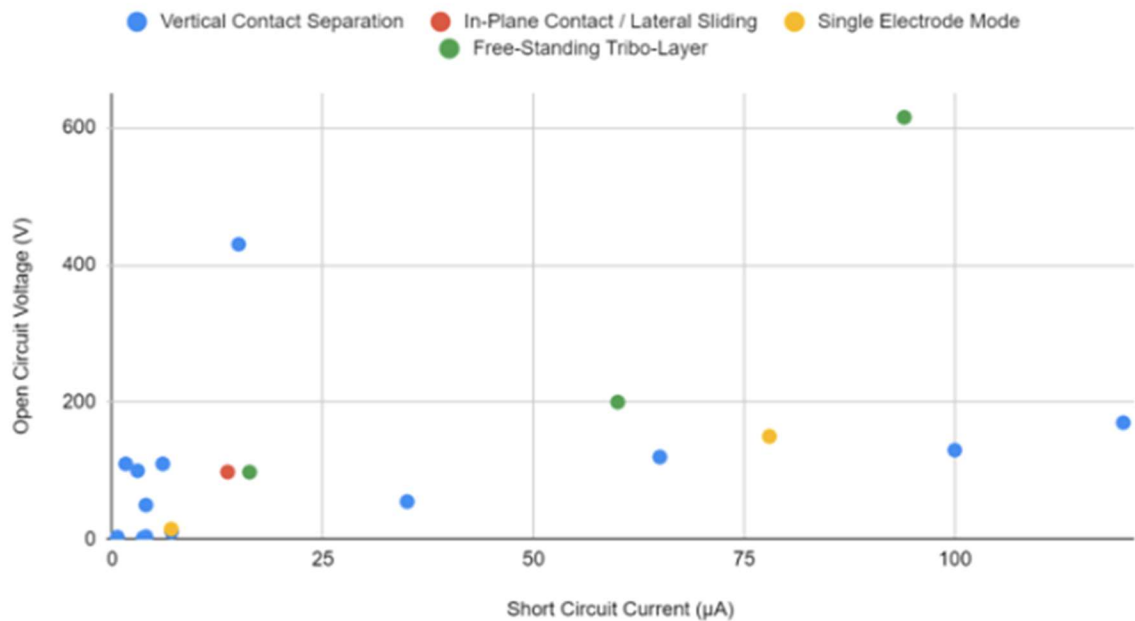


Figure 6: The Short Circuit vs. Open Circuit Voltage for TENG Modes

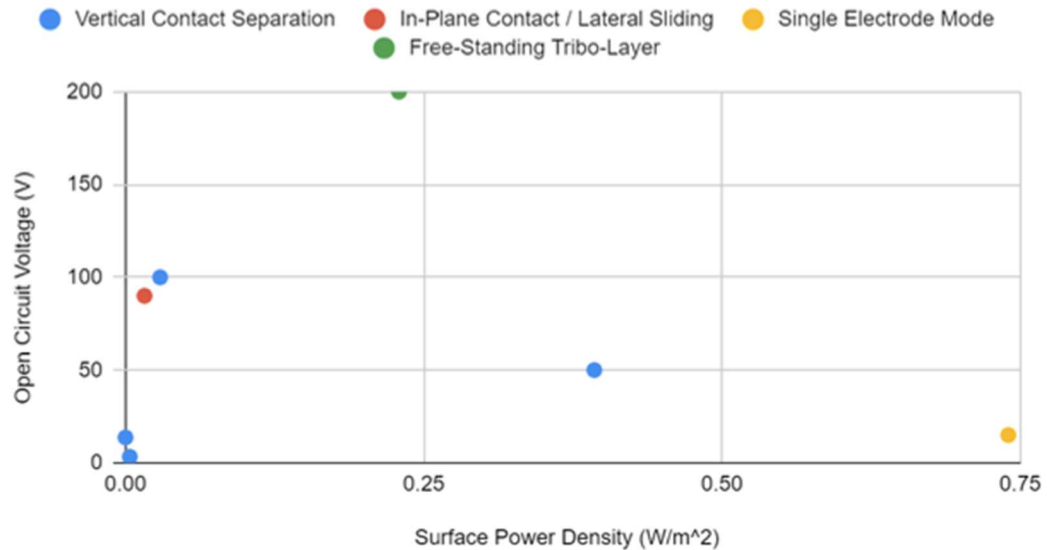


Figure 7: Surface Power Density vs Open Circuit Voltage for the TENG Modes

From prior research, the previous team observed that not every TENG mode was compatible with every design mechanism ^[27]. The team then determined the compatibility and constructed Figure 8. The notes refer to different challenges that would have been faced if those configurations were used.

DESIGN MECHANISM & TENG MODE COMPATIBILITY		TENG CONTACT MODE			
		Vertical Contact-Separation (VCS)	In-Plane Contact / Lateral Sliding (IPC/LS)	Single Electrode (SE)	Freestanding Layer (FSL)
DESIGN MECHANISM	Flexible Electrode	YES	Note 1	YES	Note 1
	Fluttering	YES	YES	Note 2	YES
	Stretchable	YES	Note 3	YES	Note 3
	Stacked (Parallel or Cross)	YES	Note 4	Note 5	Note 4
	Weaved/Fabric-Integrated	YES	Note 6	Note 7	Note 6
Process Compatibility Key		YES	NOT IDEAL	*# Refer to that note	

Figure 8: TENG Modes Compatibility Table

The overall TENG Mode and Mechanism Design Matrix was created and used to figure out the best performing TENG, paired with a mechanism, the relevance in literature, the versatility of applications, surface power density, open circuit voltage, and short circuit current ^[27]. The configurations that were compatible in Figure 8 are ranked using a similar system that was used in the material matrix. A score of 1 is least optimal, 10 is the most, and after scaling the properties, are then weighted based on importance. Relevance in literature provides a greater foundation for the configuration. The configuration with the least number of references was given a 1 while those with the most references were graded a 10. This category was given a weight of 10%. Additionally, the versatility of application was important to observe potential uses according to their sponsor. This category was weighed at 15%. The lowest number of uses in a study was given a 1 while the greatest was given a 10. The previous team determined that surface power density is the best standard metric to

determine power output. Surface power density is the measure of energy output per unit of surface area. The lowest surface power density was graded a 1 while the greatest was graded a 10. This property was given a weight of 35% because of its importance. Another parameter is the open circuit voltage. This evaluates the electrical potential between two terminals with no external load nor current. This means that the open circuit voltage is the maximum voltage possible for a circuit. The team noted that there was not extensive documentation on their circuitry. This property was given a weight of 20%. The lowest open circuit voltage was given a score of 1 while the greatest was given a 10. The short circuit current is the current flowing when the voltage is zero therefore the maximum current. The larger the short circuit current, the more electrically durable the design. The lowest current was given a score of 1 and the largest was given a score of 10. This category was weighed at 20%. All these scored categories are gathered into Figure 9. The team determined the best configurations were the weaved/fabric-integrated vertical contact-separation TENG, the fluttering freestanding layer TENG, and the fluttering vertical contact-separation TENG.

TENG MODE & MECHANISM DESIGN MATRIX	Weighted Scores per Category					Final Weighted Score (1-10)
	Use in Studies	Application Versatility	Surface Power Density	Open Circuit Voltage	Short Circuit Current	
Vertical Contact-Separation						
Flexible Electrode	0.1	0.15	0.36295	0.2	0.2	1.01295
Fluttering	1	1.5	1.414	1.176	0.718	5.808
Stretchable	0.2125	0.825	0	1.084	0.25	2.3715
Stacked (Parallel or Cross)	0.325	0.825	0.35	0	0	1.5
Weaved/Fabric-Integrated	1	0.825	1.7885	1.724	2	7.3375
In-Plane Contact / Lateral Sliding						
Fluttering	0.2125	0.15	1.1865	1.064	0.396	3.009
Single Electrode						
Flexible Electrode	0.1	0.15	0	1.542	1.366	3.158
Stretchable	0.1	0.15	3.0604	0.306	0.296	3.9124
Freestanding Layer						
Fluttering	0.2125	0.15	3.5	2	1.094	6.9565

Figure 9: TENG Mode and Design Matrix

2.5.3 TENG Selections for Design and Fabrication

In this section, the previous team combines their previous research to detail the considerations surrounding the material selection, fabrication methods, mode selection, and circuitry [27]. They note that the previous matrices were not strictly followed, but were used as a guide to weigh the pros and cons. The team evaluated the potential TENG configurations for both non-airdrop (impact) and aerial (wind) delivery applications.

For the impact testing, they concluded the most reasonable choice for the mode was the vertical contact method [27]. The vertical contact method was commonly used in literature, had a wide range of voltage to current relations, and appeared the most in the top three designs. The previous team concluded that potential applications for this type of TENG include soldier clothes, boots, and rucks. Their design configuration is pictured in Figure 10. For the wind testing, the team selected the single electrode mode. They were originally between either single electrode or the freestanding layer modes but chose single electron mode due to time constraint. The team also did not have access to equipment to make flexible and thin electrodes to allow the fluttering motion in the wind, so the team decided to have the fixed electrode on one side and the triboelectric material without the electrode on the other side. This configuration is pictured in Figure 10.

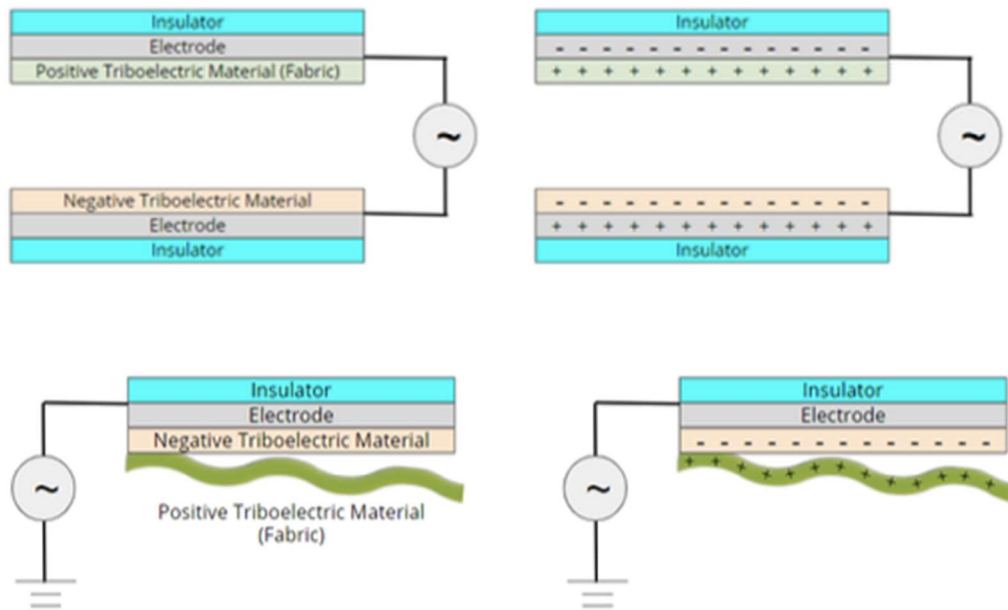


Figure 10: Impact and Wind Testing Fabrication Setup

The previous group also had discussions about the positive triboelectric materials, negative triboelectric materials, the electrode selections, and some of the fabrication methods [27]. In Figure 11, the team outlines the samples they received from DEVCOM, along with their specifications. Prior to being used, the team tested their ability to be heat treated as the curing process of the TENGs required higher temperatures. The fabrics were heat set to stabilize them and prevent shrinkage. Then the team evaluated if the coatings and the fabrics could withstand 100 degrees Celsius. After testing the fabrics and coatings, curling was found to be an issue but could be avoided with weights. The choices for the negative triboelectric materials were PTFE or PDMS. During the grading, rayon and PTFE scored the highest but the team determined that the elastic component of rayon would not have worked well with the team’s existing materials. PDMS was also presented as an option because the team is also using PDMS-Ag electrode paste and it scored well. PDMS also adheres to surfaces well while PTFE is often used in non-stick pans, possibly presenting issues in adhesion.

Fabric Sample	Application	Cloth Spec	Cloth Description	Weight (oz/sq yd)	Construction	Yarn Denier	Fiber Type	Expected Fiber Affinity	Coating	Equipment
FS-1	Shelter	USIFI PRF 44103	Class 1, Grade A - Tan/Gray	12.0	Plain	NA	Coated PET	-40 nC/J	Blackout & Flame Resistant	Shelter roof and sidewalls
FS-2	Shelter	MIL PRF 44103	Class 1, Grade B - Green/White	16.0	Plain	NA	Coated PET	-40 nC/J	Blackout & Flame Resistant	Shelter roof and sidewalls
FS-3	Clothing	MIL DTL 44436	Type I, Class 8 - Universal Camo Printed	7.0	Rip Stop	Plied	50/50% Nylon/Cotton	30nC/J, 5nC/J	Wrinkle Free Finish	Army Combat Uniform, Trouser and Coat
FS-4	Clothing	MIL DTL 32439	Type III, Class 3, 500 denier	8.0	Plain	500	100% Nylon	30nC/J	Water repellent & Back Coated	Improved Outer Tactical Vest (IOTV) GEN IV
FS-5	Air Drop	PIA C 5646	NA	4.5	Plain	Plied	100% Cotton	5nC/J	NA	Parachute components: Deployment Sleeve, Bridle and static line buffer.
FS-6	Air Drop	PIA C 44378	Type IV, 0.5-3.0 cfm, calendared, coated	1.2	Rip Stop	NA	100% Nylon	30nC/J	Fluorocarbon	Reserve and main parachute canopy cloth
FS-7	Air Drop	PIA C 44378	Type VI, 0.5-3.0 cfm, calendared, coated	1.5	Rip Stop	NA	100% Nylon	30nC/J	Fluorocarbon	Reserve parachute canopy cloth
FS-8	Air Drop	MIL DTL 32439	Type I, Class 3, Solid Shades, water repellent, back coated	12.0	Plain	1000	100% Nylon	30nC/J	Fluorocarbon & Polyurethane	Parachute containers (pack trays)
FS-9	Air Drop	PIA C 3953	Class III	18.5	Basket	1000	100% Nylon	30nC/J	Melamine Resin	Parachute containers (pack trays)

Figure 11: DEVCOM Fabric Samples

The team also needed to discuss the electrode and wiring selection for the TENGs. The highest scoring electrodes were stainless steel, nickel, and aluminum ^[27]. The team wanted to figure out a way to use the electrode in a flexible manner that would adhere to a wire. They determined that a conductive ink or a paste could accomplish both constraints. They decided that the ink would be too time consuming so they determined that a conductive paste should be used. The elastomer PDMS was used as a base material, and it was combined with silver powder to create PDMS-Ag. Due to the high price of silver, copper was used as a substitute for larger batches of TENGs. When choosing wire, the team needed to choose between an insulated wire or conductive thread. Insulated threads are more conductive and rigid. When accompanied by paste, insulated wires are prone to flexing that causes the wire to stiffen and dislodge. The conductive thread is lower in conductivity but was more conducive to their research application. Thus, the group chose to use conductive threads. They specifically used the 3-ply stainless steel thread from Adafruit.

The previous team investigated the problems with conventional bridge rectification ^[27]. The conventional bridge rectification has voltage losses that make TENG performance inefficient. The team used Texas Instruments smart bypass diodes that have a loss of 0.3 volts versus the traditional 0.6 volts. To achieve a quasi-DC waveform output, a capacitor was needed in parallel to the external load. An issue that arose was the need for both positive and negative connectivity. This problem can easily be fixed in impact testing but becomes difficult in fluttering testing because it is not bonded to the electrodes. They did not test methods to rectify this issue due to lack of time.

2.5.4 TENG Performance Evaluations

To properly evaluate the fabricated TENGs and their potential applications, impact and wind testing methods were developed ^[27]. Both of these tests involve the use of an oscilloscope to measure and record data. Before the TENGs were tested, the oscilloscope was used to evaluate the bridge rectifier. The team focused on the potential of the DEVCOM textiles rather than circuit building.

Impact testing evaluated the maximum performance of the DEVCOM materials by assessing the forces on a TENG through the use of the contraption in Figure 12. They had four analysis goals for their test:

1. *To equitably compare the performance of configurations with different insulators, electrodes, triboelectric materials, and the DEVCOM fabric samples.*
2. *To establish the relationship between voltage output, variable materials, and variable force where the voltage output would be the maximum voltage that could be expected from a given configuration.*
3. *To assess other influential parameters such as voltage density, weight, delamination, deformation, and surface defects.*
4. *To draw conclusions about the voltage output results based on experimental and theoretical data relating to relevant material affinities.*

From preliminary testing, the team determined that the height did not influence the TENG performance ^[27]. The testing was done of 2" x 4" TENGs by dropping different sized weights from a height of 6 inches. The weight classes were 0.63 lbs, 1.18 lbs, and 1.79 lbs. The testing apparatus is pictured in Figure 12. The apparatus was manually operated therefore cyclic testing was not an option. During the initial tests, the peak-to-peak voltage was recorded and plotted but peak-to-peak voltages

proved to be unreliable, so they moved on to absolute value maximum/minimum voltage (max/min voltage).

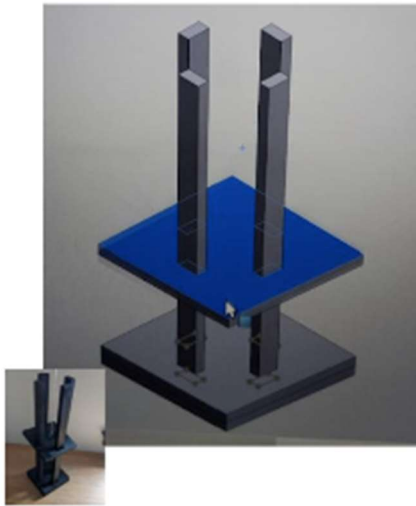


Figure 12: Impact Testing Apparatus

Wind testing was developed to evaluate the performance of TENG prototypes under constant wind speed ^[27]. There were four goals for the wind testing:

1. *To determine the effect of wind on the TENG prototypes to determine if a fluttering mechanism is possible in the single electrode configuration with our given materials*
2. *To determine the best TENG material configuration for wind-specific applications*
3. *To compare DEVCOM fabrics and determine the optimal fabrics.*
4. *To finalize the TENG configuration and create a final wind-based prototype with PDMS-Ag.*

The testing apparatus and the TENG configuration are pictured in Figure 13. A hair dryer was used to keep constant wind speed and that wind speed was measured using a handheld anemometer.

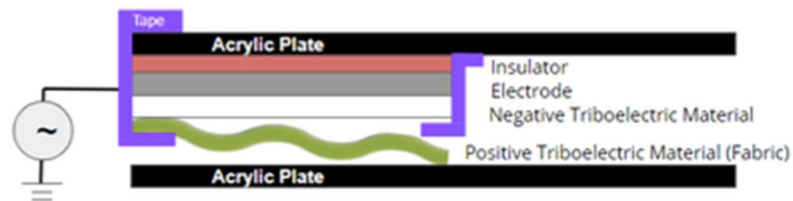
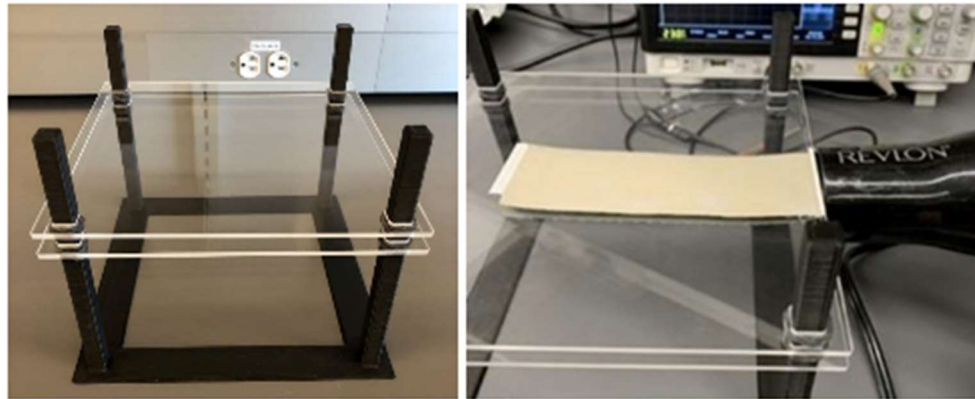


Figure 13: Wind Testing Apparatus

2.6 Fabrication Techniques

Due to TENGs being a relatively new nanotechnology, they are still used for research purposes. There is no standard way to develop a TENG currently but there are common practices that yield successful TENGs. The previous MQP team researched and experimented with the fabrication of their own successful prototypes. The following sections discussing TENG fabrication techniques discuss methods used by last year's Triboelectric Energy MQP team and recently discovered TENG fabrication techniques.

2.6.1 Bonding

There are several common methods used to bond together the layers of electrodes and triboelectric materials. A research group from Georgia Institute of Technology used solely adhesive tape to bond their layers ^[28]. Electrospinning is also a common method for bonding TENG layers. This method creates nanostructures of the triboelectric material on the electrode. The nanostructures increase the surface roughness of the TENG therefore increasing the surface area to create higher voltages ^[29]. Another method of adding triboelectric layers is spray coating. This method requires that the material is made into a liquid that will be sprayed onto a substrate using an airbrush style spray-gun ^[30]. A method that can aid the bonding process without damaging the materials are plasma treatments. Plasma is an ionized gas that is created by putting thermal energy into a gas or applying an electric field to a gas. This process creates a high electric conductivity and high thermal energy ^[31]. Plasma can be used for surface cleaning and sterilization. The plasma causes the wettability and the adhesion of materials to improve temporarily ^[32]. The changes should last long enough to apply other materials on them, potentially aiding in the entire bonding process.

2.6.2 Surface Modifications

The basic principle of a TENG is the contact and separation of two materials that creates a charge. This charge is largely based on the contact area of the materials. To improve the charge, modifications can be made to the surfaces of these materials.

Physical Modifications

A common physical modification is creating surface roughness to increase the surface area. A few ways to create this surface roughness are plasma etching, lithographic techniques, and casting [33]. Plasma etching, also known as dry etching, is a technique where plasma or etching gases are used to remove the substrate material [34]. The lithographic techniques involve depositing a photoresist layer onto a substrate before stripping and etching the layer to create a pattern to increase surface roughness.

Chemical Modifications

Another method of altering the material layers to improve performance is chemical functionalization. This method results in higher charge densities, durability, stability, or self-cleaning properties [35]. The charge density is what improves the voltage readings from the TENGs. Chemical functionalization introduces halogens through chemical adsorptions of surfactants on the surface. Halogens are the most electronegative groups so introducing them to the TENG enhances the tendency to gain electrons. The halogens are typically used with carbon-based materials because they are non-homopolymerizable. Chemical treatments can also be used to increase the charge density. Some of these treatments include ion injection, radiation treatment, and a grafting reaction through plasma. Ion injection is done with either ionized air injection or high voltage corona discharge polarization [35]. Introducing the ions across the surface is shown to increase the charge density and an increase of power. Radiation treatment done in this study gave PDMS a UV-ozone (UVO) or NaOH + UVO treatment [35]. This method controllably changes the chemical structure of the material and can be given to a wider variety of materials compared to the ion injection treatment. The plasma treatment exposes the PDMS surface to Arc plasma to oxidize the surface [35]. The plasma increases surface roughness to then increase charge density.

2.6.3 Methods of Assembly

The general method of developing a TENG is to use methods discussed above to connect the created friction layer and the electrode materials. This connection can happen in various ways, as discussed above, as long as the method does not cause interference with the contact mode.

The electrospinning assembly technique is used to create the nanofiber layer for creating a contact TENG. The nanofiber membrane is attached to the bottom electrode material using Kapton tape, as seen in Figure 14. Kapton tape is also a triboelectric material which creates some interference with the nanofiber's contact to the top electrode material ultimately hindering the current produced from the TENG pair [35].



Figure 14: Nanofiber Membrane Attached at an Electrode using Kapton Tape

Another technique used for TENG assembly is spray coating. This technique uses a liquid solution created from silk to spray onto the PET layer. This coated layer is then placed between two electrode material layers and secured with elastic straps. The straps create a curve in the layers which helps produce the space needed for the contact TENG [37].

2.6.4 Previous Triboelectric Team's Fabrication Techniques

This section will describe the various fabrication and assembly techniques used by the 2020-2021 Triboelectric Energy Generation team. The previous team had three types of TENGs they fabricated: Impact, STEP, and wind TENG [27]. They tested fabric samples provided by DEVCOM for their impact and wind testing. Following this testing they created a STEP prototype utilizing their best performing TENG and electrode. Figure 15 lists the fabrics provided by DEVCOM and their qualities.

Fabric Sample	Application	Cloth Spec	Cloth Description	Weight (oz/sq yd)	Construction	Yarn Denier	Fiber Type	Expected Fiber Affinity	Coating	Equipment
FS-1	Shelter	USFI PRF 44103	Class 1, Grade A - Tan/Gray	12.0	Plain	NA	Coated PET	-40 nC/I	Blackout & Flame Resistant	Shelter roof and sidewalls
FS-2	Shelter	MIL PRF 44103	Class 1, Grade B - Green/White	16.0	Plain	NA	Coated PET	-40 nC/I	Blackout & Flame Resistant	Shelter roof and sidewalls
FS-3	Clothing	MIL DTL 44436	Type I, Class B - Universal Camo Printed	7.0	Rip Stop	Plied	50/50% Nylon/Cotton	30nC/I, 5nC/I	Wrinkle Free Finish	Army Combat Uniform, Trouser and Coat
FS-4	Clothing	MIL DTL 32439	Type III, Class 3, 500 denier	8.0	Plain	500	100% Nylon	30nC/I	Water repellent & Back Coated	Improved Outer Tactical Vest (IOTV) GEN IV
FS-5	Air Drop	PIA C 5646	NA	4.5	Plain	Plied	100% Cotton	5nC/I	NA	Parachute components: Deployment Sleeve, Bridle and static line buffer
FS-6	Air Drop	PIA C 44378	Type IV, 0.5-3.0 cfm, calendared, coated	1.2	Rip Stop	NA	100% Nylon	30nC/I	Fluorocarbon	Reserve and main parachute canopy cloth
FS-7	Air Drop	PIA C 44378	Type VI, 0.5-3.0 cfm, calendared, coated	1.5	Rip Stop	NA	100% Nylon	30nC/I	Fluorocarbon	Reserve parachute canopy cloth
FS-8	Air Drop	MIL DTL 32439	Type I, Class 3, Solid Shades, water repellent, back coated	12.0	Plain	1000	100% Nylon	30nC/I	Fluorocarbon & Polyurethane	Parachute containers (pack trays)
FS-9	Air Drop	PIA C 3953	Class III	18.5	Basket	1000	100% Nylon	30nC/I	Melamine Resin	Parachute containers (pack trays)

Figure 15: DEVCOM Fabric Samples

Impact: ITP-F

The final prototype for the impact TENG was labeled ITP-F [27]. The ITP-F was fabricated using FS-4 and FS-3 as the triboelectric materials and PDMS-Ag as the electrode. The TENGs were to be 2 inches by 4 inches but the fabric was cut to be 2 inches by 5 inches so that weights could be used during curing of the PDMS-Ag paste to prevent curling. The PDMS-Ag is a paste created using the DOW SYLGARD™ Silicone Elastomer Two Part Kit combined with silver power. After the paste was applied, a three-ply conductive thread was pressed into the paste along the 2-inch side of the TENG.

Then the TENG had to be baked to cure. The final step to creating the TENG was to add an insulator on top of the electrode. After trying a few different methods, the group decided to use an acrylic conformal coating. Both the graphic picturing the layers (Figure 16) and a photo of the actual TENGs are below (Figure 17).

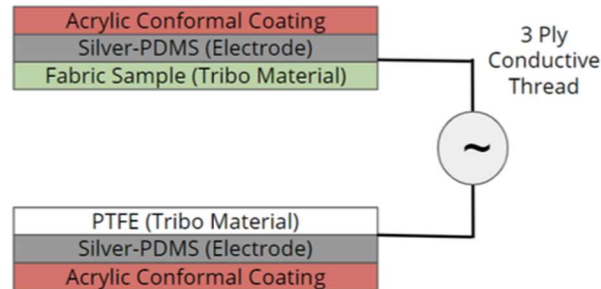


Figure 16: Impact TENG Layers



Figure 17: Photo of Fabricated TENGs

Wind: WTP-F

The final prototype for the wind tested TENG was labeled WTP-F. The material chosen was FS-7 due to its high absolute voltage ^[27]. This final prototype used a PTFE-PDMS-Ag TENG, pictured in Figure 18. The PDMS-Ag paste was used in the same way as described above. Acrylic Conformal coating was also used as the insulator. The actual TENG is pictured below in Figure 19.

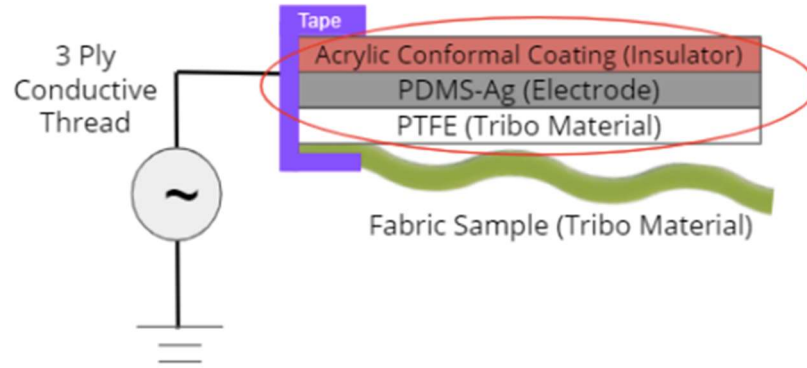


Figure 18: Wind TENG Fabrication Graphic

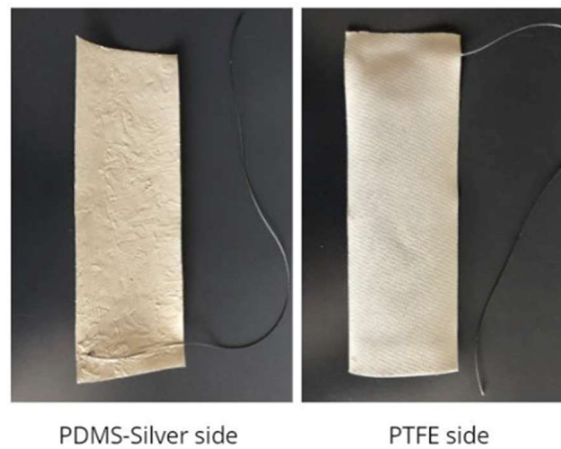


Figure 19: Photo of Wind TENGs

STEP

For this TENG, FS-4-WP and PTFE were the triboelectric materials used. PDMS-Ag was not used due to time and resource constraints, therefore copper tape was used as the electrode ^[27]. The fabrics were cut to fit into a size 9.5 wide (2E) Garmont T8 Bifida Army Boot, as seen in Figure 21. To prevent peeling, the materials were wiped down with isopropyl alcohol and then the copper tape was placed on the non-waterproof side of the TENG (the side with dulled colors) and either side of the PTFE. One inch of a ten-foot-long piece of three-ply conductive thread was placed on each material. The insulator of the STEP TENG was strips of white acrylic tape. Electrical tape was also wrapped around the 10 ft long piece of conductive thread to prevent interference. A photo of the STEP TENG is pictured below in Figure 20.

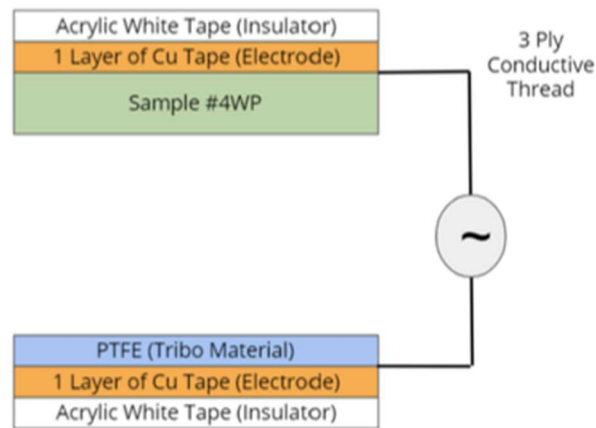


Figure 20: Step Layers



Figure 21: Photo of STEP

2.7 TENG Design

There are numerous design choices that can be made to improve the efficiency and power output of a TENG design. Modifications can be made to existing designs to reduce power decay (between surfaces) and increase vertical space efficiency, while material selection can be used to target specific properties for a given application.

2.7.1 Reducing Power Decay

In typical TENG designs, the surrounding atmosphere can cause the surface charge on the dielectric surfaces to decay. This can reduce the efficiency of TENGs when surface charges deteriorate from the permittivity of the air. To prevent decay, TENGs must be placed in a low permittivity

environment, such as a vacuum. One study tested methods to reduce surface charge decay, including adding ferroelectric polymers to the dielectric surfaces [37]. Ferroelectric polymers are polymers with low permittivity and ferroelectric properties like magnets [38]. An example of a ferroelectric polymer is PVDF, or polyvinylidene fluoride. These polymers allow triboelectric surfaces to more effectively hold onto triboelectric charge long term, without needing a vacuum. Reducing power decay is a good way to improve the power density overall.

2.7.2 Stacking

Another way to increase the power of a given TENG is stacking. Stacking refers to loading TENGs on top of one another, which improves the power per area by using more vertical space. This can be coupled with focus on thinner designs to increase the number of TENG units that can be stacked. A stacked design is excellent for use with rigid contact-separation processes. Seen in Figures 22a and 22e, there are multiple methods by which a stacking design can use vertical-contact separation depending on the energy mode [39].

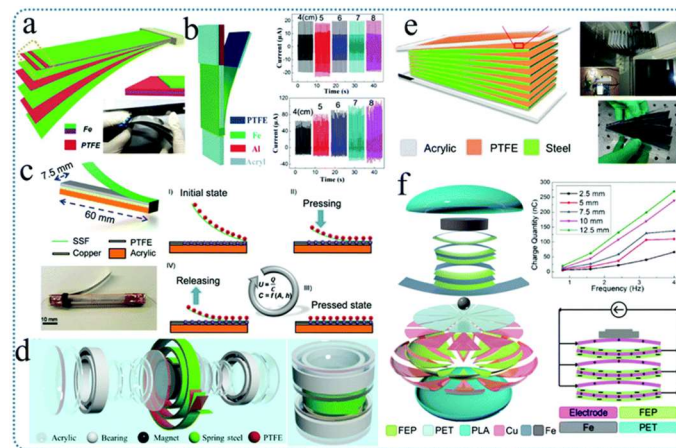


Figure 22: Various Designs using Rigid Metal are Proposed [40]

Stacking can be used in both rigid and flexible design applications. One study analyzed a stacked design for wind power applications. Seen in Figure 23, this design used ultra-thin polymer membrane to create the sub-2nm frame for each piece [40]. The study's authors found that this improved both the power output, and the directionality of the TENG.

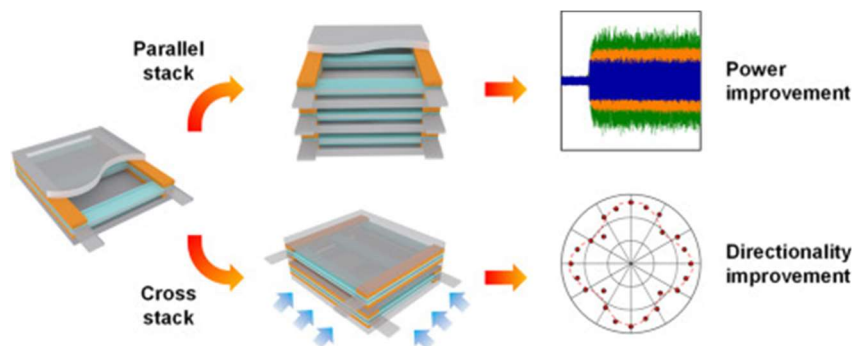


Figure 23: Ultra-thin Stacked Wind Design using A Polymer Membrane

2.7.3 Improving Applications through Materials

Flexible Applications

In fabric-based applications, both flexibility and elasticity must be considered. Many current studies that focus on improving elasticity used conductive yarn, which is coated with silicone rubber. These threads can be woven into textiles or used individually. Individual use allows for more applications of a given thread, but woven patterns like those shown in Figure 24, are more durable and flexible ^[41]. One method that also worked well for individual strands was to coil the strands in a serpentine pattern, increasing the number of strands in a given area.

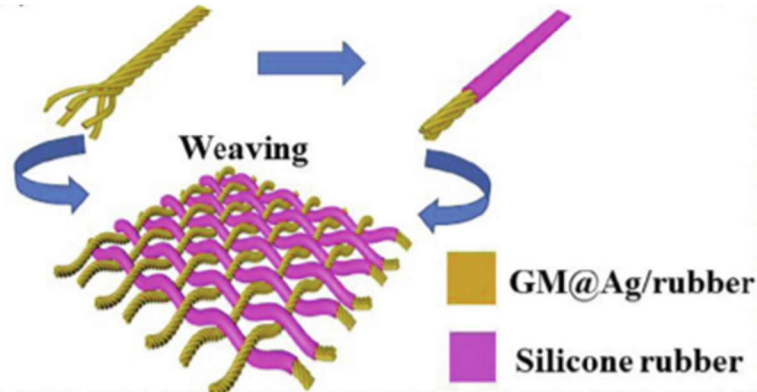


Figure 24: Individual vs Woven Threads using Silicon-Coated Silver Thread [41]

Another consideration for fabric-based applications is the weight of the fabric versus the durability. One study was able to improve the flame-retardant and durability properties of the fabric using a “mixture of EMIM/TFSI, a small amount of lithium salt, and plasticizer” ^[42]. These improved multiple properties of the fabric while partially maintaining flexibility. While it is important for most applications to be durable, the weight increase must also be considered. In applications like gathering wind energy, heavier designs limit the ability of the wind to move the fabric. When selecting a design, consideration must be made to the material’s secondary uses. One study used kevlar and stiffening gel to generate electricity through movement ^[43]. The material was able to generate electricity from movement, and kinetic energy of bullets. Materials that are good triboelectric generators and have other functions are more useful to the customer.

Rigid Applications

To improve durability, many studies used rigid metal as electrodes. Compared to copper, self-supporting elastic electrodes made of metals like spring/stainless steel are highly durable for rigid applications while remaining moderately flexible. Stainless steel shows high fatigue-resistance as a conductor. One study showcased many different designs for rigid metal, shown in Figure 20 ^[44]. Other studies commonly used a leaf spring-type design for vertical-contact separation methods, shown in Figure 25.

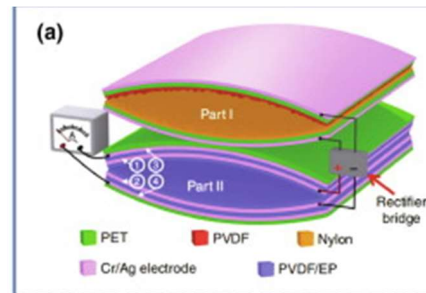


Figure 25: Leaf Spring-Type Design Used in TENG Designs and Studies [45]

2.8 TENG Applications

TENGs are unique among other kinetic energy harvesting methods for their ability to fit a wide variety of applications. Some triboelectric designs are even multi-role, or MR, meaning that they can collect energy from multiple different kinds of mechanical motion. This section will cover the wider application of the four harvesting methods discussed above.

2.8.1 Experimental Applications

This section will identify and analyze TENG designs that have been theorized or constructed and tested. Aspects of these applications can be applied to the intended final prototype our team aimed to produce at the completion of this project.

Wind Energy Harvesting

Triboelectric generators have an ability to harvest kinetic energy from moving air or wind. Traditional wind turbines are limited in their efficiency by Betz's law, which describes a limitation in wind turbines to capture more than 59.3% of the theoretical wind energy ^[46]. Triboelectric energy can have a very high-power density for their overall volume without being limited in their efficiency. Wind harvesting typically falls into four categories: buffeting, vortex shearing, galloping, and fluttering. Many sources focus on fluttering, as it works in most wind velocities and climates. Energy is collected from the oscillation of an object in the wind. As the TENG fabric flutters in the air, parts of the TENG make and lose contact with each other. This facilitates the movement of ions through the planar electrode, leading to energy generation. Some wind TENGs have external features, where the two dielectrics are clearly visible ^[47]. This is known as a double-flag type wind generator. Other wind energy TENGs use smaller scale designs. One recent study used a TENG design that used a copper-Kapton layer surrounded by PTFE surfaces ^[48]. Shown in Figure 26, the central surface oscillates in moving air, transferring charge between the two sides to generate electricity. The study showed this design has a high power density of 15kW/m^3 . The planned use in that study for this was in a breathing mask. Moving air-based TENGs have applications in large fabric objects, such as parachutes or tents, or smaller applications, like the output of a gas mask.

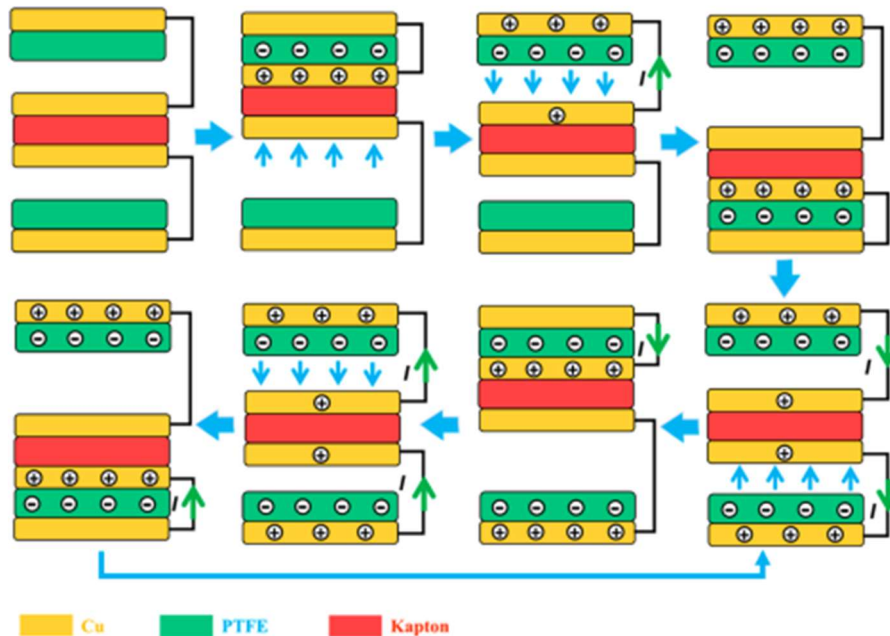


Figure 26: Diagram of the Working Model for the Thin Electrode Wind Application

Rainfall Harvesting

Another effective method of harvesting energy from the natural environment is rainfall or mist harvesting. In one study, a TENG module was completed via a solid-liquid connection, where the water droplets that form on the surface (from condensation or rainfall) share ions with the dielectric layer. The study's design, which had a surface area of $30 \times 20 \text{ mm}^2$, had a peak output of 9.5 V at 250 nA (2.37 microWatts) [49]. This could be used in conjunction with other designs to collect additional energy from the environment.

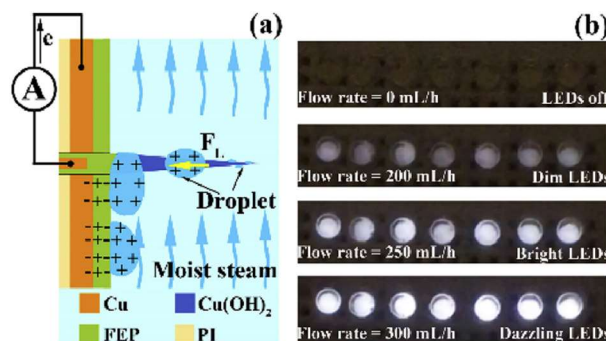


Figure 27: Micro-Scale Diagram of Water Droplet Interaction

Ocean-Based Harvesting

Multiple papers studied how TENGs could collect energy from ocean waves. One design, which uses technology known as a duck wave harvester, generates triboelectric energy as dielectric balls roll over a dielectric surface [50]. The planar electrode, which captures the energy, is located on the inside of

the device. Shown in Figure 28, the balls shift in the oscillation of the waves, they repeatedly separate and contact different areas, generating electricity. This could have an application in generating electricity on life rafts, either in the Army or in sister services, for lights or emergency communications.

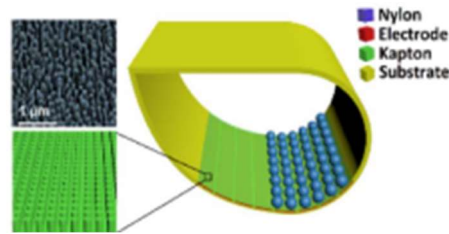


Figure 28: Duck Wave Harvester Design using Nylon Balls as a Dielectric

Rotational TENGs

Rotational TENGs utilize a variety of methods to turn rotational kinetic energy into usable electricity. One study, which utilized a ratchet-like design, had good results generating electricity from repeated contact between ABS and PTFE dielectric layers, which generated charge through the copper and steel planar electrodes ^[51]. This design was able to generate 37 mW at 60 RPM and provided a stable power source free of variability.

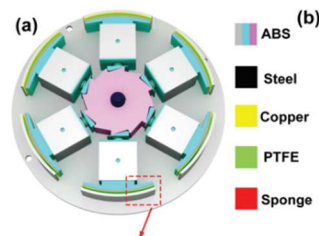


Figure 29: Ratcheting Wheel Design for a Rotational TENG

Another study, which used water as a dielectric in a rotating barrel-like design, was able to generate electricity as the barrel was turned. The water acted as a dielectric between PTFE and acrylic, with aluminum acting as the energy-collecting electrode. This design was able to generate 27.2 volts at 3.84 microamps, for a power output of 0.1044 milliwatts ^[52]. The study explains that liquid-solid contact TENGs are preferable, given they are “less likely to be affected by humidity and be damaged by friction between dielectrics...the biggest obstacle to be solved for sustainable TENG operation”. Liquid-solid contact approaches do not have to be limited to rotary motion, and we could utilize the effect in other designs.

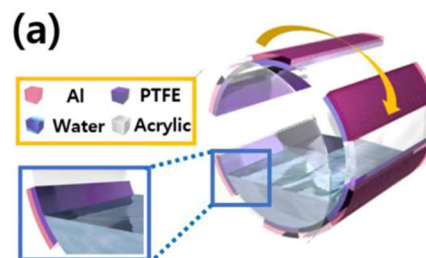


Figure 30: Water-Based Rotary Design using Typical Dielectric Materials

One unique design used multiple phases to generate power. The researchers created five distinct phases within the cycle as the different layers contact each other. At 920 RPM, the design was able to

generate 380 volts at 3.6 milliamps per square meter ^[53]. Having distinct phases in the device improved the stability of the output.

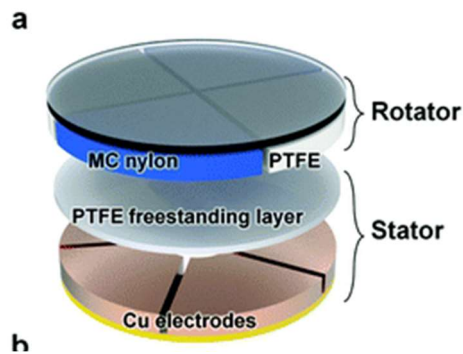


Figure 31: Rotating TENG Design

Rotational energy TENG designs can be used in a variety of roles. Rotary energy collection could act as an efficient generator for larger designs such as traditional wind turbines, as additional energy harvesters for wheels on transportation vehicles, or as specialized designs for capturing rotational kinetic energy from joints.

2.9 Flexible Printed Circuit Boards

Flexible printed circuit boards (FPCBs) are becoming more common in electrical system designs. Unlike rigid printed circuit boards (PCBs) they can be applied to small scale dynamic systems. Through the fabrication process of FPCBs the interconnecting circuit components are printed onto a thin polymer film. Using the word “printed” when mentioning FPCBs is misleading as complex processes such as photoimaging and laser imaging are the methods used to define the circuit pattern on the thin film ^[54]. With proper implementation and protection of flexible circuits, the feasibility of TENG designs that can be used as mobile devices increases.

2.9.1 Common Materials Found in FPCBs

When fabricating FPCBs, materials are selected for the thin film dielectric the circuit is printed onto and for the circuit pattern interconnecting all circuit components. A material’s chemical, mechanical, and electrical properties help manufacturers identify the most suitable material to use for their designed FPCBs ^[55]. Modern technology allows for a large range of materials that can be utilized as the dielectric thin film. These films can range in between 0.0005” to 0.01” in thickness ^[55]. The two common materials used for this component of the FPCB are polyester and polyimide ^[55]. Glass epoxy polymers have also recently been utilized for these applications ^[55]. These common material choices can endure tensile loads from about 20ksi to 100ksi ^[55]. Figure 32 below shows a polyamide dielectric film-based FPCB.

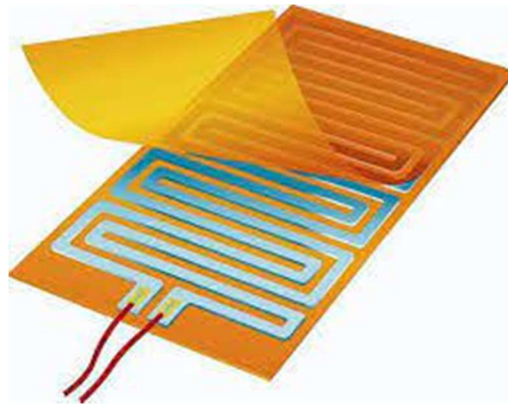


Figure 32: Polyimide Dielectric Film FPCB

Figure 32 shows the flexible advantage these dielectric polymers provide for circuit applications. The maze-like path seen in Figure 32 represents the circuit pattern that interconnects the circuit's housed components. Figure 32 shows a layer being applied to the top of the circuitry path. An adhesive layer is applied between the conductive circuitry path and dielectric film to make this layering possible. This can serve as a protective agent for the internal circuit as it can prevent the conductive materials from exposure to moisture or other harmful external agents that could cause corrosion or deterioration ^[56].

The leading conductive material used for FPCBs is copper foil. Alloys such as aluminum, nickel, gold, and silver also are used for this application ^[57]. The surface finish on the printed conductive material should be smooth in order to optimize the circuit's performance. Recent breakthroughs in additive manufacturing processes have allowed for silver pastes to be used for a FPCBs conductive wiring material. Often described as an ink-like substance, the silver paste meets the recent demands for a more flexible conductive material ^[58]. All components found within FPCBs are adhered together using epoxy or acrylic based adhesives commonly. Since the properties of the materials used in FPCBs are held to a strict standard, only the most precise fabrication processes can be used to produce these flexible circuits.

2.9.2 Fabrication Processes for FPCBs

Flexible printed circuit boards can be produced through two methods: additive and subtractive manufacturing. Subtractive manufacturing of FPCBs are more common due to their cost efficiency and provide a wider range of conductive layer configurations for FPCBs. Photo imaging is a common subtractive method used to define the circuitry patterns on FPCBs. Laser direct imaging is a popular photo imaging process. In this process, a high-intensity focused laser beam is controlled by a computer interface to define the circuit pattern onto the circuit board. CAM files are preloaded onto the computer interface which allows the laser to define circuit paths at a precise level. Figure 33 shows the layers used when manufacturing a copper circuit pattern for a circuit board.

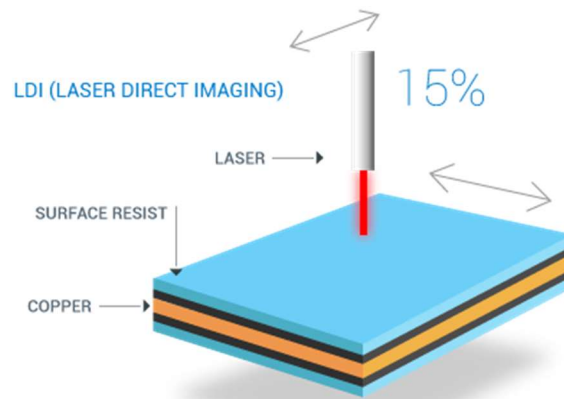


Figure 33: Laser Direct Imaging a Copper Circuit Path

The CAM program uploaded to the CNC machine operating the precise laser identifies the negative areas of the copper. In other words, it identifies what parts to cut out of the layers to create the desired circuit path. This process also cuts insert holes for inserting electrical components on the dielectric films used for FPCBs.

Additive manufacturing methods for circuit paths are driven through 3-D printing techniques. Fused-based deposition and direct ink writing through CNC 3-D printing machines have allowed manufacturers to produce flexible circuit boards at a rapid rate [59]. Fused-based deposition processes deposit melted material layer-by-layer and is commonly used outside of circuit path deposition [60]. However, direct ink writing (DIW) is the most frequently practiced additive manufacturing technique for printed circuit boards. In this process, droplet based eject the conductive materials onto the dielectric film [58]. The material is deposited to create the circuit path. Figure 34 shows the main components of an apparatus used for DIW for FPCBs.

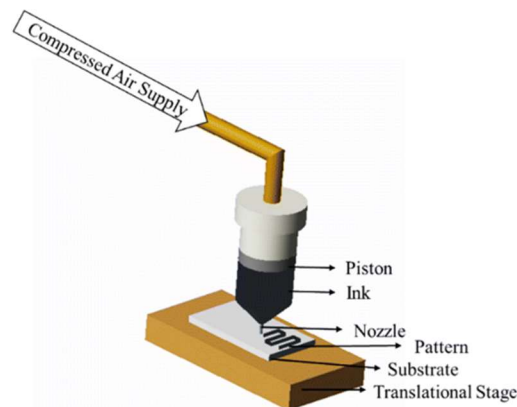


Figure 34: Direct Ink Writing for Electronic Circuits Process

This process can also be actuated through CNC machines to allow precise deposition of materials onto a circuit board. Additive manufacturing techniques such as DIW are advantageous due to their time efficient methods [60]. However, as subtractive manufacturing techniques have been practiced for a longer period the technology used in the processes allow for more precise circuitry path creation [60]. Since printed circuit paths are created on microscopic levels these subtractive manufacturing methods are more commonly practiced.

2.9.3 Voltera V-One PCB Printer

As our team aimed to implement FPCBs into the realization of our TENG design we obtained a Voltera V-One printed circuit board printer. In comparison to previous PCB printers, the V-One sells for about \$4200 which sells for less than previous available PCB printers (<https://www.voltera.io/store/v-one>). Figure 35 below shows an image of the complete V-One set acquired by our team for circuit fabrication.



Figure 35: Voltera V-One PCB Printer

The printer's technical specifications separate it from competing printers. It has a 12V power requirement which allows it to be utilized in a common living space with wall outlets. The solder material provided and compatible with the printer allows it to etch circuits onto traditional rigid and flexible layers. The printer's user interface allows for a computer to connect to the printer, upload gerber files, and then print the circuit designed on the gerber file onto a chosen surface. Additionally, the software programmed into the printer provides step by step instructions to help users successfully print their desired circuits.

When printing a circuit, the printer must calibrate its probe axis similar to a CNC manufacturing machine. The calibration process ensures no overlapping errors or created short circuits. After the calibration is complete the selected conductive ink can then be loaded into the printer. Once the designed circuit is uploaded to the printer via gerber file the conductive paste will be dispensed onto the circuit board surface. Following this step comes the solidification of the paste onto the board. The circuit board being fabricated must be flipped over so the conductive paste side is facing away from the dispensing probe. The printer's surface the paste is resting on will then be heated to 220 degrees Celsius for about half an hour (<https://www.voltera.io/store/v-one>). Once the time is up the nearly completed circuit will be cooled off for another ten to twenty minutes. This quick fabrication process allows for a fast design iteration process to help engineers fully optimize circuits with minimal time constraints.

Along with traditional epoxy or PET films used for PCB and FPCBs the V-One is capable of printing conductive paste onto fabrics. With proper heat and protection treatments circuits printed onto

fabrics can improve the realization of designs in countless fields of science. Take last year's Triboelectric Energy Nanogeneration team's STEP design as an example. They were able to produce an alternating current from a TENG pair implemented into a soldier's boot. However, they were unable to properly integrate a rectification circuit to make use of the produced voltage because of spatial constraints and harsh environmental conditions a soldier's boot will enter. With the implementation of a Voltera V-One printer into such a project, a flexible circuit could be etched onto the boot's fabric and sprayed with epoxy to ensure the design's overall resilience.

2.9.4 Multilayer FPCBs

Recent advancements in fabrication methods and commonly selected materials have allowed FPCB to be printed onto multiple layers stacked on top one another. One of the advantageous qualities of a multilayered FPCB is that it provides the option of circuit implementation into designs with small surface area limits (<https://www.allflexinc.com/multi-layer-flex/>). Although traditional PCBs are also capable of having multilayered schematics they often require more space and reduce the mobility of a design compared to FPCBs. In shorter terms, multilayer FPCBs allow for high density circuit interconnections (<https://www.treepcb.com/multilayer-flexible-circuits/>). Figure 36 below illustrates an example multilayer FPCB.

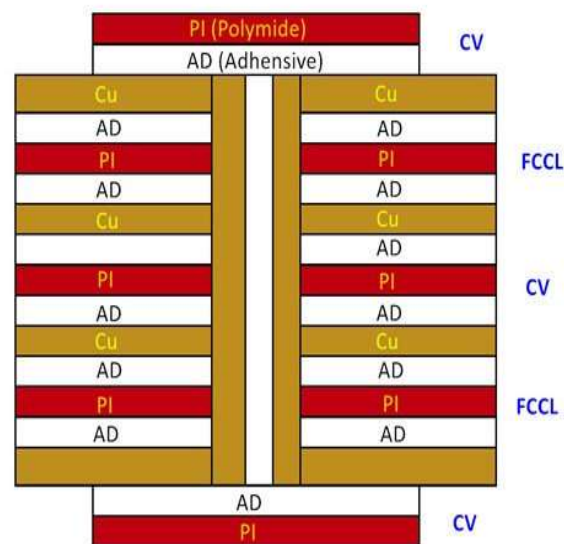


Figure 36: Example Multilayer Flexible Printed Circuit Board

The multilayer FPCB shown in Figure 36 above contains common materials utilized for FPCB assembly such as copper and polyamide film. Adhesive is used to compact the layers of the circuit together while also having plated through holes to achieve electrical interconnection between layers. Oftentimes the middle layers of a multilayer circuit consist of the power and ground layers while the remaining layers are utilized for the circuit's intended design. The applications of multilayer circuits have expanded into biomedical, computer, military and much more fields of engineering and science in the past decade. As the fabrication process becomes more automated and affordable through the innovation of DIW and LDI machines, FPCB usage has normalized and helped compact complex designs.

2.9.5 Disadvantages of FPCBs

Though flexible printed circuit boards open the door for potential electronic applications, they are not perfect. Certain limitations and weaknesses in the overall structures of FPCBs creates disadvantages that come along with FPCB implementation. Since these circuit boards require tight tolerancing and strict properties the fabrication processes of FPCBs can become complex and costly in regard to time and money. These circuit boards can be damaged or destroyed if subject to a wide variety of conditions. If one of the materials yield strengths is exceeded when a FPCB is under a load the whole system will experience failure ^[61]. Exposure to high or low temperatures can cause misalignment in circuit paths and circuit component failures ^[61]. Though fabricating FPCBs has progressively become easier over time, there are few solutions to repair these circuits ^[61]. Oftentimes if a FPCB experiences any damage or deterioration it will be replaced rather than fixed.

2.10 Power Management Module (PMM)

TENGs can produce high voltage, but at low current (~microAmps), low charge density, and high impedance. A Power Management Module (PMM) can be used to enhance energy transfer efficiency from the TENG to the power source as it is a device designed to protect the circuit from damages caused by an overload condition or shorting. An increased current output from a TENG pair would optimize its ability to charge or power a device efficiently. These modules are connected to TENGs and the energy source as illustrated in Figure 37. PMMs work to either boost the TENG performance by extracting more charge or transforming the high-voltage low-current of the TENG into low-voltage high-current depending on the designed output of the circuit ^[62]. This section will identify different PMMs that have plausible applications for TENG rectification.

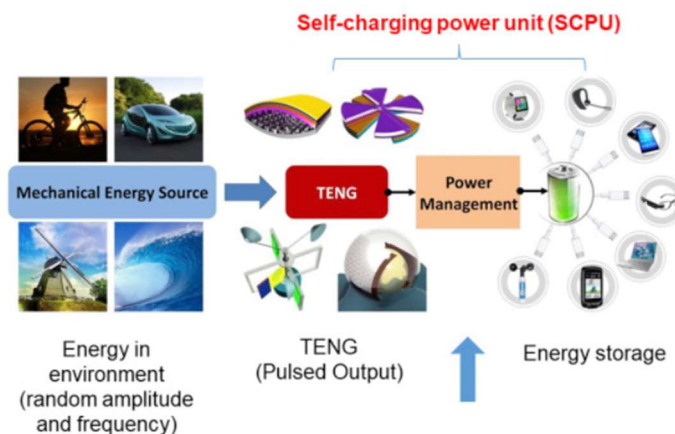


Figure 37: Steps for Charging TENGs

The first Power Management Module contains a switch in parallel with an external load (device being powered or charged). The circuit is designed to produce instantaneous short-circuit conditions. A graph charting the voltage relative to the charge of this PMM is shown in Figure 38. The switch is opened at the minimum and maximum voltage peaks. Due to this, the current flowing through the load and short circuit become equal. In theory the resistance across the load increases to an extremely high value causing the load to harvest four times the amount of energy supplied by the TENG. The short circuit charge is the voltage difference between the conductors that are supplying power to the circuit. Figure 38 shows how the short circuit current and transfer charges equal zero during the cyclic motion

of the TENG [63]. The four steps in the voltage cycle trend include the contact and separation of the TENG. The steps shown in Figure 38 are as followed:

- Step 1 - TENG is at minimum displacement and the series is open.
- Step 2 - TENG is opening and the series is closed.
- Step 3 - TENG is at minimum displacement and the series is open.
- Step 4 - TENG is closing and the series is closed.

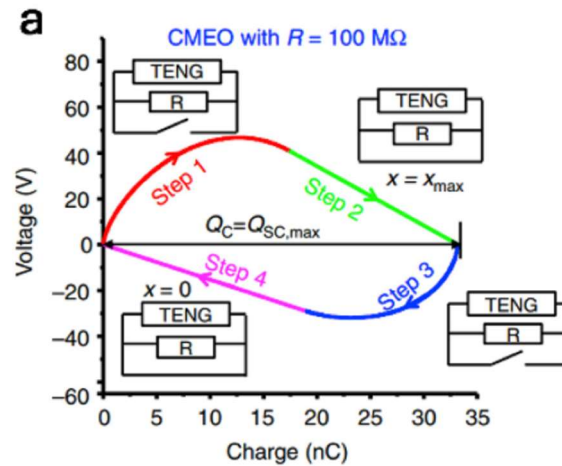


Figure 38: TENG with Parallel Switch

This cyclic motion and steps are also used for a series switch. Maximized energy output for smaller resistances can be obtained through series switches. Figure 39 graphs the relationship of charges and voltage for this configuration of PMM. When connected, the series switch discharges stored energy out of the capacitor in the TENG, making the current appear similar to a discharge curve as the instantaneous output voltage stays constant. Both parallel and series switches require a trigger switch. A trigger switch is activated from an external circuit component drawing current. Certain TENGs are created with mechanical switches, which increases the fabrication cost of the unit. There are numerous types of electromechanical switches applicable for TENG circuit designs. Self-powered trigger switches can be set up and usually include an electrostatic vibrator switch or an air discharge switch. Another switch commonly used is the potential voltage difference. This switch works through a predetermined threshold voltage. These types of switches need to come pre-designed for specific TENGs [62].

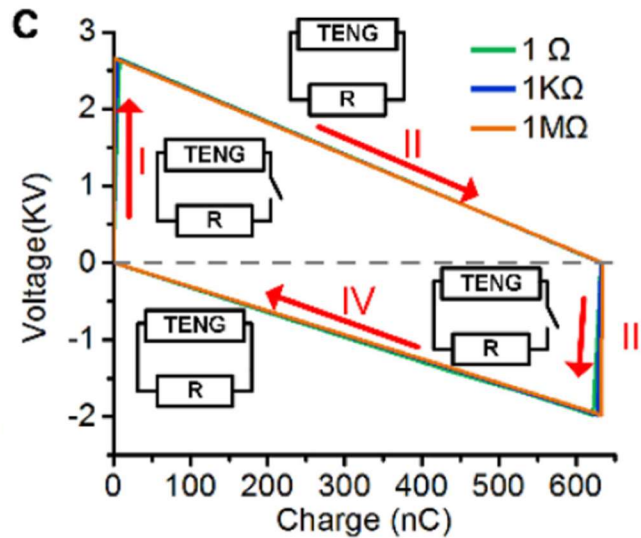


Figure 39: TENG with Series Switch

Another Power Management Module employs a parallel switch to a full-wave rectifier. Most energy of a TENG is rectified by a full-wave rectifier and then stored in a capacitor or battery. Current flow across the load will never reach zero or its highest transfer charge because of the limited efficiency of the rectifier. To prevent a brief voltage drop period a parallel switch can be added with the capacitor. The parallel switch allows the transfer charge to reach zero and maximum transfer charge, therefore improving the energy storage efficiency by up to 50% [64]. The parallel switch is compared to the normal full-wave rectifier in Figure 40. The figure includes both the voltage vs power curves and the positions of the PMM at each step.

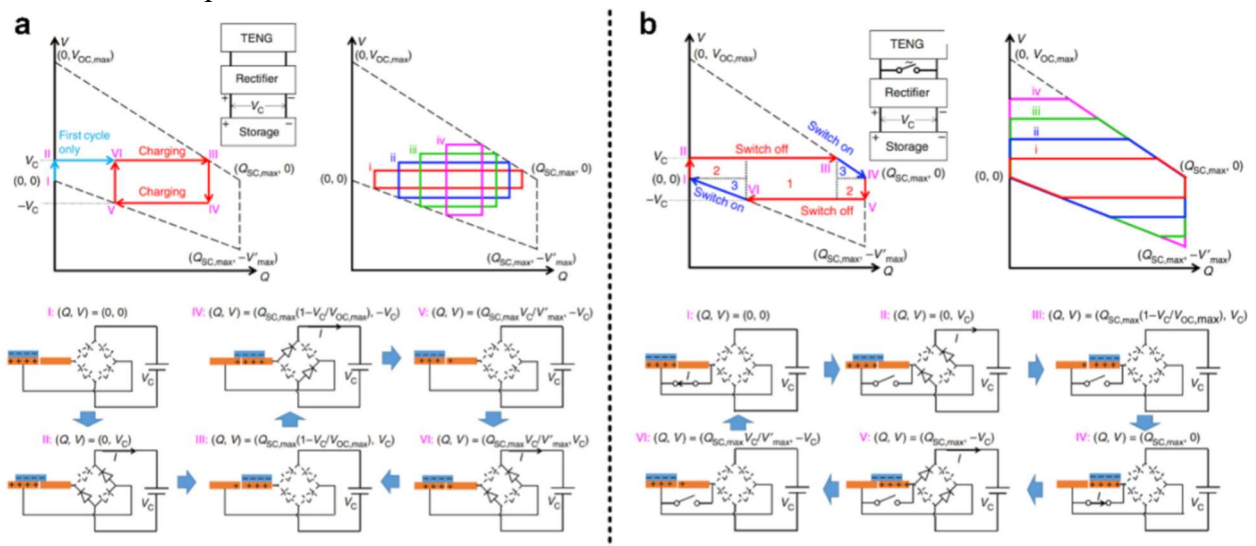


Figure 40: Comparison of Full-Wave Rectifier (Left) to Rectifier with Parallel Switch (Right)

Charge density is an important factor to take into consideration when choosing a TENG design since this property is dependent on air quality. A Power Management Module that contains a charge pump can increase the charge density of the TENG. In an air environment, the maximum charge density is 250 microcm⁻². However, with the charge pump implemented, the charge density can increase to 1020

microcm^{-2} [65]. The structure of the pump is shown in Figure 41 below which illustrates the configuration of the TENG and the output current vs time. The TENG shown in Figure 41 consists of the traditional layer on the outside and a plane-parallel capacitor structure (PPCS). The TENG will charge the PPCS, which will be connected to a full-wave rectifier, creating electrical energy. This increase in air density will increase the transferred charge, thus increasing the output energy in one cycle.

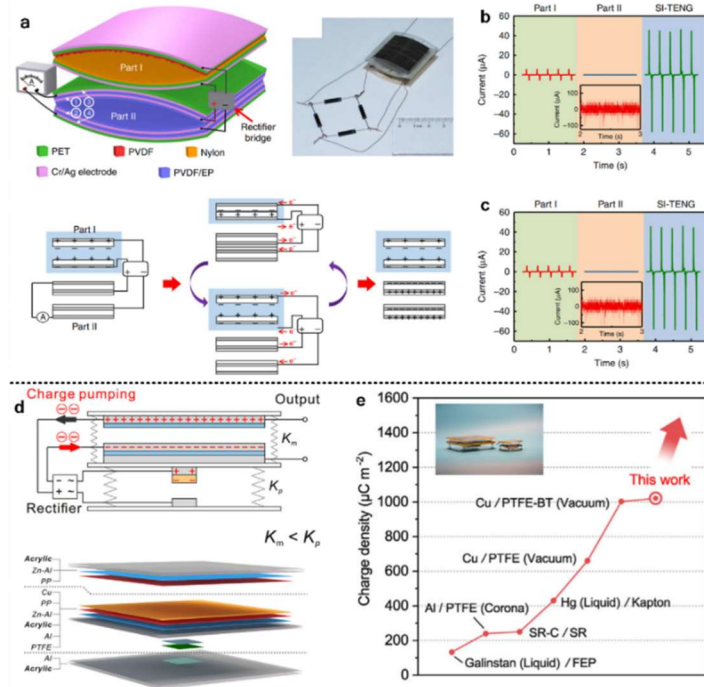


Figure 41: Charge Density PMM

Most of the Power Management Modules are complicated and include multiple components. The Bennet's Doubler Conditioning circuit is a simple diagram (shown in Figure 42). This circuit contains diodes and two reservoir capacitors in which the largest capacitor must be two times larger than the other. Reservoir capacitors help to smooth the raw rectified waveform by charging to the voltage peaks leaving the rectifier. Additionally, the circuit does not require any external controls or mechanical switches to store the energy; all the energy is stored in a reservoir capacitor [62]. In other words, despite the high energy levels this circuit can produce, the reservoir capacitor seen in Figure 39 is capable of storing all of the energy without the circuit having any irregular current flows or voltage drops.

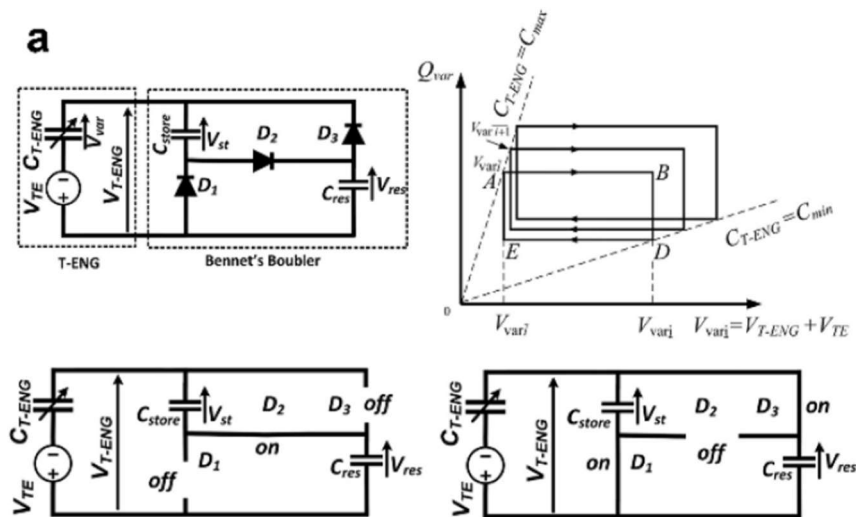


Figure 42: Bennet's Doubler Conditioning Circuit

Depending on the electrical device being powered or charged in a PMM the circuit may need to diminish the voltage produced by a TENG pair. For example, when charging a battery, too much voltage input into the battery may damage the battery or ultimately ruin the battery. To prevent this from happening, a voltage regulator circuit would have to be implemented. One way to reduce the voltage in a TENG is to incorporate inductive transformers to the Power Management Module. Transformers are composed of electrically isolated coils that take the voltage and current running through the first coil and induce an electric and magnetic field (EMF) in the second coil and the coil ratio is an important factor for tuning the voltage. This PMM also includes rectifiers, voltage regulators, and capacitors (illustrated in Figure 43). It also reduces the high voltage of TENG in order to make a direct current. Currently, the inductive transformer has only been proven to work on the rotary-mode TENG. Capacitive transformers also work to lower the voltage by controlling the short pulse at different frequencies. The PMM is made up of an array of switches that can manage different short pulses. The switches are connected in series when charging and parallel during the discharge [66].

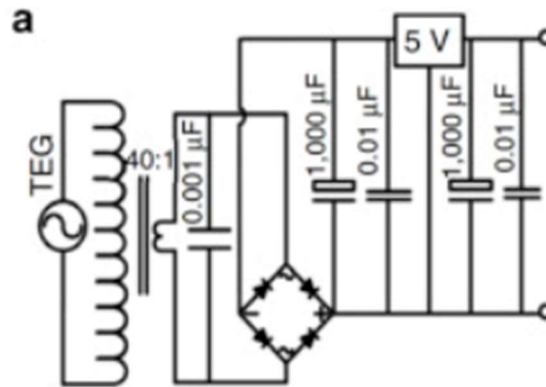


Figure 43: Inductive Transformers

The PMM can also be separated into two power stages to increase efficiency. The first stage is a temporary capacitor that is charged through a bridge rectifier while the second is to transfer the energy from the temporary capacitor to the final energy storage unit. The circuit diagram is shown in Figure 44. The energy cannot be transferred from one capacitor to the next because of the energy loss and therefore, electronic switches are added with a coupled inductor. The power efficiency of this circuit was 59.8% [67].

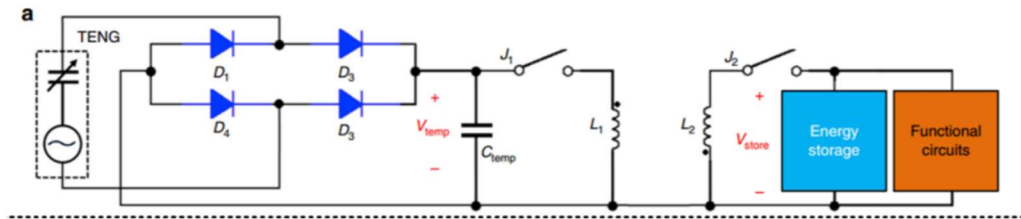


Figure 44: Two-stage PMM

Transformers, transducers, and switches all require energy or current to operate as intended. However, certain Power Management Modules do not rely on these units. One example of this type of PMM is a fractal switched capacitor converter (FSCC). A switched-capacitor converter (SCC) is an electrical component that operates based on a step-up or step-down voltage conversion within a PMM. Step-up functions increase voltage, while step-down decreases the voltage. The SCC uses the step-up and step-down function by switching from series to parallel. A fractal is a geometric shape of which each part has the same character as a whole, therefore, fractal design helps to create a direct current applicable towards electrical devices. The FSCC is formed by placing multiple simple SCC into a similar design. Each fractal has three diodes and two capacitors [68]. The circuit design is pictured in Figure 45. Figure 45 depicts all three steps of the design, initiation, charging in series, and discharging in parallel. FSCC has a high efficiency rating of 94%.

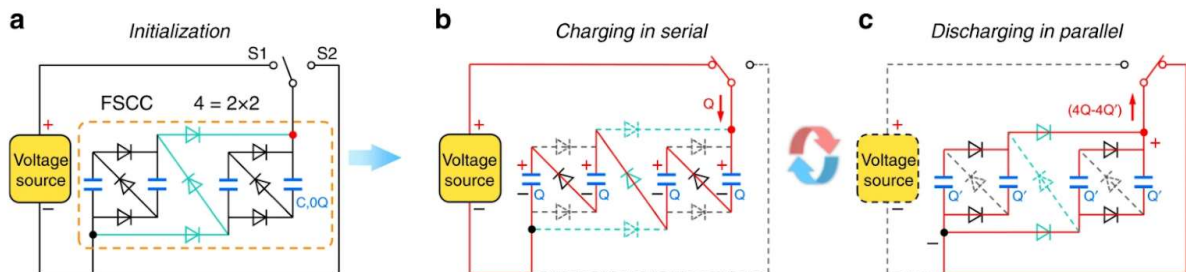


Figure 45: Fractal Switch Capacitor Converter

Chapter 3: Project Scope and Objectives

This chapter explains the scope and overall objectives for this project based on resources, advisor/sponsor expectations, and team goals. Having general goals for this project improved the efficiency of the team's efforts.

In this project, we aimed to develop and evaluate TENG designs implemented within Army footwear equipment. Project focus areas were outlined in order to further understand potential subsystems that produce an optimal TENG design. This year's project was defined by the following objectives:

- Design an automated tester capable of evaluating TENGs performance relative to walking.
 - Design and test circuits capable of rectifying current inputs similar to that of a TENG and supplying power to external devices.
 - Design and evaluate iteration of the TENG design to increase voltage output.
 - Develop separate prototypes modified for different locations in footwear.
 - Construct a final design that optimizes results from previous testing.
-

Chapter 4: Rectification Circuit Design and Evaluation

Out of the rectification circuits described in Section 2.1, Power Management Modules, six circuits were picked for analysis and construction. A table summarizing the pros and cons found in the literary review concerning the individual circuits is shown in Table 3. During the preliminary assessment, the team built the circuits on National Instruments' *Multisim* software. This allowed us to test for effectiveness to analyze the circuits before construction. The first purpose of the software was to test the theoretical feasibility of each circuit. If the circuit failed to work in the simulation, we eliminated that circuit knowing it would not work on breadboards either. After eliminating some circuits, the software helped optimize each circuit's composition prior to assembling and testing. Running these simulations also allowed us to understand the effects of each component within these circuits and specify desired quantities and qualities for these components. We analyzed each circuit under ideal conditions to first understand the general function of each circuit. An ideal power source would produce a consistent current like a DC current. To simulate this, we implemented a high-frequency AC voltage supply within each circuit. A higher frequency within the circuit produces its peak voltages more consistently throughout a time interval than a supply with a lower frequency. The more consistent frequency allows the circuits to produce smoother, constant voltages. Next, the voltage supply was changed to match the 2020-2021 Triboelectric Energy Generation team's results. We choose the results from the top performing TENG pair from the previous group's tests and set their highest voltage as the peak-to-peak voltage for the simulated circuits' power sources. The fabric that performed the best, MIL DTL 32439 (camouflage fabric), produced the highest peak voltage of about 2.3V during the previous team's STEP prototype tests. In the simulation, the voltage used to represent the TENG voltage was an AC power source with a peak voltage of 2.3 volts and a 1 kHz frequency. An AC power source was chosen because the TENG produces both a positive and a negative voltage similar to an AC voltage. A table with the output results of the simulated circuits is shown in Table 3.

Circuit	Pros	Cons	Viable from Preliminary Assessment?
Bennet's Doubler Conditioning Circuit	- Does not need external controls	- A large number of components (comparatively) - Faster discharge rate	Yes
Fractal Switch Capacitor Converter	- Highest researched outputs	- Complex - Requires switches not available - Requires external controls	No
Full Wave Rectifier	- Does not need	- More complex than Self Doubled	Yes

	external controls -The previous team researched this	Rectification Circuit and Half Wave Rectifier	
Half Wave Rectifier	- Simplistic - Does not require external controls	- Only captures positive voltage - Fast discharge rate	Yes
Parallel Switch Circuit	- Simplistic	- Requires external controls - Unable to replicate in multisim	No
Series Switch Circuit	- Simplistic	- Requires external controls - Unable to replicate in multisim	No
Self Double Rectification Circuit	- Simplistic - Does not require external controls	- Only shown through theoretical research	Yes

Table 3: Simulated Circuit Results Summary

4.1 Circuit Schematics and Simulation Results

The following subsections will summarize the designed construction and simulation results for each rectification circuit. As stated before, the top-performing circuits advanced to a breadboard testing and evaluation stage.

4.1.1 Bennet's Doubler Rectification Circuit Schematic and Simulation

The Bennet's Double Conditioning Circuit uses diodes and reservoir capacitors to rectify the input TENG voltage. The breadboard configuration is shown in Figure 46. The diodes rectify the voltage while the capacitors smooth the rectified voltage after it leaves the diodes. Bennet's Doubler does not require external controls or switches to store energy because it is stored in the reservoir capacitors. The Multisim model and the output readings are shown in Figure 47. The readings show that with a peak voltage of 2.3 volts, the circuit can produce 1.611 volts. These results prove that the circuit can rectify the AC current while producing a positive voltage.

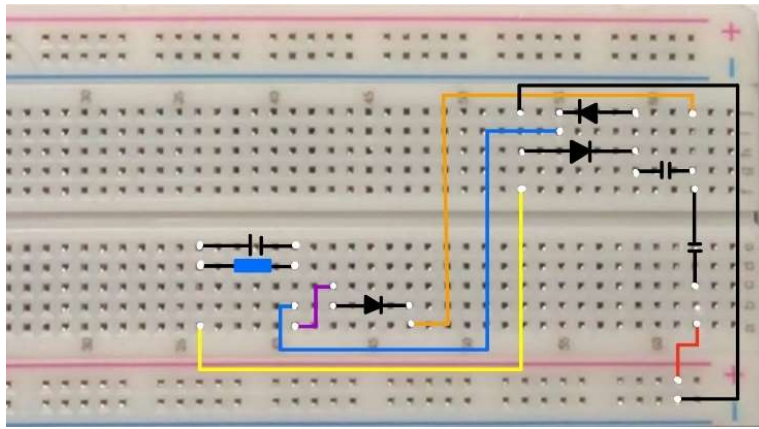


Figure 46: Bennet's Double Conditioning Circuit on Breadboard

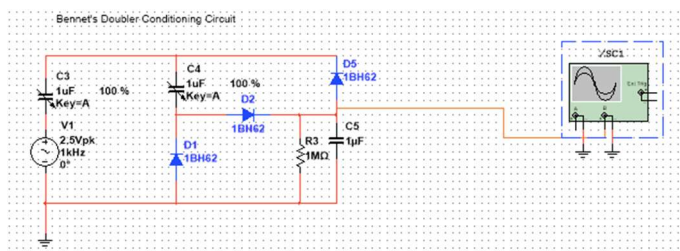
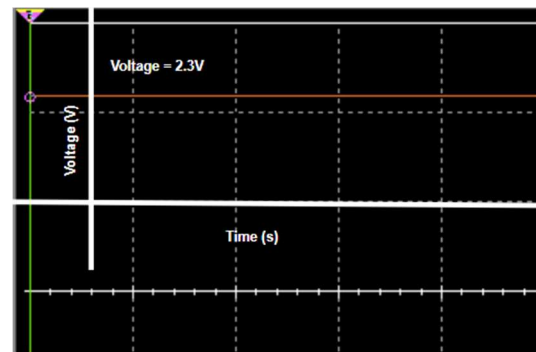


Figure 47: Multisim Circuit and Results of Bennet's Doubler



4.1.2 Fractal Switch Capacitor Converter Schematic and Simulation

The Fractal Switch Capacitor Converter rectifies TENG voltage using multiple switch-capacitor converters (SCC). The SCCs create step-up and step-down conversions in which the voltage is either increased or decreased, respectively. It accomplishes this by switching the circuit from series-to-parallel or parallel-to-series. A breadboard circuit was not built due to the complexity and amount of breadboard space required. The Multisim Model and its output readings are shown in Figure 48. Based on the complexity and the results shown, the team decided not to proceed with this circuit. The simulated results are seen below in Figure 48. The simulated output signal was not ideal as the current still behaved in an alternating current manner.

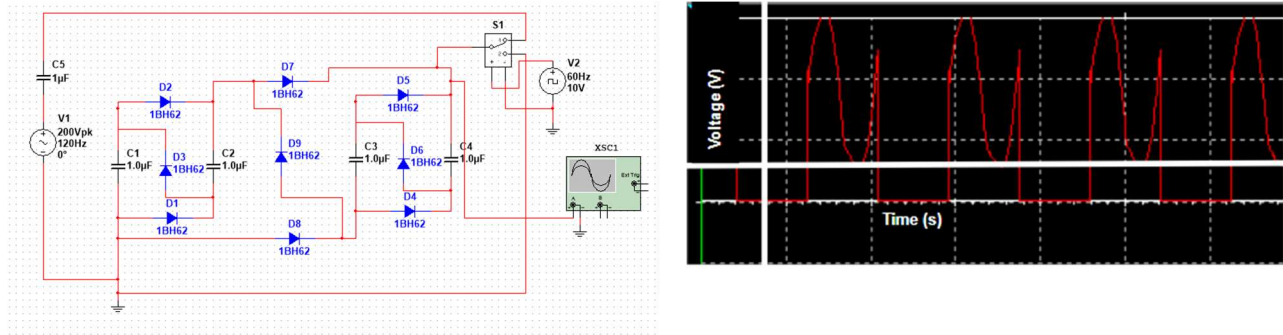


Figure 48: The Multisim Circuit and Results of the Benet's Doubler

4.1.3 Full Wave Rectification Circuit Schematic and Simulation

The Full Wave Rectifier is the circuit that the previous MQP team used to start exploring the circuitry attached to the TENG. The breadboard configuration is shown in Figure 49. The Full Wave Rectifier uses a full bridge rectifier which consists of four diodes and a capacitor. This circuit also does not require any external controls or switches to store energy, as the capacitor stores it. The Multisim model and its output results are shown in Figure 50. In this preliminary assessment, the circuit could produce 2.379 volts with a peak voltage of 2.5 volts. Based on the output results, the team decided to further explore this circuit.

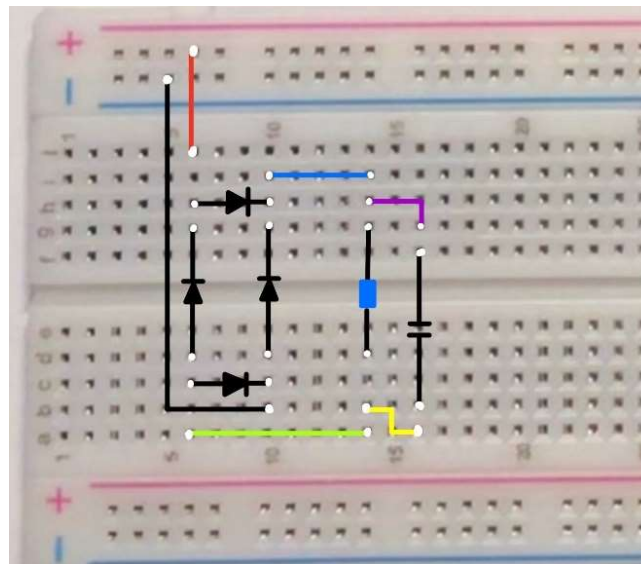


Figure 49: Full Wave Rectifier on a Breadboard

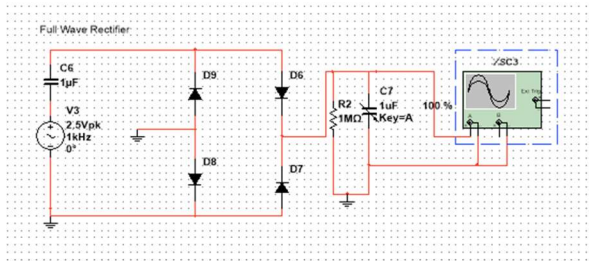
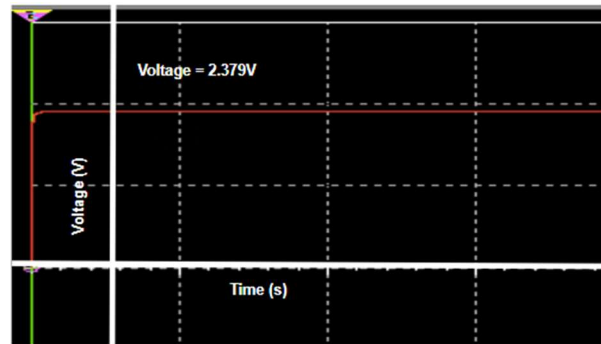


Figure 50: Multisim Model and Results of the Full Wave Rectifier



4.1.4 Half Wave Rectification Circuit Schematic and Simulation

The Half Wave Rectifier is derived from the Full Wave rectifier. The breadboard model is shown in Figure 51. The Half Wave Rectifier uses two diodes and a capacitor to correct the TENG input voltage. The Multisim model and the output results are shown in Figure 52. With a peak input voltage of 2.5 volts, the preliminary results show that it could produce 93.83 millivolts. Even with the low voltage readings, the group decided to continue exploring this circuit.

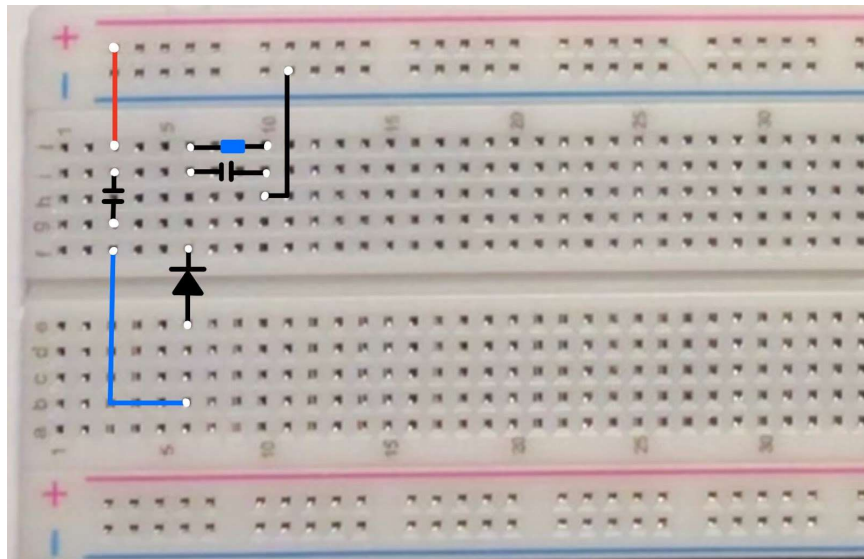


Figure 51: The Half Wave Rectifier on a Breadboard

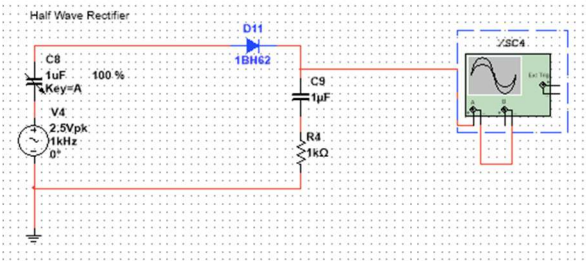
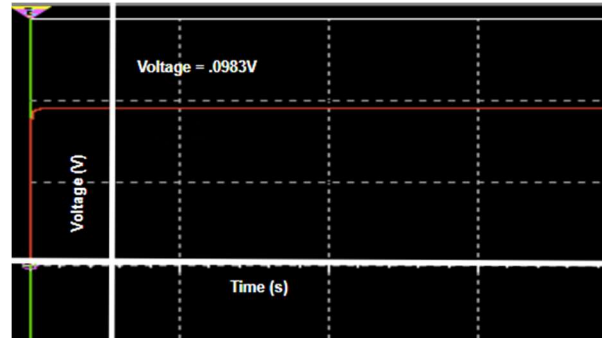


Figure 52: Multisim Model and Results of the Half Wave Rectifier



4.1.5 Parallel Switch Circuit Schematic and Simulation

The Parallel Switch Circuit is constructed using switches in parallel to rectify the input TENG voltage. The breadboard configuration is shown in Figure 53. The switch discharges the stored energy out of the capacitor in the TENG, creating a current that appears similar to a constant voltage output. It also requires a trigger switch that is controlled by another source. The Multisim Circuit and its output readings are shown in Figure 54. As seen in the readings, this circuit is not a viable option for this project. After discussions with advisors, the team concluded that the circuit had been too simplified to be useful for our end goal.

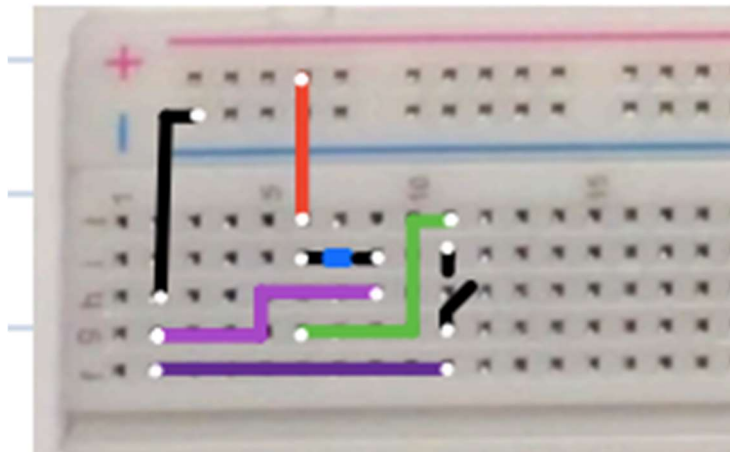


Figure 53: The Parallel Switch Circuit on a Breadboard

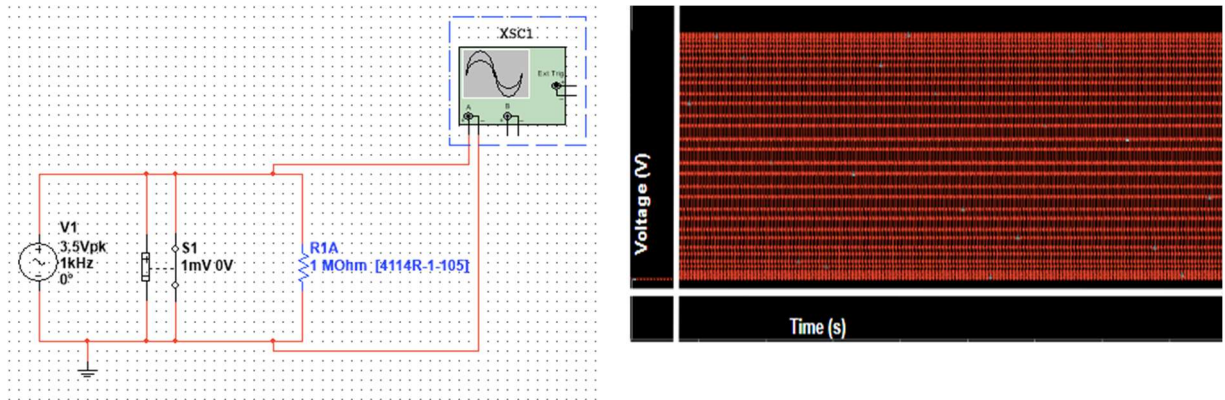


Figure 54: Multisim Model and Results of Parallel Switch Circuit

4.1.6 Series Switch Circuit Schematic and Simulation

The Series Switch Circuit is similar to the Parallel Switch Circuit except that the switches are in series. The breadboard model is shown in Figure 55. This circuit also requires a trigger switch that is controlled by another source. There is a possibility to use an automatic switch that relies on things such as a voltage threshold. The Multisim circuit and its output readings are shown in Figure 56. Similar to the Parallel Switch Circuit, this circuit's results show that it is not a viable option for this project and has been too simplified to meet the project's needs.

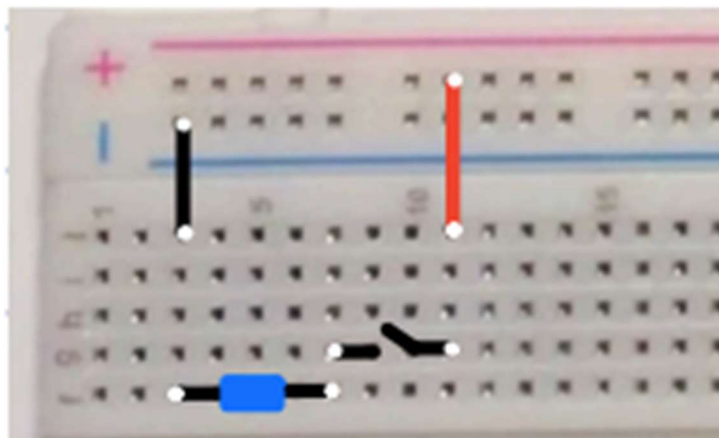


Figure 55: The Series Switch Circuit on a Breadboard

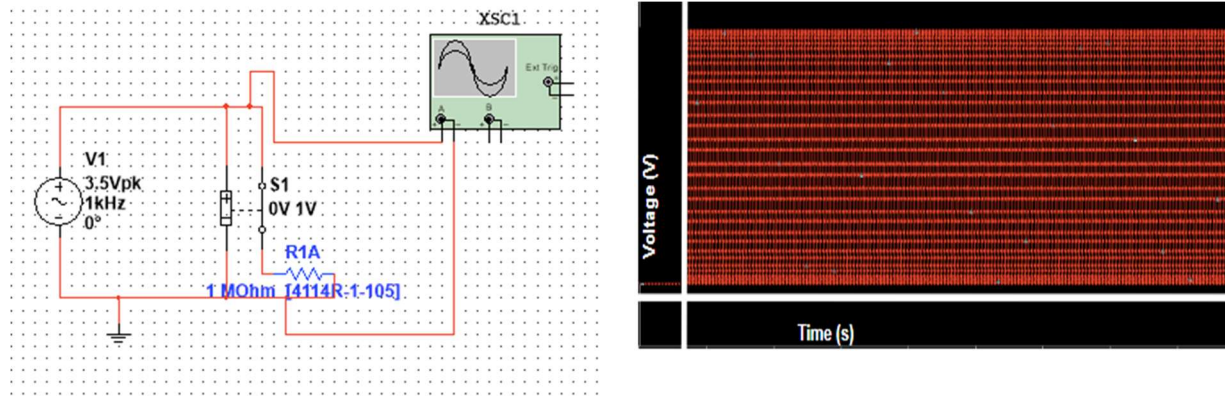


Figure 56: Multisim Model and Results of the Series Switch Circuit

4.1.7 Self Doubled Rectification Circuit Schematic and Simulation

The Self Doubled Rectification Circuit has a similar structure to that of the Half Wave Rectifier. The breadboard model is shown in Figure 57. The preliminary Self Doubled uses two diodes and a resistor to rectify the TENG input voltage. The Multisim model and the output results are shown in Figure 58. At a peak voltage of 2.5 volts, the circuit outputs 2.218 volts. The initial readings showed potential, so the team decided to further investigate the circuit.

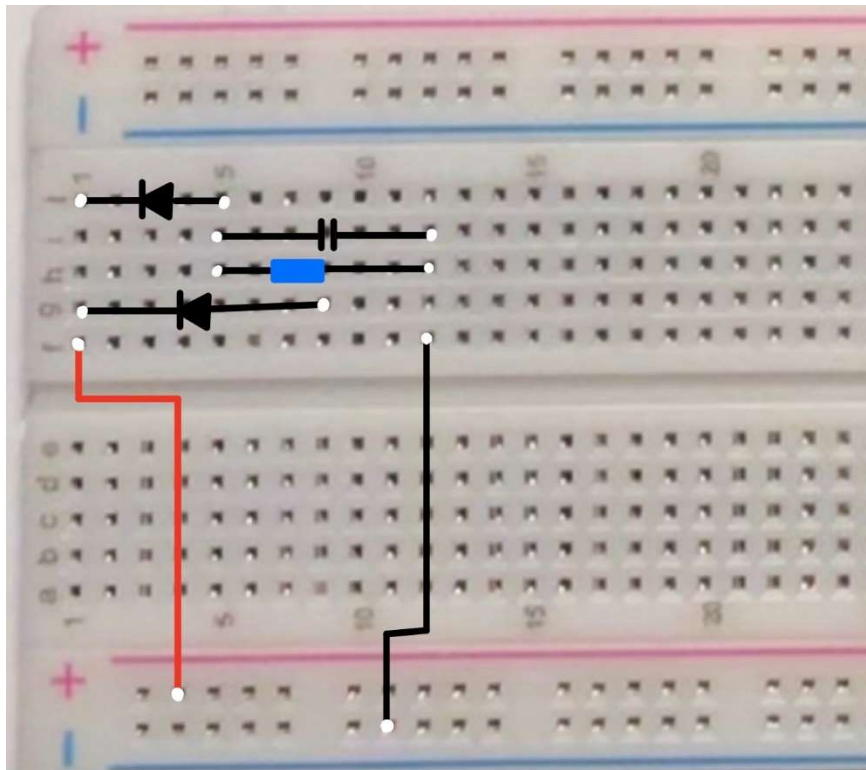


Figure 57: The Self Double Rectification Circuit on the Breadboard

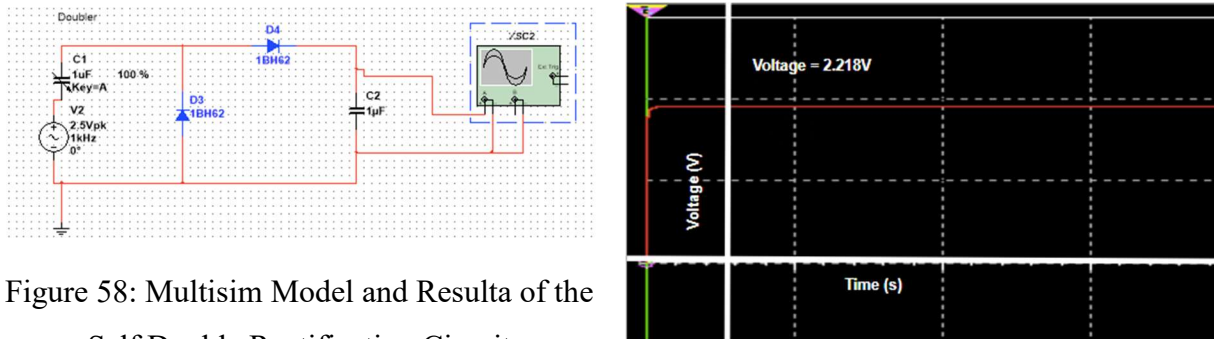


Figure 58: Multisim Model and Results of the Self Double Rectification Circuit

4.2 Simulated Circuit Changes and Improvements

Following the initial simulations, we moved towards modeling a power source with a functional output similar to the output generated by our designed TENG pair. Originally, we represented the TENG in our simulations as a sinusoidal wave AC power source. After reviewing the mechanics of the STEP design, we determined our represented TENG power source to be inaccurate. To improve upon our simulated model, we assumed that soldiers would walk most of the time while wearing our STEP design. The current flow output by the STEP TENG was simulated using a PWM voltage supply with a ten percent duty cycle. The ten percent duty cycle means that the force will be applied on the TENG for only one-tenth of each step. The frequency of the output was changed from 1kHz to 10Hz to account for the walking pace. The final change made was changing the peak voltages to (+/-) 2.3V as that was the average voltage last year's STEP prototype produced during their walking test trials. We believed the culmination of these changes would best resemble the produced power supply from our STEP design while a soldier was walking at a constant pace. After implementing these changes, we recorded the peak voltage values across a resistor used to represent the electrical device being powered or charged by the circuit. Voltage readings were taken after one second, ten seconds, and thirty seconds. After running the simulations, we recorded the difference between each circuit's produced voltage before and after implementing the newly modeled power supply.

The Bennet's Doubler Rectification Circuit produced a higher voltage after the implementation of the PWM power source. Figure 59 and 60 below show the Multisim model of the circuit with the PWM power source and the oscilloscope's voltage reading across the resistor used to represent the electrical device being powered or charged by the circuit.

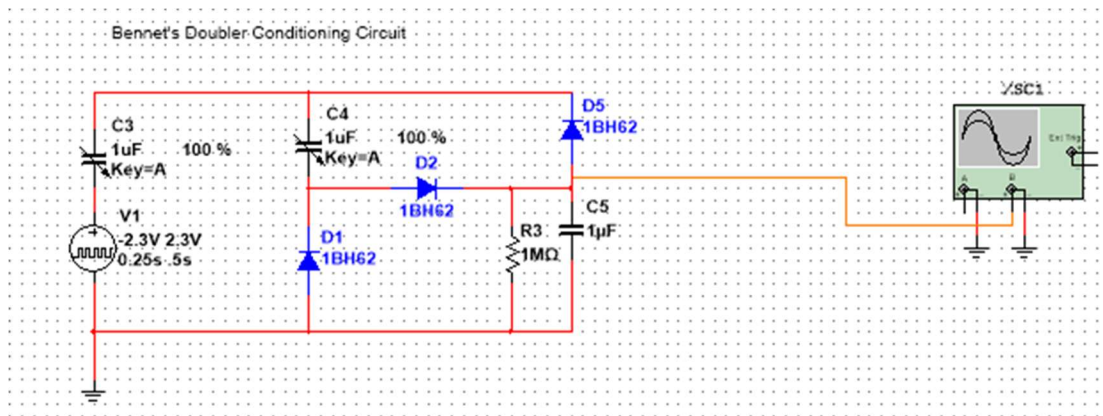


Figure 59: Bennet's Doubler Rectification Circuit with PWM Power Source

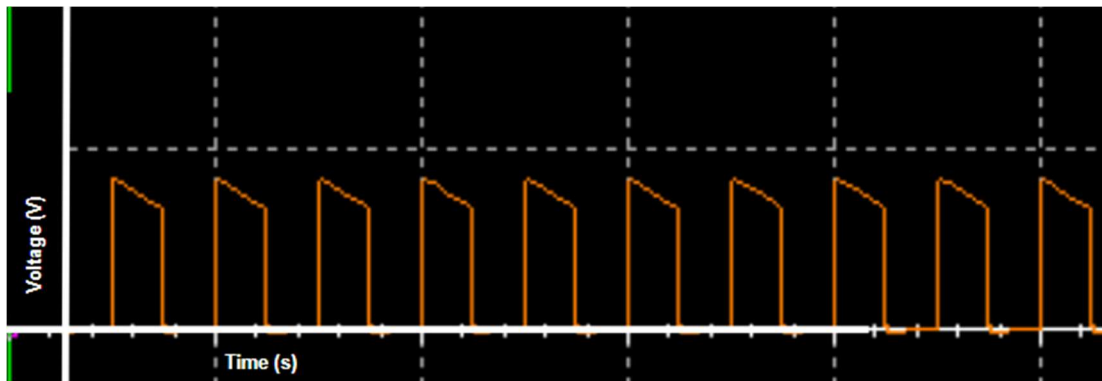


Figure 60: Bennet's Doubler Rectification Circuit with PWN Power Supply Voltage Supply

Figure 60 shows the voltage output for Bennet's Doubler rectification circuit. This circuit worked in converting the oscillating positive and negative voltage to an all-positive voltage. A negative attribute found within this circuit is the oscillations seen during the steady voltage state. There was a 0.07V increased average voltage during the steady state after implementing the PWM power supply.

The full wave rectification circuit was the only circuit to negatively change upon the implementation of the PWM power supply within our simulation. The circuit's voltage output across the resistor was similar to its voltage output generated during our initial simulations. As seen in Figure 61 below, the voltage across the resistor progressively steps from 0V to 1.435V over an approximate 2 second time interval.

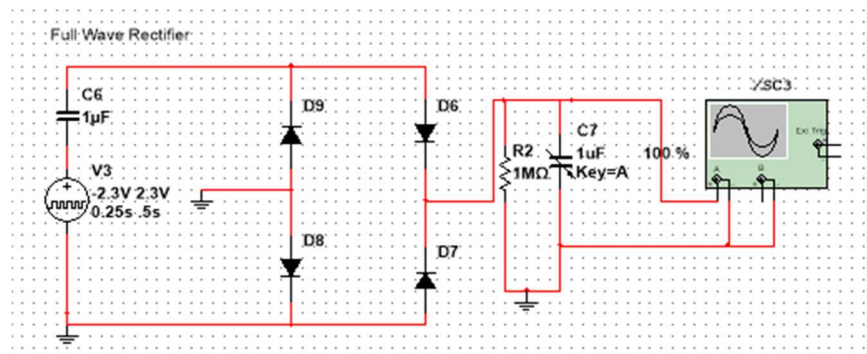


Figure 61: Full Wave Rectification Circuit with PWN Power Source

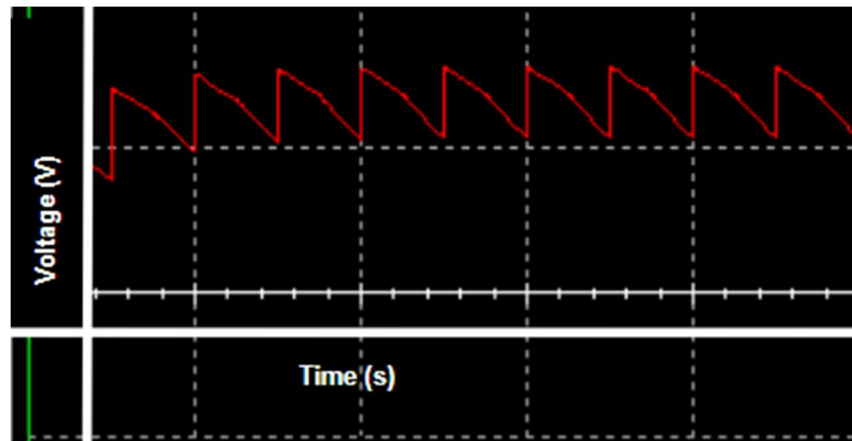


Figure 62: Full Wave Rectification Circuit Voltage Reading

The voltage peak seen within this simulation was 0.924V less than the steady stage peak voltage recorded during our initial simulations. We believed that increasing the capacitance within the smoothing capacitor (C6) would help increase the voltage across the resistor (R2) seen in this circuit. We hypothesized this because an increased capacitance allows for the component to build up more charge for a longer period. If the capacitor is discharged over a time period it allows for constructive voltage interference across (R2) creating a higher steady-state voltage value.

Similar to the initial simulations, the half-wave rectifier produced the smallest steady-state voltage during this stage of our simulation trials. The output function is read across the resistor (R4) seen in Figure 63 below.

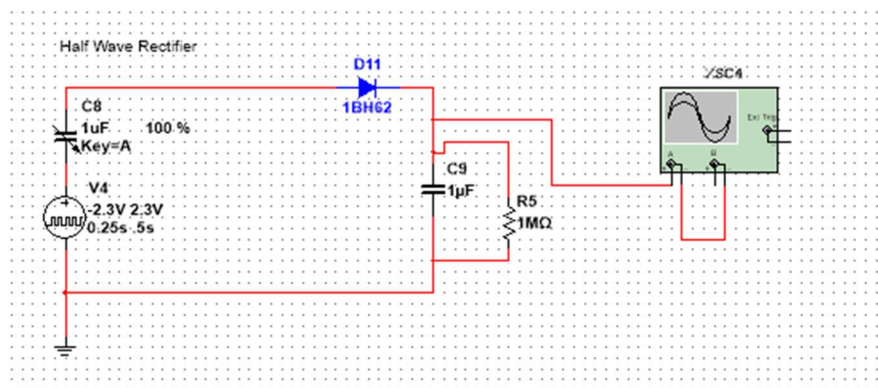


Figure 63: Half Wave Rectification Circuit with PWM Power Source

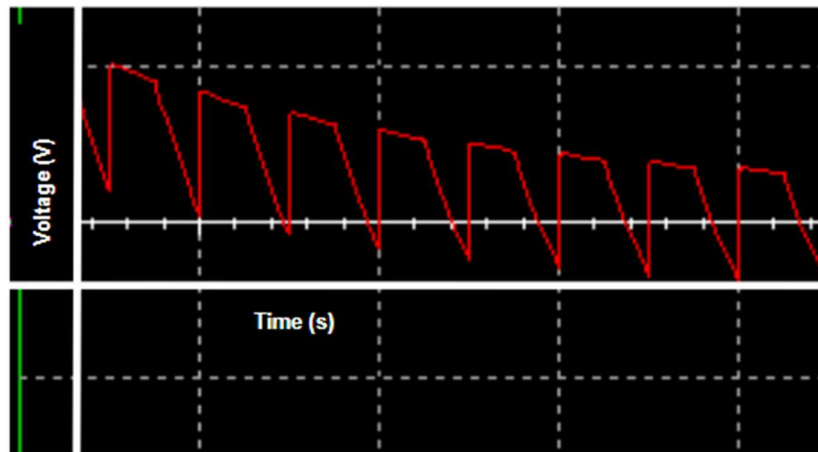


Figure 64: Half Wave Rectification Circuit (R4) Voltage Reading

Referring to Figure 64 above, a step function following a curved pattern can be seen. The peak voltage was 1.269V which was the lowest of our recorded peak voltages from this simulation trial period. The voltage decline seen at the end of each excitation period is from the capacitor discharging. We hypothesized that increasing the capacitance seen within C7 would allow for a more constant DC-like voltage output. This would occur because the capacitor would allow a larger charge build-up and discharge for a longer period of time. The negative attributes of this circuit were the inconsistent voltage supply and a small peak voltage supply.

The self doubled rectification circuit, though containing only one more capacitor than the half-wave rectification circuit, produced the highest peak steady-state voltage recorded during this simulation trial run. Figure 66 below shows the voltage output of the self doubled rectification circuit across resistor R1 shown in Figure 65.

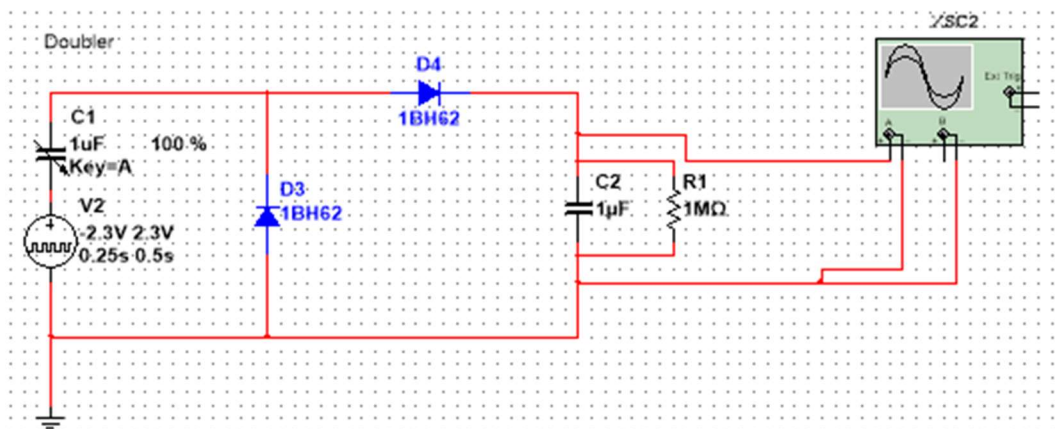


Figure 65: Self Doubled Rectification Circuit with PMW Power Source

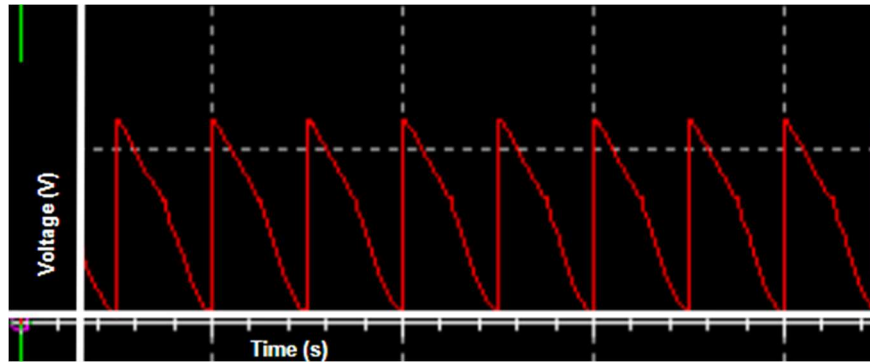


Figure 66: Self Doubled Rectification Circuit Voltage Output

The voltage output across resistor RX, seen in Figure 66, would jump to its peak and then in a linear manner decrease to zero. A voltage of 2.346V was read across resistor RX after the circuit reached a steady state. This was the highest voltage recorded during this simulation trial run. Before building the circuits, we delved deeper into simulation analyses within the Multisim circuit models. The next period of simulation testing was focused on the effect of varying capacitance values on the generated output voltage across the resistors used to represent an electrical device within all four tested circuits.

4.3 Simulating Change in Capacitance

Three separate simulations were conducted on the four remaining rectifiers to both increase the output and simulate all possible scenarios in the TENG. In the first test, both the internal capacitor and the smoothing capacitor(s) were changed at the same rate to see the effect an increased capacitance had on the circuits. In the next experiment, the smoothing capacitors were held at 20 μF , while the internal resistance changed. This experiment was meant to understand how the results would change if the internal capacitor was not a set value. In the last experiment, the internal capacitor was deleted from the circuit, while the smoothing capacitor's value varied, simulating the effect that no internal capacitance would have on the circuit.

The first simulation was conducted by changing the values of the capacitors in the self doubled rectifier, Bennet's doubler rectifier, full-wave rectifier, and half-wave rectifier. All the capacitances were set to 1 μF , and then the simulation was run on Multisim for approximately 30 seconds. After 30 seconds, the output across the resistance was recorded using the Multisim oscilloscope at 5, 10, and 30 seconds. These results are shown in Table 4, along with the calculated average voltage from these three points. This process was repeated for a variable of capacitance values from 1- 100 μF .

Self Doubled						
	C1 (μF)	C2 (μF)	Output Voltage (t=5)	Output Voltage (t=10)	Output Voltage (t=30)	Average Voltage

	1	1	2.208	2.208	2.208	2.208
	2	2	1.972	1.971	3.529	2.491
	5	5	4.224	4.225	3.635	4.028
	10	10	4.575	4.469	4.264	4.436
	20	20	4.551	4.612	4.557	4.573
	40	40	4.685	4.697	4.7	4.694
	50	50	4.674	4.694	4.707	4.692
	100	100	4.615	4.708	4.715	4.679
Bennet's Doubler						
C3(uF)	C4 (uF)	C5 (uF)	Output Voltage (t=5)	Output Voltage (t=10)	Output Voltage (t=30)	Average Voltage
1	1	1	1.661	0	1.591	1.084
2	2	2	1.783	0.234	1.831	1.283
5	5	5	1.943	2.781	2.569	2.431
10	10	10	3.384	3.878	4.135	3.799
20	20	20	3.071	3.968	4.323	3.787
40	40	40	3.736	4.183	4.584	4.168
50	50	50	3.702	4.346	4.654	4.234
100	100	100	3.652	4.303	4.68	4.212
Full Wave Rectifier						
	C6 (uF)	C7 (uF)	Output Voltage (t=5)	Output Voltage (t=10)	Output Voltage (t=30)	Average Voltage
	1	1	3.101	3.008	2.146	2.752
	2	2	3.454	3.462	2.885	3.267
	5	5	3.749	3.748	3.504	3.667
	10	10	3.868	3.868	3.857	3.864
	20	20	3.896	3.876	3.898	3.890
	40	40	3.911	3.915	3.912	3.913

Table 4: Capacitances and their Output Value Across Resistors

To analyze the data collected in Table 4, the average voltage was plotted against the capacitance-voltage. The results from all four of the circuits are shown in Figure 67. All four of them illustrate the same trend, the voltage increases at a decreasing rate until around 20 uF. After 20 uF, all the voltages stay constant as the capacitance increases. The self doubled rectifier has the largest voltage of 4.5 volts, while Bennet's Doubler and the full-wave rectifier are 4 volts. The half-wave rectifier produced a 2.5V output. This was the lowest voltage compared with the other three circuits. These results explain that any capacitance from 20 uF to 100 uF can be selected and the circuit will be optimized.

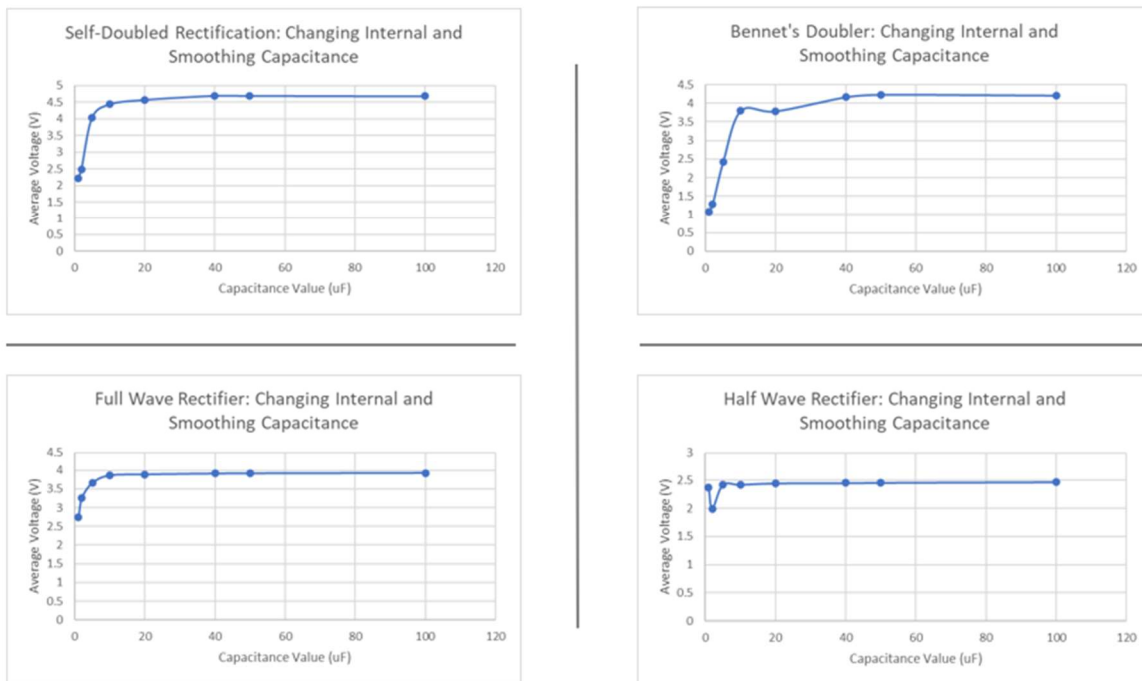


Figure 67: Graph of Average Voltage vs Capacitance

The internal capacitance of the TENG does not stay constant when a load is exerted upon it. Because of this quality, tests were performed to examine the effect of varying internal capacitance was chosen to be tested. The smoothing capacitors were kept constant at 20 uF due to the results from the last simulation. First, all four circuits' internal capacitance was set to 1uF, and then the simulation ran for 30 seconds. The voltage was measured across the resistor at 5, 10, and 30 seconds and recorded in Table 5. This process was repeated for different internal capacitances up to 100 uF. The average voltage and the percent difference between the internal capacitance to the smoothing capacitor were recorded using the equation $C1/C2 * 100$.

Self Doubled	C1 (uF)	C2 (uF)	% Difference (C1/C2 *100)	Output Voltage (t=5)	Output Voltage (t=10)	Output Voltage (t=30)	Average Voltage
	1	20	5	1.063	1.431	1.751	1.415

Half Wave Rectifier	C8 (uF)	C9 (uF)	% Difference (C1/C2 *100)	Output Voltage (t=5)	Output Voltage (t=10)	Output Voltage (t=30)	Average Voltage
	1	20	5	0.240	0.240	0.238	0.240
	2	20	10	0.374	0.374	0.374	0.374
	5	20	25	0.987	0.919	0.919	0.942
	10	20	50	1.583	1.629	1.582	1.598
	40	20	200	3.229	3.229	3.263	3.240
	50	20	250	3.464	3.464	3.464	3.464
	100	20	500	4.078	4.051	4.051	4.060
	150	20	750	4.293	4.293	4.293	4.293

Table 5: Change in One Capacitance Across Resistance

The results from Table 5 are shown in Figure 68. The four graphs are the capacitance difference (internal/smoothing capacitor) for each rectification circuit. Three of the circuits (SDR, bennet's doubler, and full-wave rectifier) reach the maximum voltage between 50-200 percent of smoothing capacitance. The half-wave rectifier creates a greater voltage at a larger capacitance value because there are fewer components to the circuit, thus a higher internal capacitance helps to smooth the voltage from the TENG.

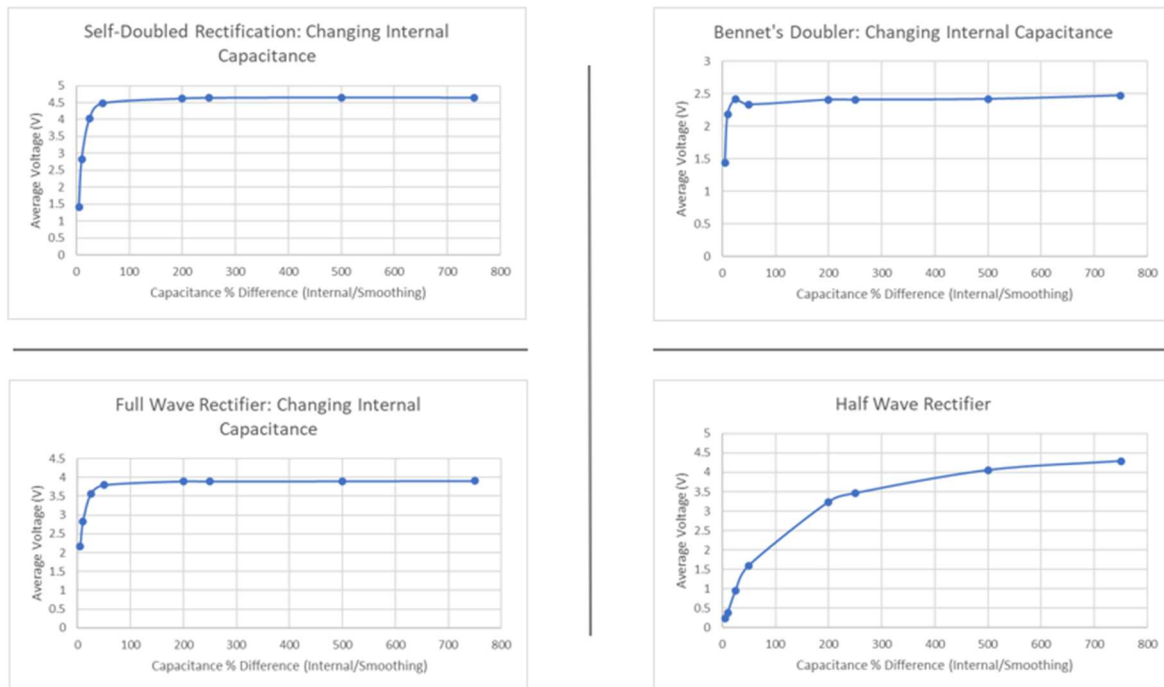


Figure 68: Graphs of Average Voltage vs Difference in Capacitance

The internal capacitance can also be small or close to zero. Therefore, the circuits were run with no internal capacitance. The smoothing capacitance was also changed to see if a higher capacitance is needed when there is no internal capacitance. The results were run similar to the previous two, except only the smoothing capacitance varied from 1 uF to 100 uF. The average voltage was also taken from running the simulation and collecting the voltage through the resistor at 5, 10, and 30 seconds. These voltages were recorded in Table 6

Self Doubled						
C1 (uF)	C2 (uF)	Output Voltage (t=5)	Output Voltage (t=10)	Output Voltage (t=30)	Average Voltage	
0	1	2.463	1.652	0.602	1.572	
0	2	2.342	2.342	2.413	2.366	
0	5	2.25	2.25	2.404	2.301	
0	10	2.307	2.307	2.346	2.320	
0	20	2.347	2.347	2.328	2.341	
0	40	2.368	2.373	2.363	2.368	
0	50	2.376	2.376	2.374	2.375	
0	100	2.38	2.382	2.383	2.382	
Bennet's Doubler						
C3(uF)	C4 (uF)	C5 (uF)	Output Voltage (t=5)	Output Voltage (t=10)	Output Voltage (t=30)	
0	1	1				
0	2	2				
0	5	5				
0	10	10				
0	20	20				
0	40	40				
0	50	50	When the internal capacitance is missing, the voltage resorts to AC, which means the battery would not be able to be charged. We would need to figure out a way to add internal capacitance to run the simulation.			
0	100	100				
Full Wave Rectifier						

C6 (uF)	C7 (uF)	Output Voltage (t=5)	Output Voltage (t=10)	Output Voltage (t=30)	Average Voltage
0	1	1.812	1.812	2.004	1.876
0	2	1.975	1.975	1.975	1.975
0	5	1.952	1.952	1.969	1.958
0	10	1.989	1.989	1.973	1.984
0	20	1.973	1.973	1.978	1.975
0	40	1.983	1.983	1.981	1.982
0	50	1.983	1.989	1.983	1.985
0	100	1.985	1.985	1.985	1.985
Half Wave Rectifier					
C8 (uF)	C9 (uF)	Output Voltage (t=5)	Output Voltage (t=10)	Output Voltage (t=30)	Average Voltage
0	1	1.889	1.889	1.007	1.595
0	2	2.297	2.297	2.43	2.341
0	5	2.297	2.297	2.38	2.325
0	10	2.32	2.32	2.319	2.320
0	20	2.405	2.4	2.373	2.393
0	40	2.396	2.396	2.413	2.402
0	50	2.416	2.417	2.4	2.411
0	100	2.406	2.42	2.422	2.416

Table 6: Tables of No Internal Capacitance

Data from Table 70 was plotted into separate graphs using the smoothing capacitance value vs average voltage. The benet's doubler was not able to be graphed because the circuit depends on an internal capacitance to run. The other three circuits (Self Doubled, full-wave, and half-wave) have similar results. All of them reach their maximum voltage at around 10 uF, which is smaller than when there is an internal capacitance. For the Self Doubled and full-wave rectifier, the maximum voltage is around 2.5 volts, which is 1.5 volts lower than experiment one. However, the half-wave rectifier had the same peak voltage of 2.5 volts, meaning an internal capacitance was not needed for the half-wave rectifier.

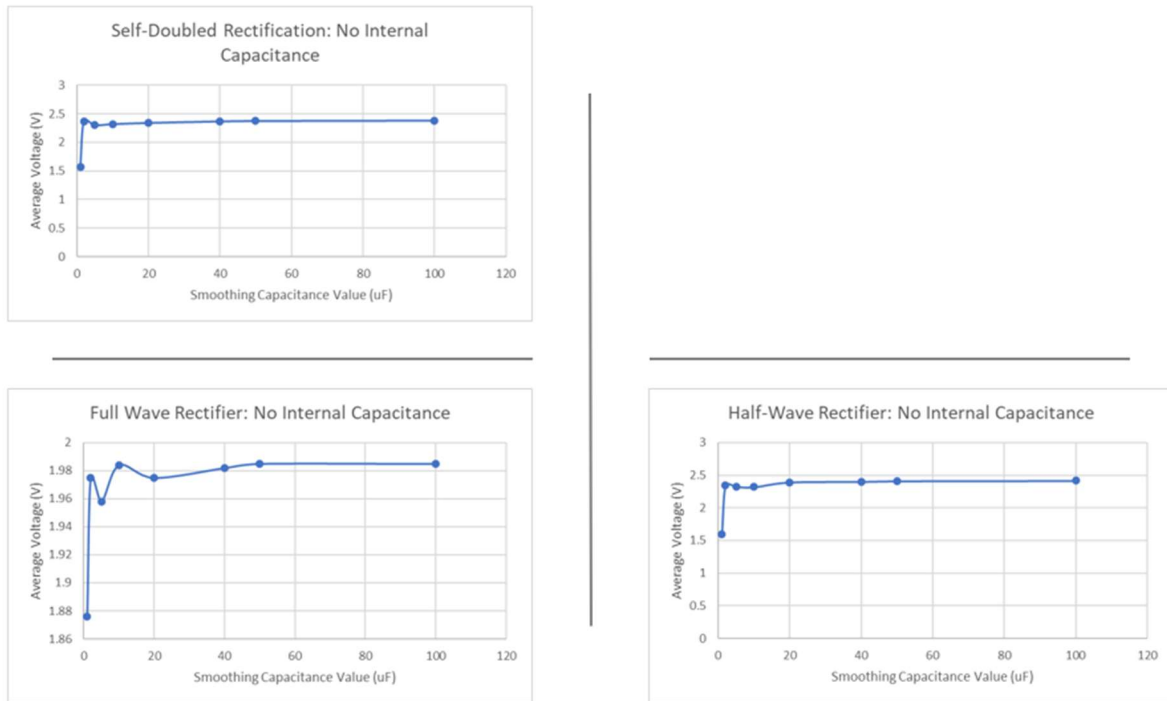


Figure 69: Smoothing Capacitance vs Voltage for No Internal Resistance

4.4 Breadboard Rectification Circuits Testing and Evaluation

Following the simulation trials of each rectification circuit, our group used breadboards and through-hole circuit components to build each circuit. Sections of the breadboard rectification circuits were then wired to an oscilloscope to provide a power supply and measure the voltage that would be produced across the rechargeable battery interface. Beyond quantitatively analyzing the performance of each circuit, notes were taken on the complexity and implementation feasibility. These tests were also performed to ensure the overall reliability of each circuit. Troubleshooting and improvements were prioritized during this stage to prevent future interface issues while testing complex TENG designs. The voltage produced across the resistor loads within each tested circuit was plotted over a time interval to help compare their overall performance.

4.4.1 Half Wave Rectification Circuit Breadboard Evaluation

Figure 72 depicts the voltage across the load within a half wave rectification circuit. The circuit was powered for thirty seconds. Following the initial thirty-second time period, the power supply was disconnected. Data on the voltage across the resistor load was taken to analyze the discharge process due to the capacitor.

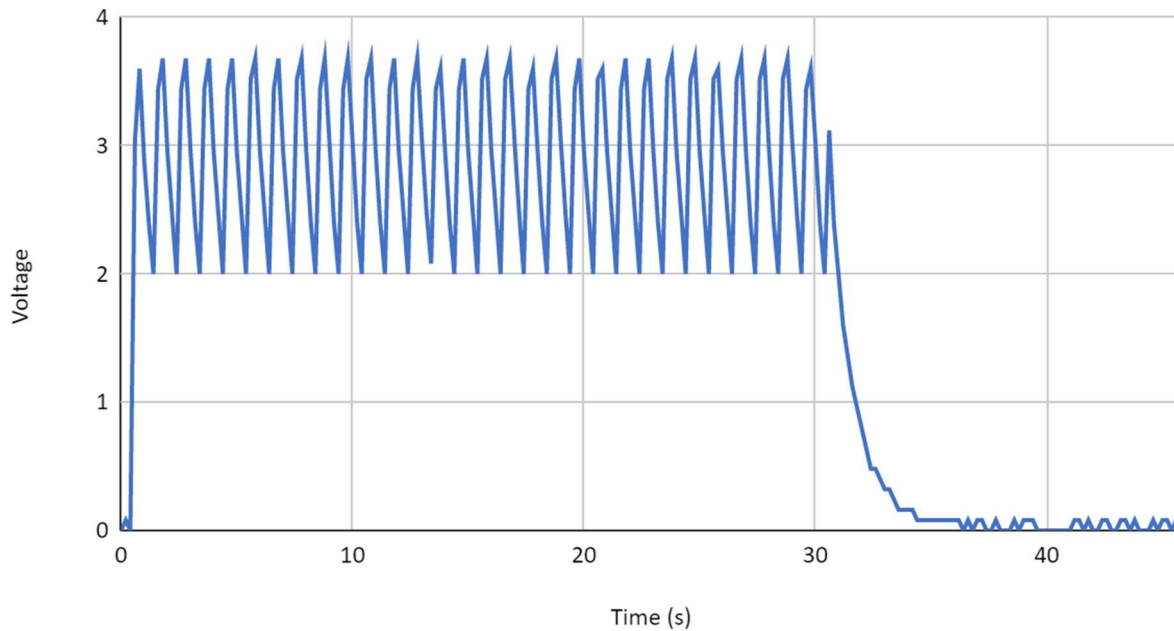


Figure 70: Half Wave Circuit Breadboard Voltage Output

The output voltage recorded for the half wave rectification circuit oscillated between 2V and 3.74V. The undesirable aspect of this circuit was the amplitude of the signal oscillating since the rectification circuits are designed to produce a linear direct current. The circuit discharged in approximately six seconds following the disconnection from the power supply. This discharge time was the lowest of all circuits. The unsteady signal produced across the oscilloscope and the fast discharge time brought us to rank the half wave rectification circuit last when comparing the performance of each circuit. The discharge time can be improved within this circuit by integrating a larger capacitor in parallel with the measured load. However, as the overall size of the circuit is crucial to our TENG system's optimization and applicability, only a certain sized capacitor could be implemented.

4.4.2 Bennet's Doubler Rectification Circuit Evaluation

Figure 73 plots the voltage across the load within the Bennet's doubler rectification circuit. The steady state signal produced across the load, similar to the half wave rectification circuit, oscillated voltage levels between 1.25V and 1.75V.

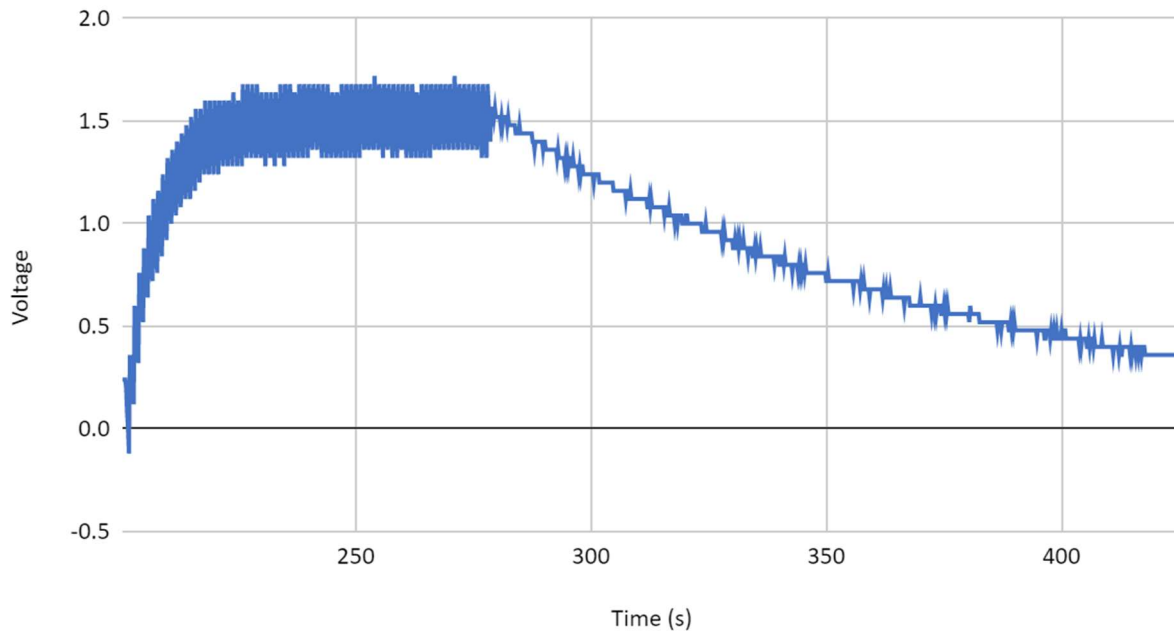


Figure 71: Bennet's Doubler Breadboard Circuit Voltage Output

Unlike the half wave rectification circuit, the discharge time interval allows the circuit to provide power to a device for minutes even if there is no mechanical interactions occurring within a connected TENG. The bennet's doubler rectification circuit produced the smallest average voltage within its steady-state period of 1.5V. Due to this circuit producing the smallest voltage it was ranked below the self doubled rectifier and full wave rectifier. These two circuits produced a more ideal direct current power supply at higher voltage levels.

4.4.3 Self Doubled Rectification Circuit Breadboard Evaluation

Both the self doubled rectifier and full wave rectification circuits produced a steady-state DC voltage of approximately 4.1V. Both circuits also discharged in a logarithmic decrement pattern over a similar time frame. Figures 74 and 75 plot the voltage across the loads within the self doubled rectification and the full wave rectification.

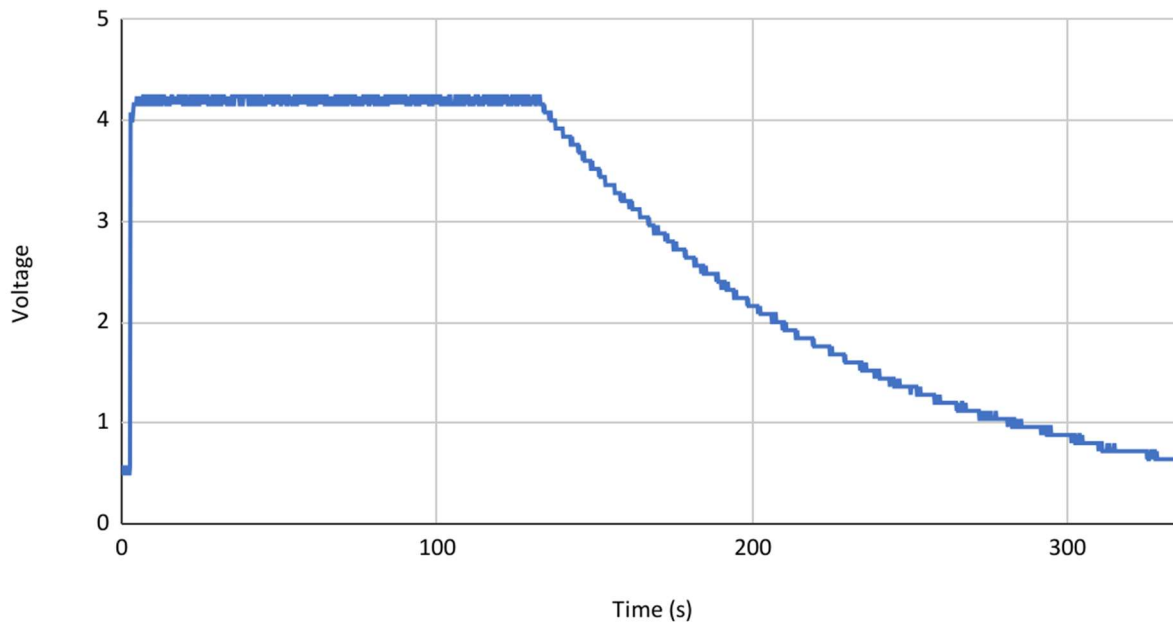


Figure 72: Self Doubled Rectification Breadboard Circuit Voltage Output

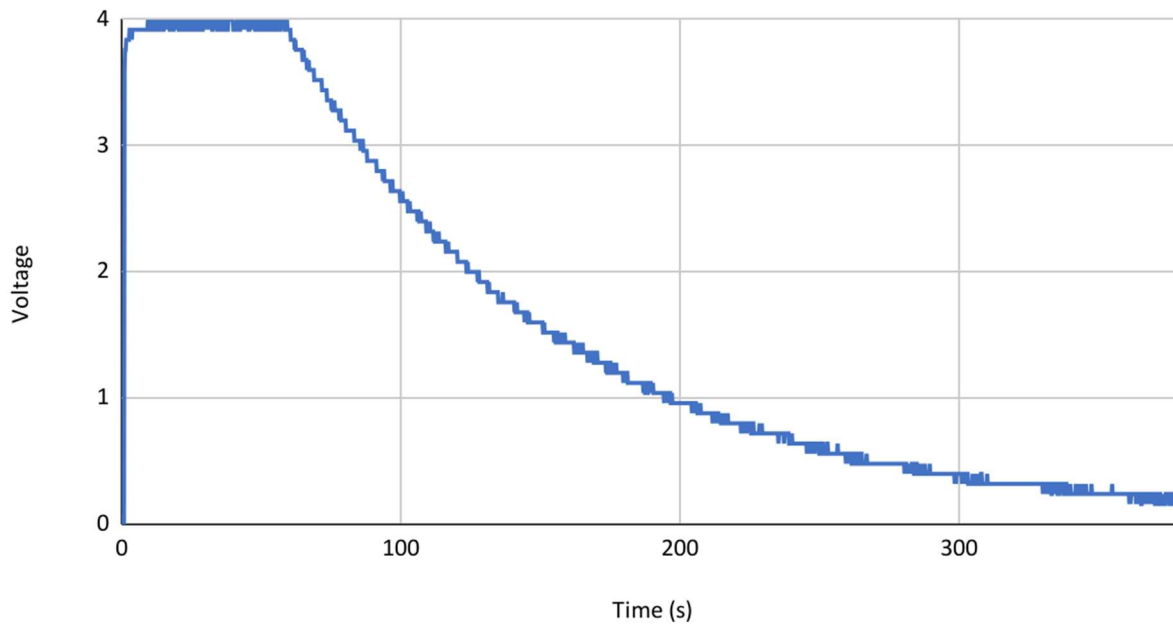


Figure 73: Full Wave Rectification Breadboard Circuit Voltage Output

Due to the SDR and Full Wave rectification circuits performing similarly and being of the same complexity, our team decided to test both circuits under more complex conditions. Following the completion of the breadboard testing phase, our group designed and fabricated flexible printed circuit boards (FPCBs) for both the self doubled and the full wave rectification circuits.

4.5 Flexible Printed Rectification Circuit Fabrication and Performances

The Voltera V-One circuit printer was utilized to help optimize the overall compactability and mobility of our prototypes. PET film was used to print conductive ink and interconnect small surface mount components and produced our two designed rectification circuits. Circuit schematics were updated to improve the compactability and efficiency of each circuit. Our ideal fabricated circuit would not be damaged in use or limit the movement of a TENG footwear prototype. This ideal FPCB would also produce a signal similar to those produced within the tested breadboard circuits.

4.5.1 Rectification FPCB Schematics

The Voltera V-One standard flex ink cartridges were used to fabricate each circuit. The chemical composition of this paste is optimized for printing resolution and durable qualities such as resilience. Our team utilized KiCAD, a circuit design program, to design the schematics of the self doubled rectification circuit and the full wave rectification circuit. Figures 76 and 77 below show the designed schematic of each FPCB. A benefit of utilizing FPCBs, aside from mobility improvements, is the dimensions of the circuits. The smallest breadboard we had available was 44.80cm². The design features utilized within KiCAD allowed for us to design both circuits to have a surface area of 30cm². Figures 76 and 77 below show our team's designed flexible rectification circuit schematic.

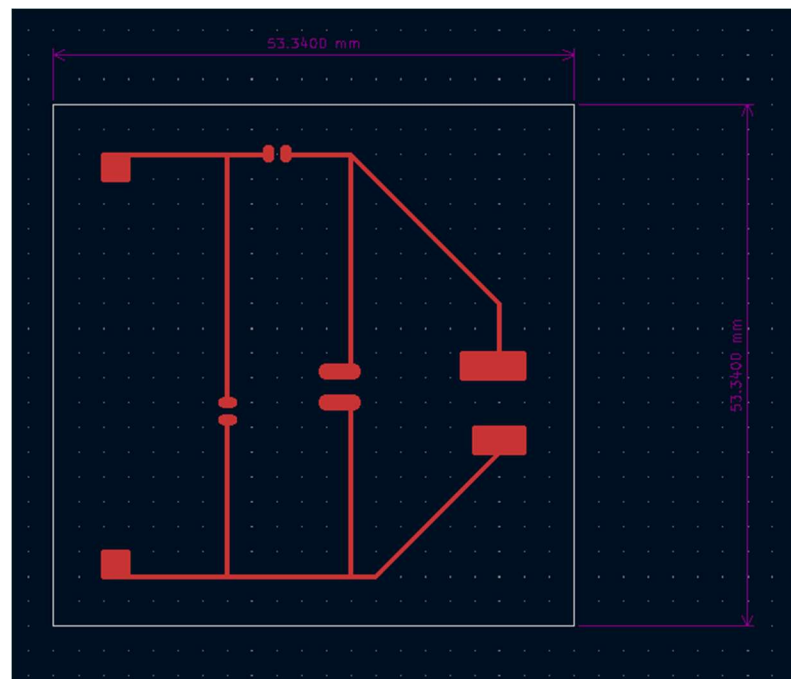


Figure 74: Self Doubled Rectification Circuit KiCAD Schematic

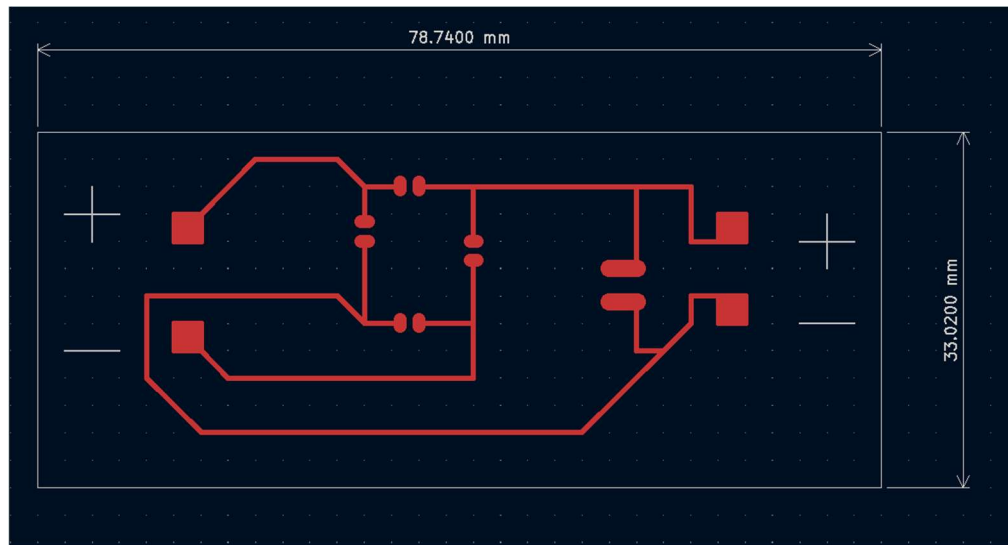


Figure 75: Full Wave Rectification Circuit KiCAD Schematic

Note the V-One printer is capable of processing and printing far more dense circuits. However, since the surface area of the FPCBs met the intended requirements for housing the circuit within STEP prototypes, we finalized these as the set dimensions for the FPCBs. Following the completion of these circuit designs, our team uploaded the circuits to gerber files in order to be compatible with the V-One printer.

4.5.2 FPCB Components and Fabrication

Compared to the through-hole insertable circuit components utilized for the composition of our breadboard circuits, the surface mountable diodes and capacitors were significantly smaller. Figure 78 below shows an image of the $47\mu\text{F}$ surface mountable capacitor (3.5mm x 2.6mm) integrated into our FPCBs.

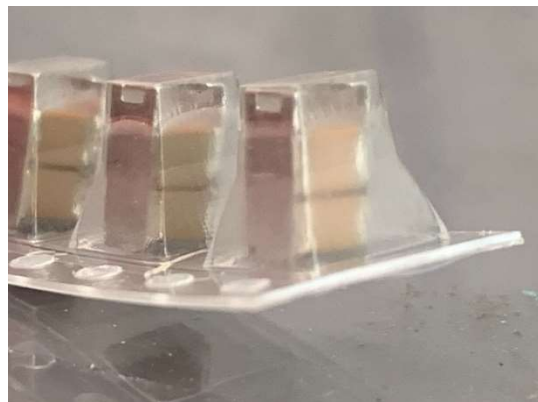


Figure 76: Surface Mount Capacitor Component

Even at such a small scale, the surface-mountable capacitor was large in comparison to the diodes utilized in our FPCBs which were X by Y in dimensions. Due to the size of the diodes, a microscope was utilized to place the diodes at their correct positions within the circuit. This ensured the

polarization and placement of the diodes were oriented correctly. Figure 79 below shows the diode under the microscope and Figure 79 shows the virtual image taken while placing the diode on the substrate.



Figure 77: Surface Mount Diode Component as Seen Under Microscope

Note that the conductive pastes branching from this diode were reprinted over to ensure full conductivity throughout the circuit.

After printing the conductive paste to create the interconnections between each circuit component the V-One heated the substrate to solidify the paste. A similar reflow process was performed following the dispensing of the solder paste and placing the components within the circuit. Figure 80 depicts the SDR FPCB circuit prior to soldering all components onto the substrate.

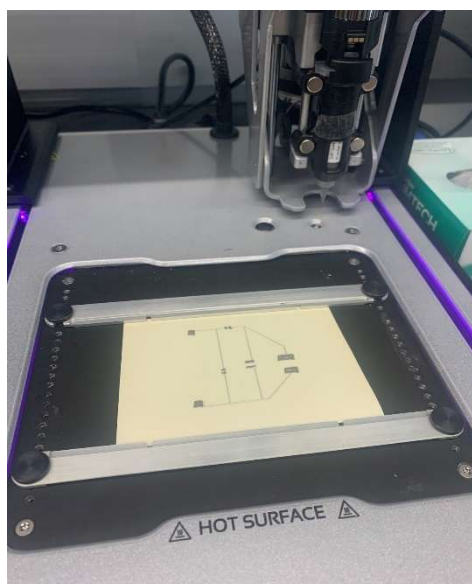


Figure 78: Self Doubled Rectification Circuit Mounted onto Voltera V-One Printer

Once the conductive solder paste was dispensed onto the substrate, components were then placed onto it. Following the reflow process both circuits were ready for testing and implementation. Figures 81 and 82 show the final rectification of FPCBs.

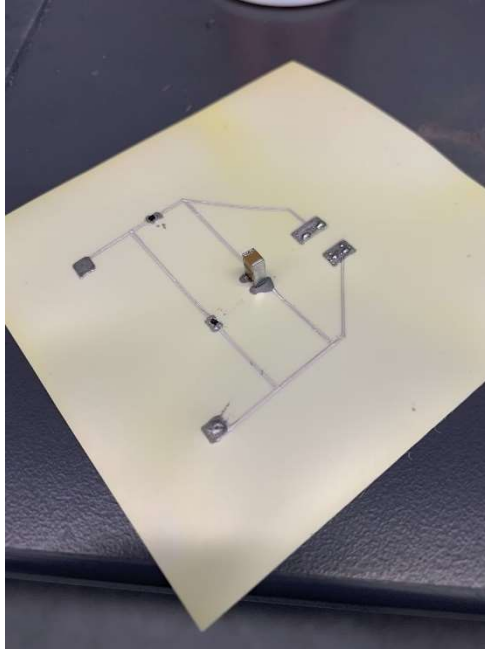


Figure 79: Self Doubled Rectification Circuit with Soldered Components

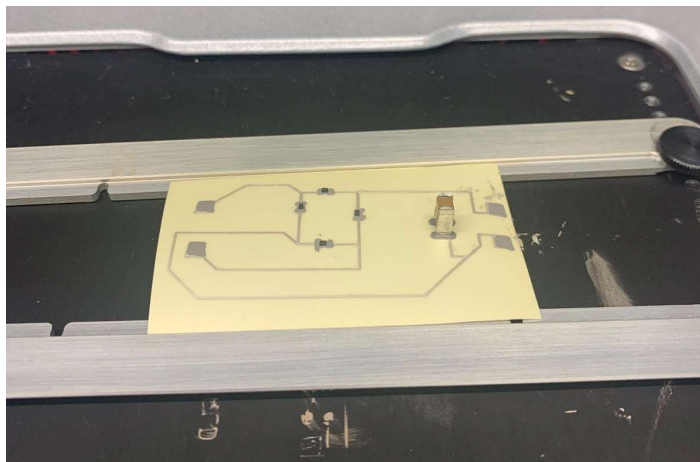


Figure 80: Full Wave Rectification Circuit with Soldered Components

Following the fabrication of both rectification FPCBs, both circuits' voltage output was tested and analyzed. Lead wires were soldered to the input and output points on both rectification circuits. The TENG iteration was then connected to the input wires while an oscilloscope probe was connected to the

output wires to measure the voltage across this section. Figure 83 below shows the self doubled rectification circuit with soldered input and output lead wires.

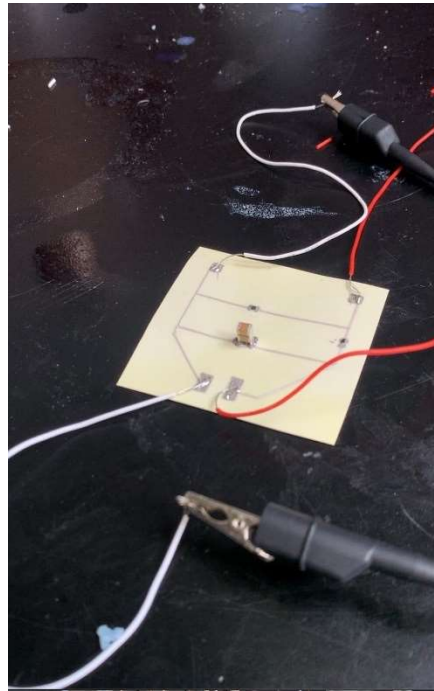


Figure 81: Self Doubled Rectification Circuit with Soldered Lead Wires Connected to Oscilloscope

4.5.3 FPCB Evaluation and Conclusions

Figure 84 below shows the voltage measured across the output section of both rectification circuits. The same power input settings set while evaluating the breadboard circuits were held constant for this evaluation as well.

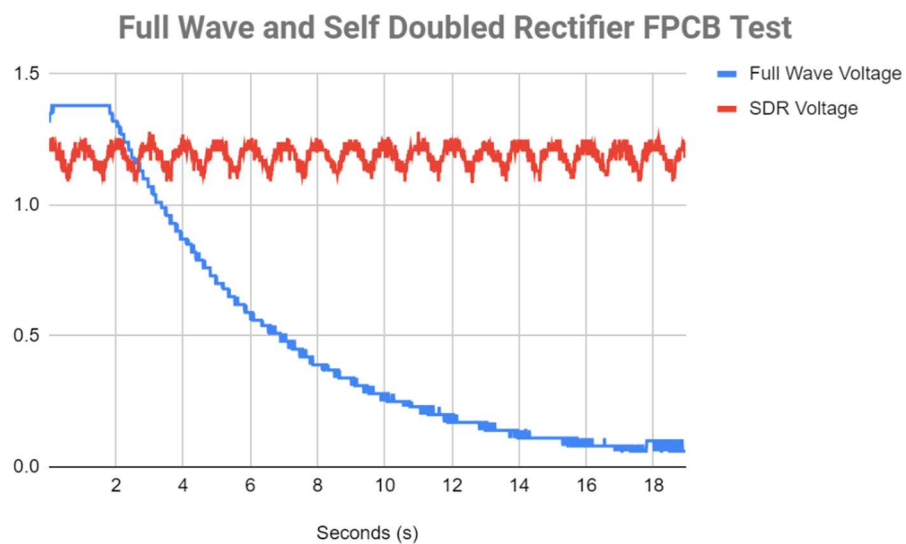


Figure 82: Graph of Rectification FPCB Test Voltage Output

Around 3 seconds into testing the full wave rectification circuit, the voltage began to logarithmically decay. We theorize this is due to a voltage spike larger than the SMD capacitor's voltage rating of 10V. The signal output for both circuits was quite similar to the measured results from the simulation and breadboard testing stage of this project. Before the capacitor was blown, the full wave FPCB output a linear current reaching 1.3V. The self doubled rectification would produce an oscillating voltage between 1.1V and 1.3V. This signal output is due to the relationship between the current and the overall capacitance of the circuit's smoothing capacitor. If a capacitor with a larger capacitance was selected, then the signal output would be linearized more. However, if a capacitor with a larger capacitance was selected then the smoothing component would most likely increase in size. The height of the selected capacitor was larger than the height of other utilized components such as the diodes or soldered wires. Several times, the capacitor would disconnect from its soldered position if a large enough force was applied to it. To improve this section of both circuits, a capacitor smaller in height should replace the currently selected component. Both circuits can be densified further to allow for larger ease of implementation within TENG designs. While there are many benefits to densifying the designs of the two circuits it should be noted that decreasing the size narrows circuit components suitable for the two circuits.

After testing the FPCB circuits' voltage output produced with programmed power input, both circuits were tested with a TENG connected as the power supply. The triple-fold TENG sample was placed in the automated tester, with the same timing and force settings held constant throughout the prototype testing stages. Unfortunately, both circuits did not produce a current across the external load sections. We theorized this was due to a voltage drop across different circuit components and an irregular current input from the TENGs. The power output of a TENG in this case can vary significantly due to the speed and impact force per step. Though the automated tester had constant applied forces over the same interval, there are still other factors that vary the power output per step. This variance can cause signal interference within specific sections of the circuit. Certain areas within both circuits have wire or tracing intersections designed to combine currents of the same polarity prior to traveling across an external load. It was hypothesized that the timing and consistency of the TENG's current output caused destructive interference at such intersections in both circuits. With more time to develop and test these circuits, our team would have looked into implementing a transistor or similar device before the previously designed rectification circuits in order to regulate the current inflow. This would allow the current input of the circuit to act as a signal, similar to what we set the input to be when testing these circuits with an oscilloscope power input. Further research could also be done into implementing circuits optimized for a current input similar to that of a TENG. Further research and development of circuits designed for TENG applications will help achieve the main purpose of our intended STEP application.

Chapter 5: Automated Tester

5.1 Design Parameters

Before designing the automated tester, we determined the parameters of the sample that would be tested. Through research and a meeting with an Army ROTC student, the average “loadout” for Army infantry was found. The loadout includes everything that the soldier would wear on a given mission. The Army has implemented a target weight of 50 pounds for all individual soldier’s packs, so this was assumed the max weight. Through research, the average weight for a female and a male soldier is 130 and 170 pounds respectively, as seen in Table 5. The maximum weights were found to be 1.25 times the initial weights^[69] as the heel struck the ground, seen in Figure 85 under “R:HS”. After combining the soldier weight, the loadout, and applying safety factors, the maximum weight was considered to be 330 lbf.

The gait cycle, or how often the shoes strike the ground, was found by meeting with an Army ROTC student and cross-checking their numbers with research. This was researched to determine the impact interval settings to program the automated tester to operate at. The data they provided was 120 steps for every 100 meters or 60 steps on each foot for 100m. We used the rucking standard for the Expert Infantryman Badge (19 km within three hours in the full pack) and calculated the total steps for that ruck to be 11,400 steps. Given those standards, we expected the average infantryman to have a walking pace of 1.06 steps/second, or 1.06 Hz frequency.

Item Name	Weight (lbf)
Army helmet w/ night vision goggles	9
Pack	50 (target)
Improved outer tactical vest (IOTV) ^[63]	27
Weapon (M4 carbine) ^[64]	7 (3.1kg)
Human body weight (<i>Female/Male</i>)	130/170
Total (<i>Female/Male</i>)	223/263

Table 7: Weight of Item in Average Loadout

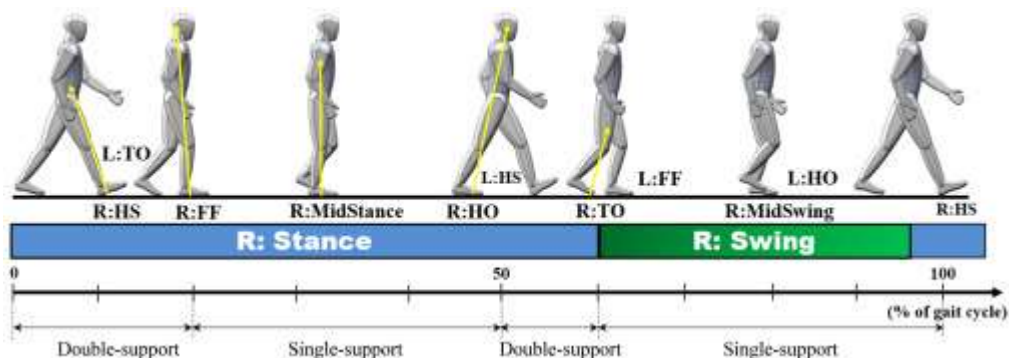


Figure 83: Gait cycle for average humans.^[70]

5.2 Summary of Designs

There were four initial designs considered for the automated tester. These designs fell into two categories: designed to simulate the striking pattern of a human foot, and those designed to impact a sample directly with a flat face. The designs included a pneumatic tester that simulated a walking gait, a weight-based tester that simulated a walking gait, a pneumatic tester that impacted the sample straight on, and finally a weight-based design that impacted the sample straight on. The weight-based tester that simulated a human's gait did not make it past the initial stage, due to the unnecessary complexity of the design.

5.3 Pneumatic Gait Design

The first concept, illustrated in CAD in Figure 86 was a rolling design to simulate the striking pattern of a human foot. The use case for this machine was to test both the rough simulated output of a human over a period and how long each sample would continue to output energy before breaking. The device used two pneumatic cylinders controlled by an Arduino Mega to press the impact surface into the base of the machine, which would be covered with plywood. This would give some indication of its power output over average terrain. This shared many similarities with the final design, given both are pneumatic systems. The bill of materials for this system is detailed in Appendix 1A. We decided against this design because of the unneeded complexity in trying to simulate a human walking pattern and the cost of the system. After a few meetings, it became clear that the purpose of the automated tester was to test samples for output and failure time rather than replicating a footstep for an extended amount of time. It was concluded that testing the accurate power output of a footstep would be done with a footwear prototype during a walking test.

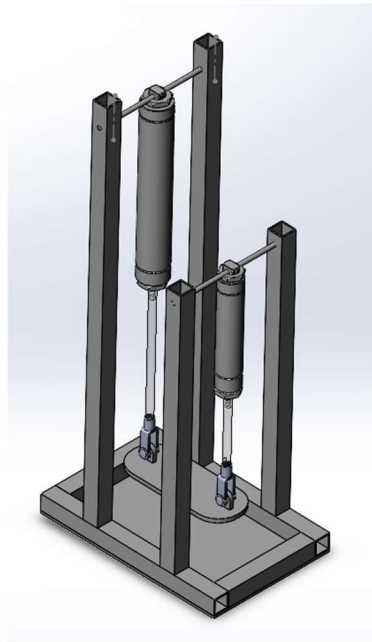


Figure 84: Pneumatic gait design.

5.4 Weight-Based Design

Another initial concept used physical weight to act as the force of the tester. This design used a scotch yoke mechanism to lift the weight up and drop it onto the sample repeatedly as seen in Figure 87. The scotch yoke mechanism was used to limit the amount of required torque and provide a smooth and controllable cycle. The impact surface would press the sample into the plywood base of the tester, simulating a given weight. The bill of materials is detailed in Appendix 1B. The disadvantages of this system include the complexity, cost, and impracticality. Most parts of the machine would need to be precisely cut from sheet metal in order to work well. This would have increased the development time and the cost. However, the largest cost would come from the A/C motor that would require a significant max torque to move the weight. The machine would have needed to be able to scale up to 350 pounds of weight, which would take up space. The initial concept was to use either weight from the WPI recreation center, limiting its use, or cement from a hardware store, increasing its size. For these reasons, it was decided to not use this design or any further iterations of it.

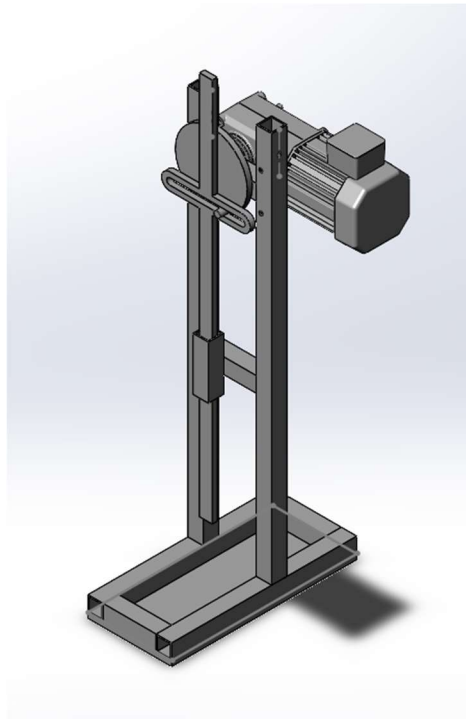
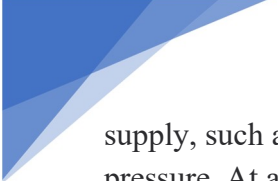


Figure 85: Weight-based Design

5.5 Final Design - Pneumatic Straight Tester

The final and selected design was a single-axis tester based around a pneumatic cylinder. A CAD model of this system is shown in Figure 88. The design used a double-acting pneumatic cylinder that repeatedly pressed the sample into the plywood base. The base, which would be held in place by fasteners, could be removed and replaced with additional plywood sheets as needed. This tester used an Arduino Mega, which controlled the cycle of the cylinder. The pneumatic system used a fixed air



supply, such as those in Washburn or Higgins, which went through an adjustable regulator to control the pressure. At a 2.5-inch bore diameter, the pneumatic cylinder provided 250 lbf at 50 psi through 750 lbf at 150 psi. This cylinder was selected for its bore diameter, which allows it to provide forces above 350 lbf at pressures below 100 psi. This was important, as the air compressors around WPI are limited to 100 psi. We selected a cylinder with a four-inch stroke length because it decreased the required flow rate of air while allowing us to easily put samples in place. After the regulator, the air flowed through an electrical valve which prevented the air from working when power was shut off, or when the Arduino sensed that someone had opened the safety door. After the electrical valve, the air flowed through a directional control valve, which allowed air to escape through one side while supplying air through the other. This was found to be the best way to control a double-acting cylinder. The entire pneumatic system is detailed in Figure 89. The system ended at the cylinder, where it would move up or down and push air out of the muffler, which reduced the noise of operating the machine.

Structurally, the machine was made from welded steel framing rail, which provided enough support for the cyclic load the cylinder created. The sections were cut out using an abrasive chop saw, squared using an angle grinder, and MIG welded together. To MIG weld the sections into the correct place, each frame was clamped onto a metal welding table in the correct square position. Then, each side was welded to create the two square frames. The pneumatic cylinder was bolted in place to a metal bar cut out of a steel sheet. The tester was designed to be able to disassemble for storage, and so that the cylinder could be semi-adjustable by adding spacers beneath the bolts. All steel sheet sections were cut using a handheld hacksaw, and milled using a MiniMill. The drawings of our frame can be seen in Appendix 2. Finally, the impact head of the pneumatic cylinder was cut out from plywood. This allowed the point of failure to be the impact face, rather than the tester itself. We analyzed the design to ensure that the frame could handle above the expected stress, the calculations of which can be seen in Appendices 3. The entire machine was covered in thick plastic sheets, to keep important objects out of danger, and prevent any debris from flying out.

On the electronic side, the code for the machine was modeled on a state machine shown in Figure 90. The code can also be seen in Appendix 4. The device would move through extending and retracting the cylinder. While it moved through those cycles, the state machine would constantly check whether the safety door reed switch had been disconnected, or the stop button had been pressed. In addition to the stop button, the machine had an emergency stop switch that cut power to the safety valve and Arduino. Externally, there were three colored LEDs to communicate to the operator when the device was prepared, started, and eventually stopped. The original design included collecting data on the current power output and saving it to an SD card. An INA219 sensor would measure both the voltage and current to calculate the power output. If the power output was zero for a period of time, it would shut off the machine and record the failure in the SD card. The time of failure would be logged using an RTC module. These features were removed, as a separate operating system was required and the oscilloscope provided much needed resolution.

Given the eventual agreement that the design would primarily be used to failure-test small samples, this design was the lowest-cost solution. The basic tester cost a total of \$864.98. These costs are broken down in Appendix 1C.

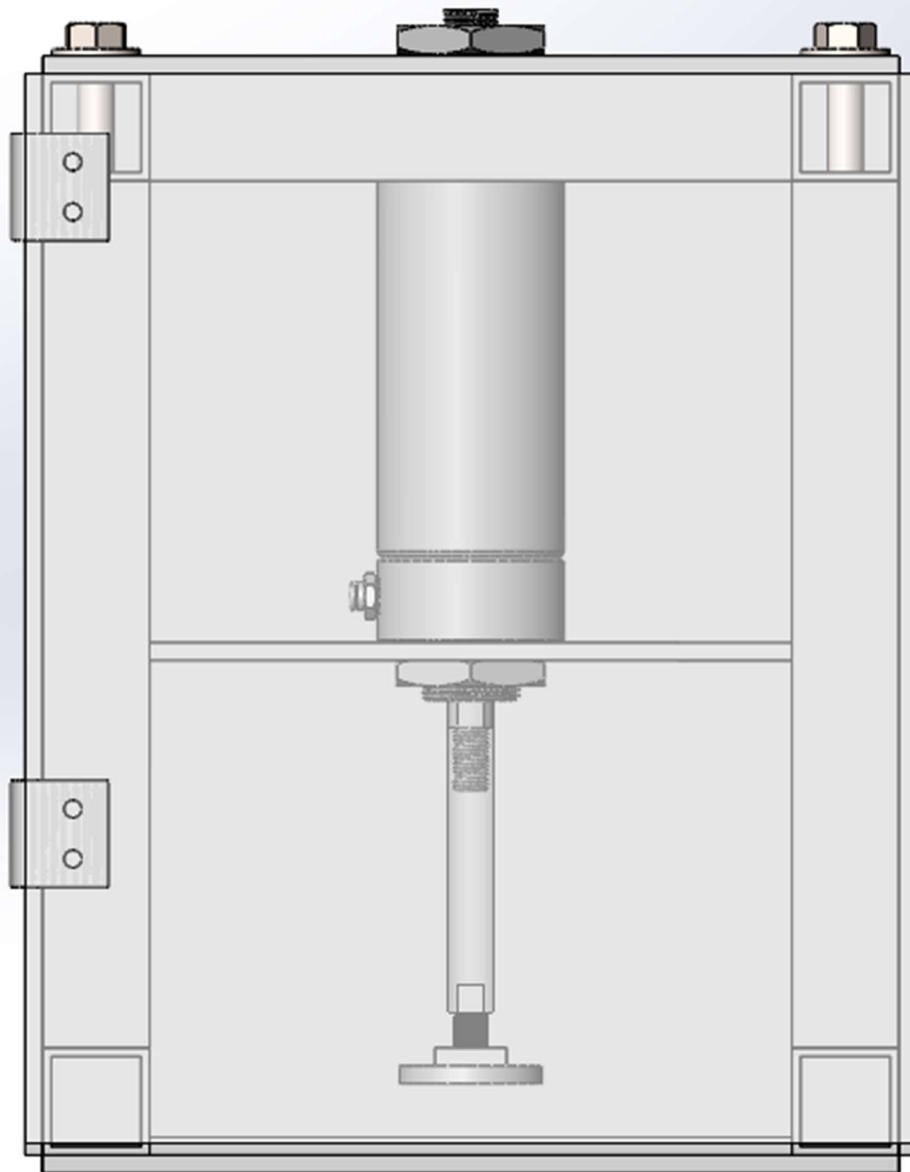
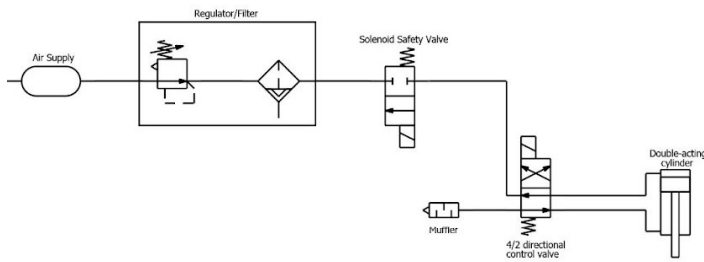


Figure 86: Pneumatic Straight Design



Code	Name	Model	Comment
A1	Cylinder, Double acting, Single rod	6498K491	Double-acting cylinder, 2.5" bore, 4"L
V1	4-port, 2-Position, Single solenoid, Spring return, Direct	62095K4	Electrical Air Directional Control Valve
P1	Regulator	60115K42	Compressed Air Regulator/Filter
P2	Air tank	Higgins Air Supply	>100 PSI
V2	2-port, 2-Position, Normally closed, Spring return, Direct	5489T411	Solenoid Safety Valve
L1	Filter, With auto drain	60115K42	Compressed Air Filter/Regulator
P3	Silencer	8535T23	Muffler

Figure 87: Pneumatic system for the final design

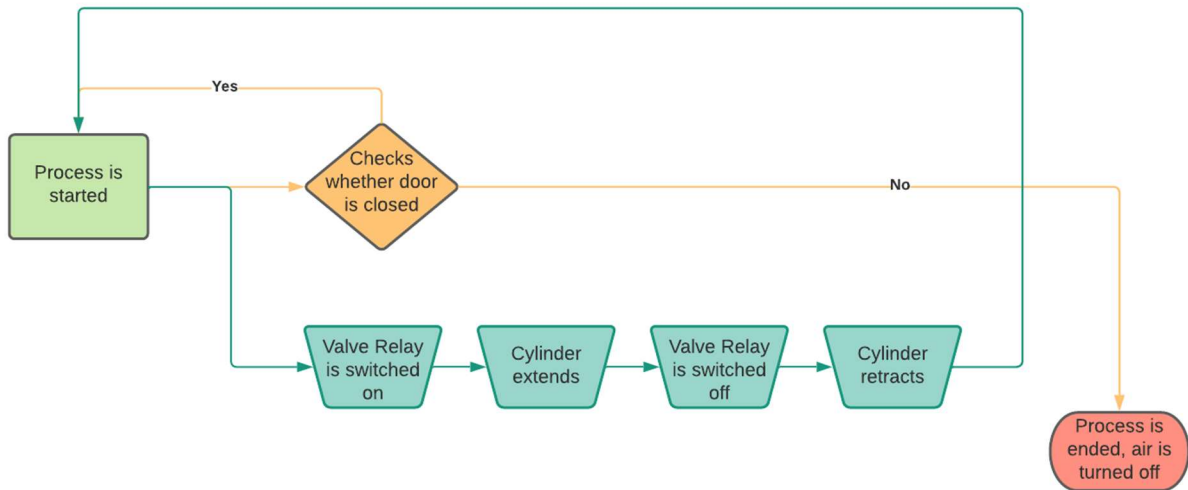


Figure 88: Final flowchart diagram for Arduino code and decision-making process

Chapter 6: TENG Iterations

To improve the voltage and current produced by the TENG implemented in our prototype, we developed and evaluated different 2”x2” samples. Prior to this development process, different TENG designs feasible for our design were researched. These designs included adding more wire throughout the TENGs, folding the TENGs, increasing surface area, adding different combinations of sponges, and adding a layer of foam. All designs were tested using the automated tester. These iterations were evaluated based on their voltage outputs shown in Table 7. The next step for the project was integrating the best results into the final prototypes.

6.1 Research for Criteria of Voltage Increase

Researching variables that could be tested to increase the voltage and current was the first goal of this iteration process. An increased voltage and current would produce a larger power output. Since our team planned to insert a TENG within footwear, our research focused on increasing vertical contact separation. The equation for voltage output during vertical contact separation is given in the formula below ^[71].

$$V = -Q \left(\frac{1}{C_1} + \frac{1}{C_{gap}} + \frac{1}{C_2} + V_{oc} \right) = -\frac{Q}{S\epsilon_0} \left(\frac{d_1}{\epsilon_{r1}} + x(t) + \frac{d_2}{\epsilon_{r2}} \right) + \frac{\sigma x(t)}{\epsilon_0}$$

Table A: Symbols and their Meanings

Symbol	Meaning
Q	Transferred charge amount between electrodes
C ₁	Capacitance of positive layer
C ₂	Capacitance of negative layer
C _{gap}	Capacitance of air gap
V _{oc}	Open Circuit Voltage
S	Effective contact area
ε ₀	Free space permittivity
ε _{r1} , ε _{r2}	Relative dielectric constants of positive and negative triboelectric layers
d ₁ and d ₂	Thickness of positive and negative triboelectric layers
x(t)	Distance between triboelectric layers
σ	Surface charge density of triboelectric layers

Table 8: Variable Definitions for Voltage Equation

Most of these variables in the equation above were predetermined by the environment and material selection. The capacitance and thickness of both materials were factors chosen by the previous group and could not be easily altered. The free space permittivity and the relative dielectric are constants in this equation that cannot be fixed. Additionally, one can assume V_{OC} is zero for the design setup. Thus, the variables needed to change the voltage are the distance between the triboelectric layers and the effective contact area. The equation illustrates that increasing the distance will increase the voltage, while the effective contact area decreases the current. However, an effective contact area plays a crucial part in increasing the current of the TENG.

Based on the equation and previous research, the team needed to look into different design iterations that changed either the contact area or increased the gap between the two triboelectric materials. One way to increase both surface area and force separation is by folding the materials to create tension ^[72]. This is shown in Figure 91 below, where the pink fold is one material and the green fold is the other. They are folded 90 degrees from each other to force separation while increasing the contact area. The folds are meant to act similar to a spring and compress under an applied load. Taking these traits into account both the current and voltage will increase.

Another way to increase the separation is to add compressible material in between the layers. This can be shown in Figure 91 below. This idea was found in a research paper titled, *Smart Shoe Based on Battery-Free Bluetooth Low Energy Sensor* ^[73]. This design features different layers of positive and negative TENG materials that were all separated by a foam material in the four corners of the TENG. The foam is added to create measurable space between the TENG. The foam-spacer and folded TENG iterations influenced the design of twelve separate iterations that utilized changing the size of the TENG and the separation.

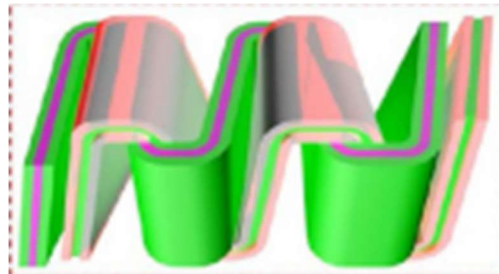


Figure 89: Folded TENG from Literature

Another way to increase the separation is to add a compressible material in between the layers. This can be shown in Figure 92 below. This idea was found in a research paper titled, *Smart Shoe Based on Battery-Free Bluetooth Low Energy Sensor* ^[73]. This design features different layers of positive and negative TENG materials that were all separated by a foam material in the four corners of the TENG. The foam is added to create measurable space between the TENG. The foam-spacer and folded TENG iterations influenced the design of twelve separate iterations that utilized changing the size of the TENG and the separation.



Figure 90: Spacing for TENG from Literature

6.2 TENG Iteration Composition

All TENGs were made using the same materials (conductive copper foil electrical tape, conductive thread, PTFE, acrylic tape, and MIL DTL 32429 type 1 class 8 universal camouflage print fabric). Keeping the materials used consistent helped to reduce the variability between designs to isolate the change in voltage that occurs in the different designs. The different types of iterations tested were how the wire was applied, different levels of folding, and increasing spacing through adding material between the layers.

6.2.1 Influence of Wire Geometry

During TENG construction, the 3-ply conductive thread was used on both the layers of the TENG to capture the displacement of electrons. The wire went in between the camouflage print fabric and copper tape as well as the PTFE film and copper foil. Last year's research group only applied the wire at the end of both sides of the TENG. We decided to test a different method by snaking the wire throughout the entire space between both designs of the positive side and negative side. This test was done to both increase contact between the wire and the materials as well as create a small gap between the sides. Winding the wire creates a small amount of separation from the individual materials to the copper tape that can be compressed during impact. This is especially true on the PTFE side where the PTFE does not adhere well to both the wire and copper tape.

Shown below in Figure 93 is the positive side (PTFE) with the wire running through the TENG. The wire was first applied on top of the PTFE in the position pictured and held down as the copper tape was placed on top of both the wire and PTFE. We made sure two people helped to apply the tape, so the wire could not move. Additionally, there was a gap between the wire and the edges to make sure the wire stayed in between the layers of the TENG to avoid wire contact with the environment.

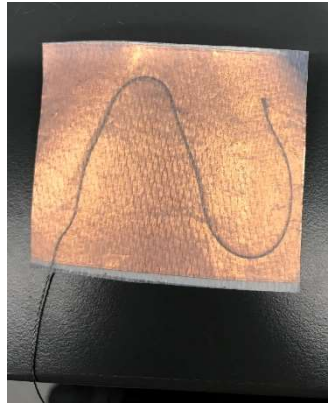


Figure 91: Image of Wire Through

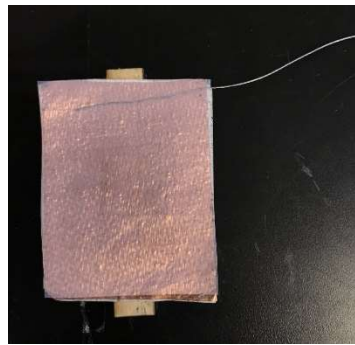


Figure 92: Image of Wire at the End of the TENG

6.2.2 Folded Iterations

This subsection of designs focused on the effect folding the TENGs would have on the voltage. The PTFE structure resists bending, helping to keep the space between the folds when force is not applied. To test out the effects of the fold, three separate prototypes were designed (single-fold, double-fold, and triple-fold). As a fold was added, the contact surface area increased by 4 inches². The construction of the single fold is shown in the CAD below. Both sides of the TENG were made to be 4"x2" in size. First, the negative fabric was folded so the acrylic tape was on the outside. In Figure 95, this feature is highlighted; the copper tape is colored white, while the camouflage fabric is green. Figure 96 shows the completed TENG. Then, the positive side was folded so that the PTFE was on the outside and the acrylic tape was on the inside. This is illustrated below as the PTFE is shown with orange and the acrylic tape is white. The positive layer was then inserted into the negative layer so that the fabric and PTFE are in contact. By folding the TENGs, layers are created easily to increase surface area. The TENG can also be seen both folded and unfolded.

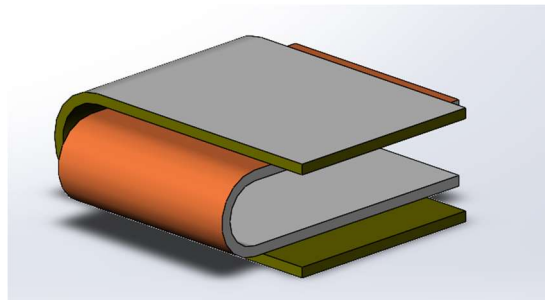


Figure 93: CAD of Single-Folded TENG

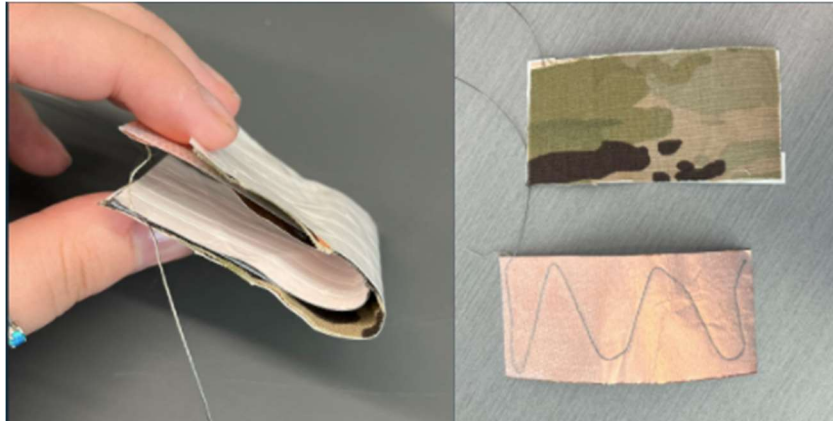


Figure 94: Image of TENG Single-Folded

Another prototype was created with two folds on both the positive and negative sides. This was accomplished by increasing the area of the TENG by another 4 inches². This TENG is double the contact surface area of the original 2"x2" sample. The negative side was folded first in an accordion style with the acrylic tape facing the outside. The positive side is composed of PTFE folded in the same manner but with the PTFE facing the outside. In a similar manner to the single-fold, the positive side was inserted into the negative so that the PTFE and camouflage fabric are always in contact. These folds are shown in the pictures below, with the PTFE and camouflage touching each other three times. Each of the folds is a 2"x2" for the automatic tester. Figure 97 shows the prototype model. Figure 98 shows the completed TENG.

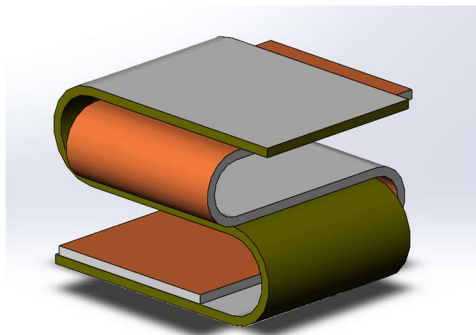


Figure 95: CAD of Double-Fold TENG

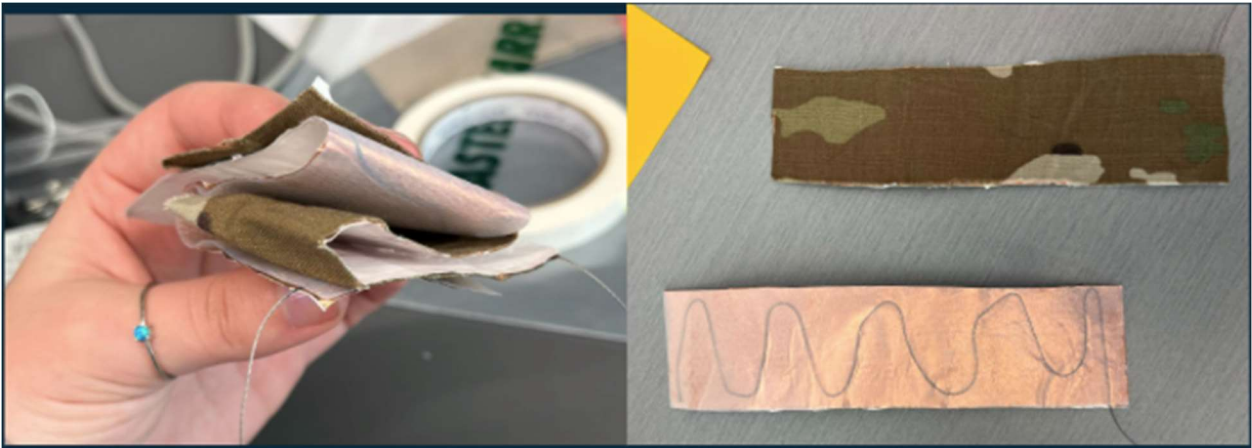


Figure 96: Image of Double Fold TENG

The triple-fold was made in the same way as the last two folds. It is 2"x2" larger than the second fold, making it eight inches long and two inches wide. This allows for three folds on each side with four places for the contact between the PTFE and camouflage material. The more folds in the material allow for more separation between the layers as the PTFE is resistant to folding. Figure 99 shows the CAD model of the three-fold prototype. Figure 100 shows the completed TENG.

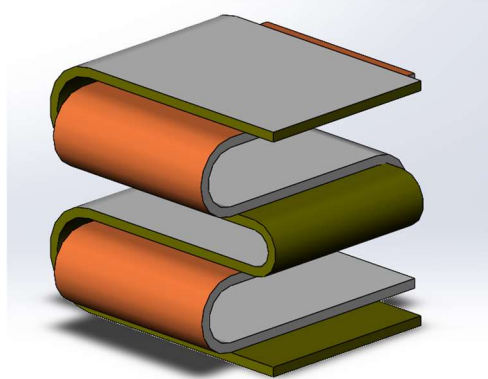


Figure 97: CAD of Triple-Fold

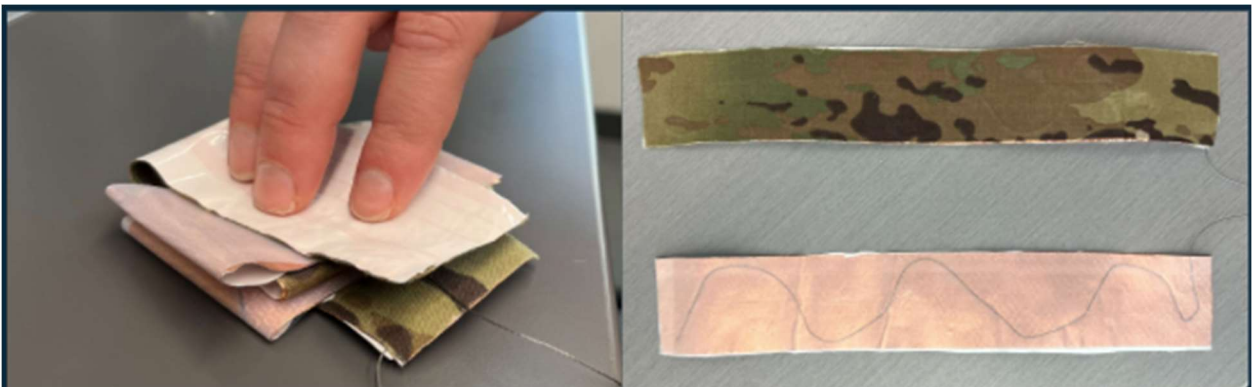


Figure 98: Image of Triple-Fold

All three of these samples were first tested unfolded to compare the effects of surface area on the voltage output. These iterations were compared with both the original sample and the other iterations.

6.2.3 Inducing Spacing Between TENG Layers

The space iterations tested how the gap between the positive and negative layers affects the voltage output by a TENG. The material chosen in the first iterations was a sponge because sponges are easily compressible, allowing for the materials to come into contact when force is applied. Additionally, sponges have a high resilience easily taking their original shape once the force has been taken off the TENG. The first design was assembled by cutting up a sponge into four 0.5" x 0.5" pieces. These pieces were then sewn into the four corners of the TENG. Sewing was chosen over tape and glue because sponges have difficulty adhering to glue and tape. The first iteration of one layer of sponge with four corners is shown in Figure 101 below.

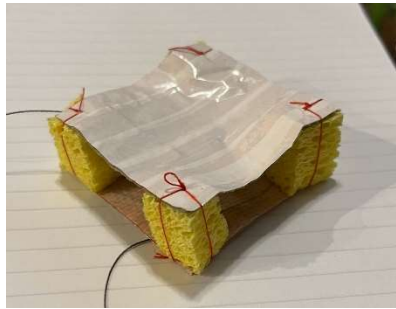


Figure 99: Image of Sponge Four Corners

Another iteration was made by cutting the sponges to half their original height, seen in Figure 102. This decision was made to see how the height of the sponges affects the voltage. The half layer of the sponge was constructed the same way as the other sponge iteration, with four pieces of sponges in the four corners of the TENG.

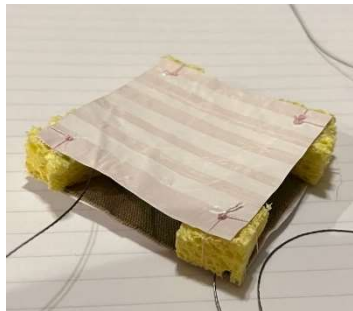


Figure 100: Image of Sponge Four Corners Half Height

The last sponge iteration, seen in Figure 103, was made by having only one piece of 0.5"x0.5" in the middle of the sample. The point of only one sponge is to increase the surface area of the TENG. By only having a singular sponge, the impact can only be applied directly to the center, or the positive and negative layers do not overlap each other perfectly.

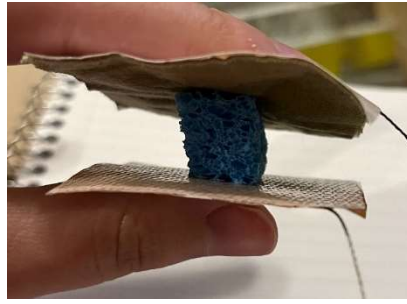


Figure 101: Image of Sponge in Center

When the sponge samples were exposed to air, we noticed that they seemed to dry out and become brittle. This became an issue for testing because the sponges were no longer compressible making it harder for the positive and negative sides to touch. Thus, we constructed another sample made with polyurethane foam. These foams were cut into four 0.5"x0.5" samples for the four corners of the TENG. As the force was applied, the foam compressed and decompressed more efficiently than the sponge.

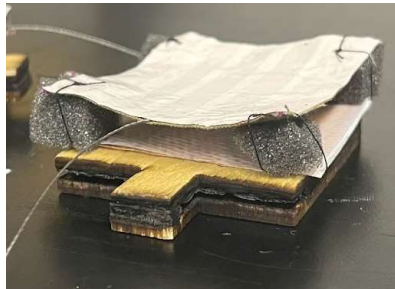


Figure 102: Image of Foam Four Corners

All these iterations were placed under the automated tester with the oscilloscope attached to record the voltage. The automatic tester was set at the same pressure value of 100 psi to ensure the impact and frequency stayed the same. The tests were run for 30-60 seconds and then the data was recorded on the oscilloscope and saved on the flash drive for analysis.

6.3 Results for TENG Iterations

The saved data from the oscilloscope was exported to excel for analysis. The oscilloscope gave a time versus voltage, which was graphed with voltage as the y-axis and time as the x-axis. During this stage, the automated tester and the surrounding environment produced a large amount of noise in the data. This noise was around -100 millivolts and 100 millivolts. Using a filter, all data points from that range of -0.1V to 0.1 V were removed and only the points out of that range were plotted. This difference can be illustrated in Figure 105 below, as the second graph only has the data from the impact of the automated tester on the TENG.

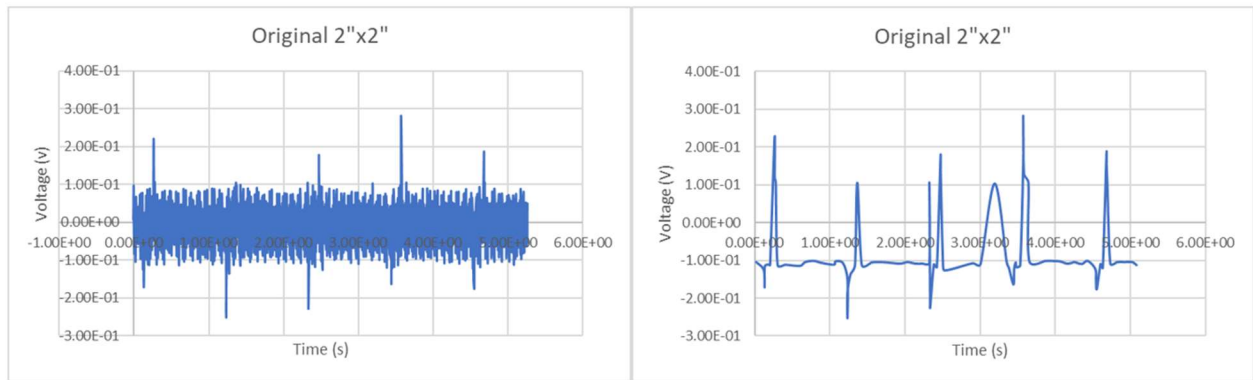


Figure 103: Filtering Out Noise from Data

Once filtered, the average positive value and negative value were calculated. The difference between these two values was the average peak-to-peak voltage, which shows the average output that each impulse will produce. Along with this data, the maximum and minimum values were collected to determine the maximum peak voltage. All this data is summarized in Table 7. Additionally, the average peak-to-peak voltages of all the samples were graphed on a histogram. With both these peak values, along with the graphs of each sample, decisions were made about the prototypes and final design.

	Max (V)	Min (V)	Max Peak-to-Peak (V)	Average Positive Value (V)	Average Negative Value (V)	Average Peak-to-Peak (V)
Original	.282	0.252	0.534	0.145	-0.121	0.266
Wire Through	.684	0.206	0.890	0.365	-0.145	0.510
Folded Once	.344	0.459	0.803	0.167	-0.154	0.322
Folded Once Unfolded	.390	0.401	0.791	0.197	-0.161	0.358
Folded Twice	.218	0.157	0.375	0.131	-0.117	0.249
Folded Twice Unfolded	.489	0.498	0.987	0.192	-0.166	0.358
Folded Three Times	.573	0.723	1.30	0.300	-0.262	0.561
Folded Three Times Unfolded	.516	0.653	1.169	0.183	-0.146	0.329
One Layer Sponge Center	.279	0.175	0.454	0.122	-0.113	0.235
One Layer Sponge Four Corners	.183	0.274	0.457	0.134	-0.150	0.284
Half Layer			0.313	0.128	-0.113	0.242

Sponge Four Corners	.161	0.152				
One Layer Foam Four Corners	.784	0.319	1.10	0.211	-0.128	0.338

Table 9: Results from All Iterations

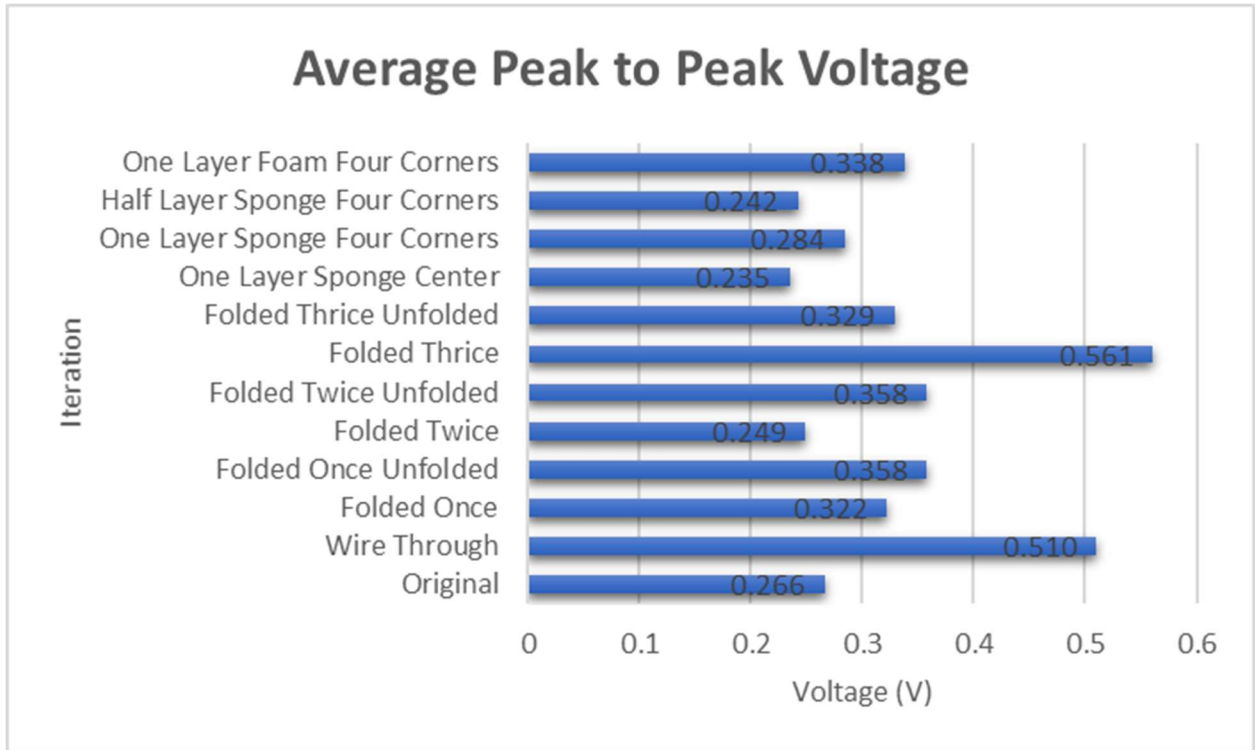


Figure 104: Average Peak-to-Peak for Iterations

6.3.1 Influence of Wire Geometry

The wire iteration outperformed the original sample with the average peaks being 0.510V over the 0.266V produced by the original sample. Adding a wire through the entire sample nearly doubled the voltage output per impact. The increase in voltage is due to the additional wire in contact with the triboelectric material and copper. This additional area not only allows for the wire to capture the electron transfer at a faster rate but creates a small gap in the PTFE that is compressed and released in each step. The data for both can be seen in the comparison graph below. The maximum and minimum peaks range from 0.2V to -0.2 volts for the peak-to-peak of 0.4V for the original sample with only the wire at the end. Wire through produced a voltage with peaks from 0.5 volts to -0.2V for a peak-to-peak of around 0.7V. Moving forward, all tested samples had a wire looped through all the samples as the data suggests an increased voltage through adding additional wire.

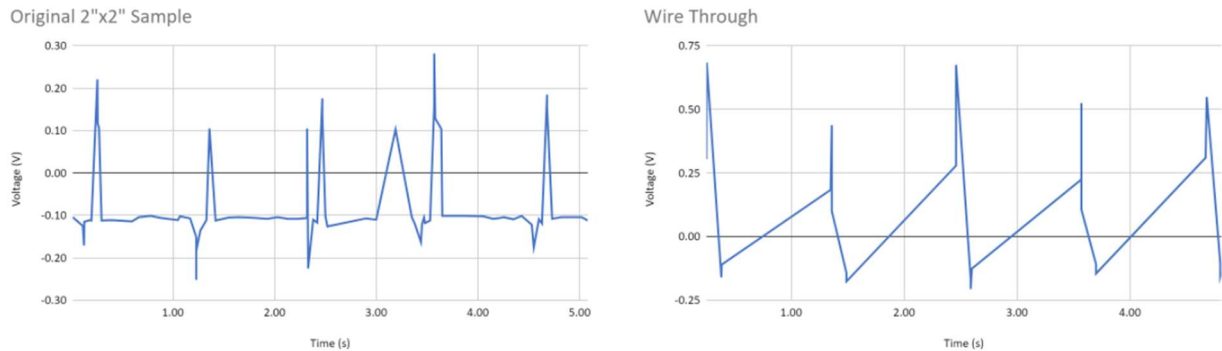


Figure 105: Graph Comparison of Original Sample to Wire Through

6.3.2 Folded Iterations Results

Folding the TENGs allowed the effect of a gap and increasing surface area to be tested. As shown in the equation, the voltage should drop with increased surface area. However, as the voltage increases with the folds that means that the folds help to create a large voltage while the surface area will improve the current of the TENG. The first iterations were the singular folds. The tested unfolded sample produced an average peak-to-peak voltage was 0.358V which was less than the singular 2”x2” sample of 0.510V. This iteration was approximately half the voltage and doubles the contact surface area of the wire through the sample. This suggests that the surface area does reduce the voltage of the TENG. The single folded sample produced a voltage that stayed around the same with an average peak-to-peak voltage output of 0.322V. Shown from the graphs, the folded once has a more uniform voltage difference between the negative and positive peaks. The more uniform voltage allows for easier rectification as it models the AC current more directly.

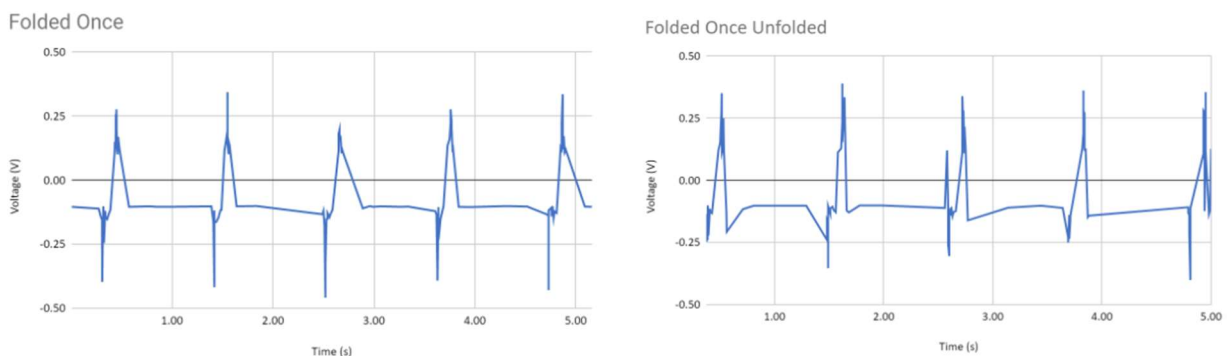


Figure 106: Comparison Once Folded to Unfolded Iteration

The double-folded TENG sample produced the least favorable results of the three different types of fold. The voltage did not drop with an increase of surface area from the last iteration of once folded. The average peak-to-peak voltage was the same value for the unfolded sample and double unfolded sample. This implies that at a certain surface area other variables affect the voltage more than the contact area. When folded twice, the voltage dropped below the unfolded average peak-to-peak voltage to an average peak-to-peak voltage of 0.249V. The data for the double-folded sample is pictured below in Figure 108. The maximum peak-to-peak for the double-folded was only 0.375V which was less than the unfolded by around 0.5V. We hypothesized there is interference happening with the layers interacting to

reduce the voltage. One of the positive sides or negative sides could have contact with the acrylic tape that would create no voltage when in contact.

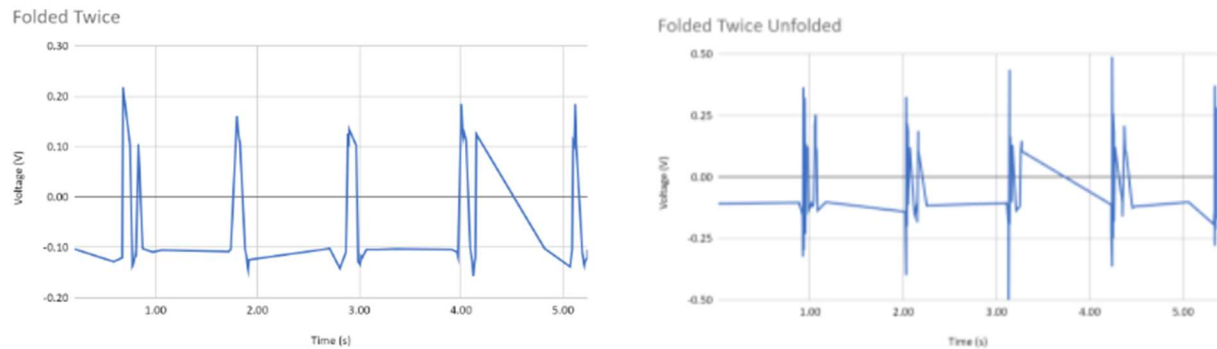


Figure 107: Graph Comparison of Double-Folded to Unfolded

The three-fold sample produced the best results of all the iterations. The three-fold average peak-to-peak voltage output was 0.561V with the maximum peak-to-peak being 1.30V. The unfolded sample produced a voltage that followed the same trend as the other folded iterations and had a peak-to-peak voltage of around 0.329V. Folding the TENG samples increased the average and maximum voltage output by 0.2V. Figure 110 pictures the folding, creating a more uniform peak output from both the positive and negative voltages. Our team theorized the three-fold sample produced its results because the PTFE was bent three times, allowing two of the bends to be on the same side. The two bends found in the sample worked together to resist the folding and push the TENG apart after the force was applied. This force allowed the separation needed to increase the voltage. The results of this test allowed for the folded three times to be integrated into the prototypes and the final design.

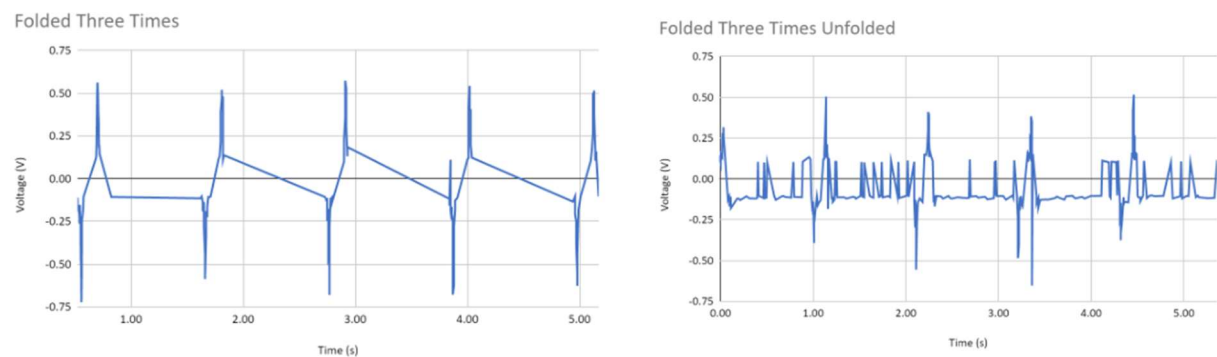


Figure 108: Graph Comparisons of Triple-Folded to Unfolded

6.3.3 Inducing Spacing Between TENG Layers

Sponges were used to test the effects of adding spacers within a TENG design. At full compression, the TENGs still had a slight separation because the sponges act as a barrier, keeping the materials from touching. In addition, as the tests continued the sponges started to deform and compress at angles instead of linearly. This shift prevented the positive and negative layers from overlapping correctly and led to the data below. All have small voltage readings around -0.15V to 0.15V. These low

values led us to discontinue developing and testing TENG samples with a sponge as the spacer material. Instead, we moved forward with the other iterations in the prototypes. Furthermore, the sponges would not be a good addition to the prototype design because the sponges are susceptible to damage easily or come apart from the sewn string, affecting the longevity and durability of the prototypes. These results are shown in Figure 111 below.

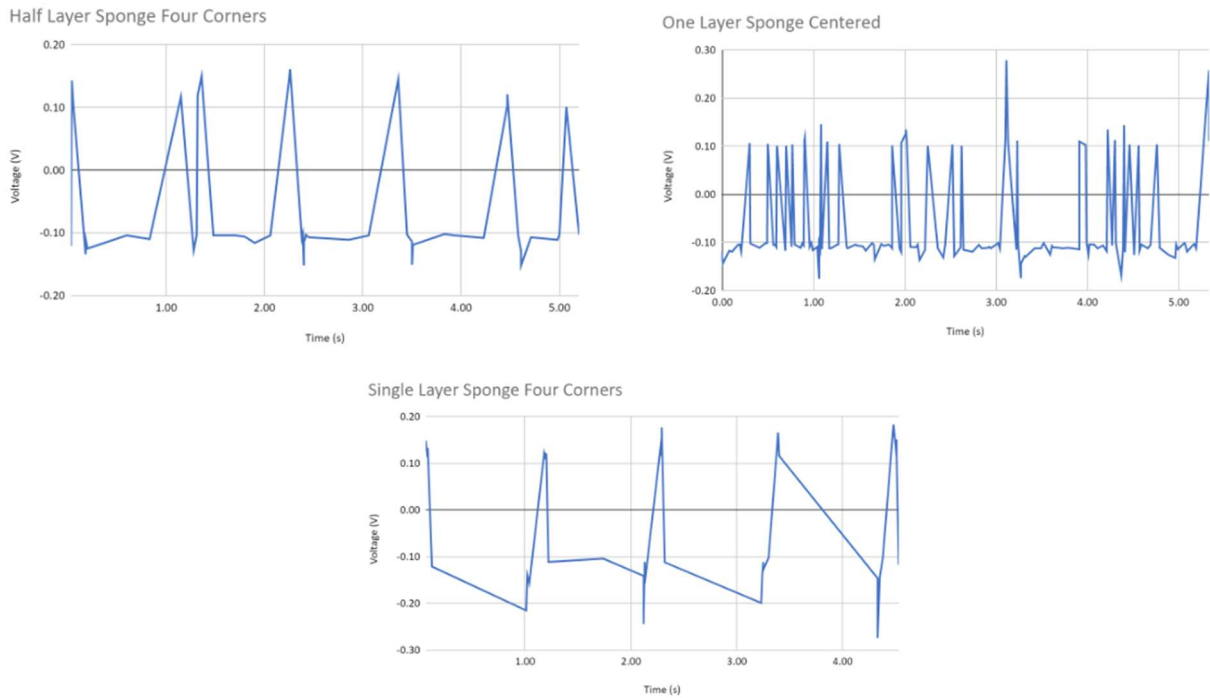


Figure 109: Comparison Graphs of Sponge Layers

The graph below compares the polyurethane foam corners to the sponge corners. The foam corners produced better results than the sponges with an average of 0.338V applied peak-to-peak. The foam corners allowed for more compression on the TENG, creating more contact between the surfaces. The results from the foam corners were still not promising compared to the folds, thus the iteration was not continued through the prototypes.

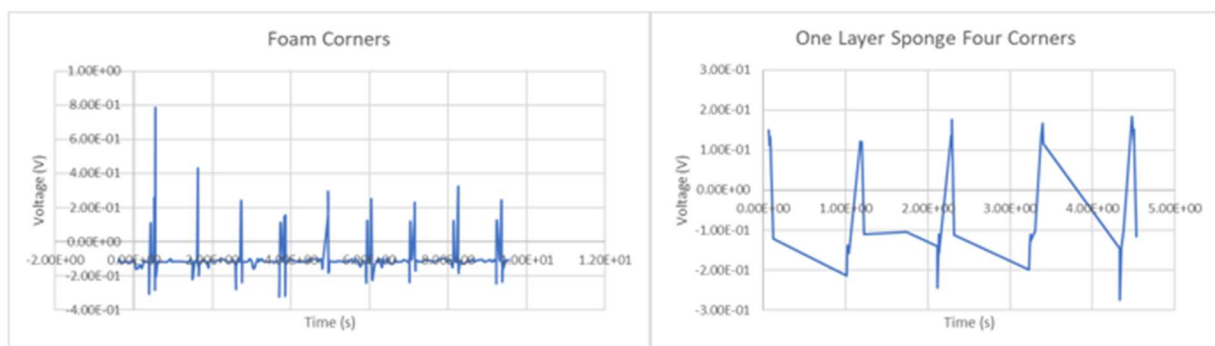



Figure 110: Comparison Graphs Foam vs Sponge



This iteration process aided the team in the design of the final TENG configuration and prototype design. Based on the results, the most successful iterations were increasing the wiring throughout the TENG as well as folding the TENG three times.



Chapter 7: Prototyping Stage One

The end goal of this project was to create a TENG system that can be integrated into soldier's footwear to power an external device. This was first accomplished by establishing where the TENG material would be placed in the foot. Three separate rounds of prototypes were conducted to narrow down the optimal location as well as design as TENG design. We started the design process with initial brainstorming, then iterations of promising TENG placements were conducted.

7.1 Initial Design Concepts

During the initial brainstorming session, our team began by identifying areas to insert a TENG for optimal performance. After this brainstorm period we identified five prototype concepts: the sock, the insole, a sock-sole combination, the midsole, and the bottom of the shoe. In the application of an Army boot, our team decided that the bottom of the shoe would not be the best application due to a potential lack of traction from the TENG materials. The two materials have less friction and grip than the rubber sole, which makes it harder for a soldier to walk in. With the remaining prototype concepts, our team formulated basic designs and weighed the pros and cons associated with each concept.

Our first idea was to embed the TENG into a slit made in the rubber midsole on the boot. A rough sketch of the idea is seen in Figure 113. The rubber would act as insulation for the TENG allowing there to be space to separate the layers of the TENG while providing a barrier between the environment and the soldiers' foot. The circuitry would be placed beneath the crease line of the boot and the battery would be placed above the crease line in a zipper pouch. The pros of this design are its durability, insulation, and ability to increase space. The cons of this idea are that it would be hard to manufacture, it could compromise shoe support, and the shoe/TENG would be hard to replace.

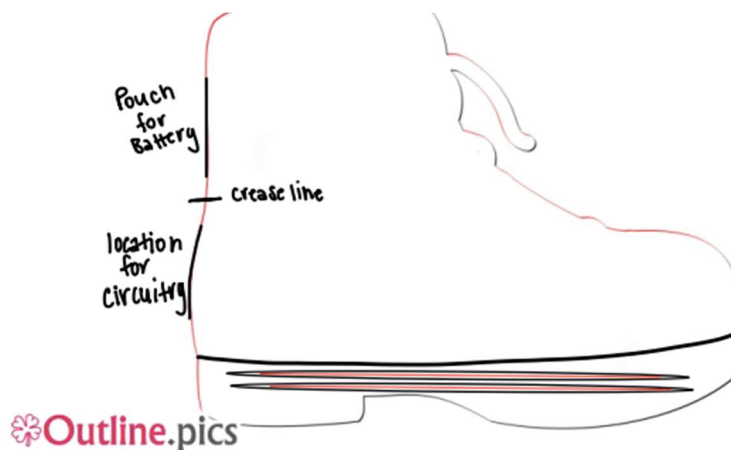


Figure 111: The Basic Midsole Design Idea

For the basic sock design concept, the TENG would be placed at the bottom of a sock. In this design, the TENG would be integrated into the sock instead of the boot. A sketch of the idea is shown in Figure 114. The circuitry would be placed near the calf when the sock is worn. Furthermore, the battery would be attached to the sock by a strap, velcro, or a clip mechanism. The pros of this design are low

cost, easy replaceability, there would be no boot modification, and the circuitry would be contained to the sock. The cons of this idea are that it could be hard to implement the circuitry, weak tensile strength, and moisture possibly affecting the operation.



Figure 112: The Basic Sock Design Idea

The sock-insole design concept attaches the layers of the TENG to both the sock and insole of the boot. The rough sketch is shown in Figure 115. One layer of the TENG would be attached to the bottom of the sock while the other would be attached to the insole. The circuitry could either be placed on the boot or be printed on the sock. This would be the same for the battery placement. The pros for the sock to insole design include ease of implementation and the ability to create more gap space. The cons of this idea are possible slippage, inconsistencies in the gap between TENG layers from different levels of wear on the boots, moisture build-up that could cause potential circuitry malfunctions.



Figure 113: The Sole to Sock Design Idea

Finally, the basic sole design concept integrates the TENG into the insole of the boot and is similar to the previous team's design. Figure 116 shows the rough sketch of the design. The TENG could potentially be the insole of the shoe or could be an additional insert on top or below the original boot insole. The circuitry and battery would be implemented in the same way as the midsole design idea. During this concept stage our team thought of another TENG configuration that involves using spacers, shown in the top right corner of Figure 116. The spacers would help create a gap and maximize surface area. The pros of this design idea include the guarantee of last year's research and ease of manufacturing. The cons of this design include the need for an insulator material, moisture, and its alteration options.

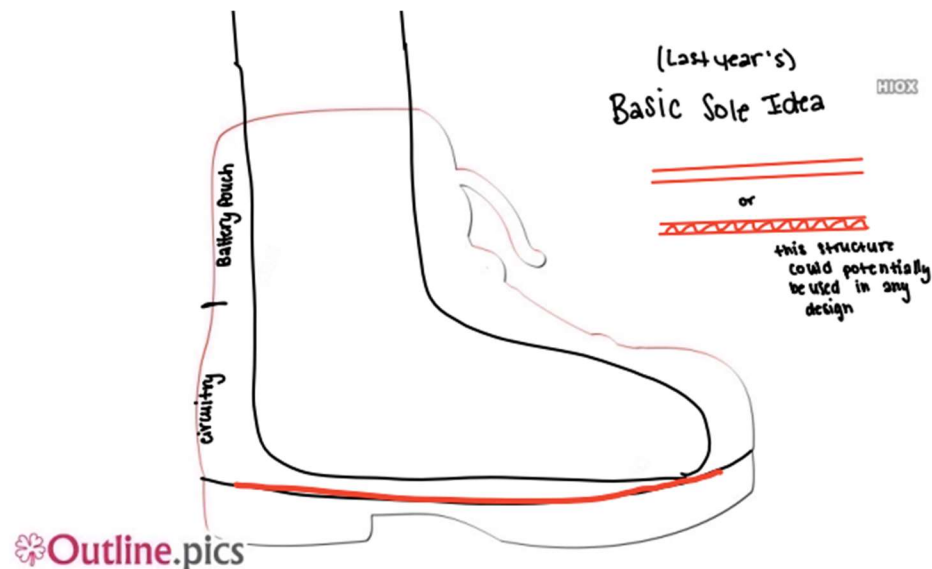


Figure 114: The Basic Sole Design Idea

After this ideation stage, our team built the four designs to evaluate which one would be the most effective. The first prototype stage only evaluated the effect location of the TENG had on the voltage output. This was accomplished by creating a simple TENG iteration.

7.2 Stage One Prototype Construction

In stage one of the prototype building, the team created all four of the original design ideas using the camouflage fabric and PTFE with copper and acrylic tape. We used the 3-ply wire thread between the fabric and copper tape layer of the TENG. For this iteration, the wire was only placed at the back edge across where the heel would go. The wire leads were about five feet long and insulated using electrical tape.

7.2.1 Midsole I

For the initial midsole prototype, our goal was to separate the rubber sole from the rest of the shoe, place the TENG pair within the cut, and secure the shoe back together for testing. The tough

material in the rubber sole was cut through using a handsaw. The TENG was placed within the cut and was secured using rubber bands for the walk test. The prototype without the rubber bands is shown in Figure 117.



Figure 115: Midsole I Prototype

7.2.2 Sock I

For the initial sock prototype, the goal was to create a pocket at the bottom of the sock to encase the TENG pair. The team took two socks and cut one into what resembled a low cut sock. The constructed prototype is shown in Figure 118. The camouflage fabric layer was sewn onto the bottom of the full sock and the PTFE layer was sewn into the bottom of the cut sock. This was done to aid in the gap space and to keep the layers secure. The two socks were then sewn together to complete the TENG sock.



Figure 116: Sock I Prototype

7.2.3 Sock-Insole I

The sock-insole prototype design was intended to maximize the gap between the TENGs by attaching one layer of the TENG to the sock and the other to the sole of the shoe. As the user walked, the sole of the foot - and therefore sock - would separate from the sole of the shoe and the separation of the TENG pair could produce higher outputs. For this prototype, the camouflage fabric layer was sewn into the bottom of the sock while the PTFE layer slipped into the shoe like a normal insole. A photo of the camouflage fabric layer sewn into the sock is shown in Figure 119.



Figure 117: Sock to Insole I Prototype

7.2.4 Insole I

The insole prototype was modeled based off the previous team's STEP design. Both layers were inserted into the shoe just as a regular insole would be. A photo of the TENG pair with the boot is shown in Figure 120.

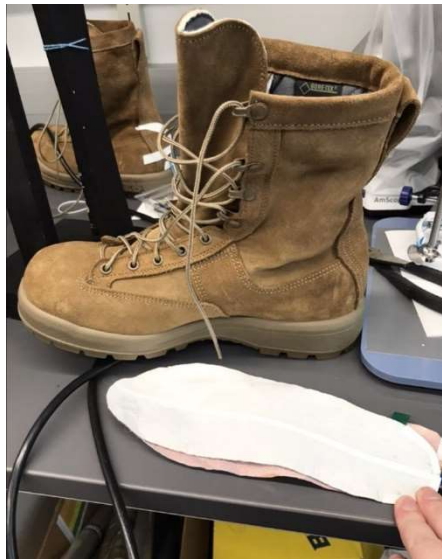


Figure 118: Insole I Prototype

7.3 Stage One Prototype Tests and Results

There were two tests performed in the first round of testing. The first test performed was a walking test in which the prototypes were worn and tested using a treadmill to evaluate the comfort level and structural integrity. During this test, the evaluator would be wearing the prototype on one foot and a regular shoe on the other for comparison. We then used the automated tester to evaluate the voltage outputs. For this stage of testing, the TENGs were attached to the self doubled rectification (SDR) circuit. Though we had not determined which rectification circuit would be best applied to our

prototype, we chose to test the initial prototypes with the SDR circuit due to time constraints. While testing the TENG pairs with circuits early on, the full wave rectification (FWR) circuit would often fail due to a blown diode or capacitor. Rather than spending time troubleshooting and repairing the FWR circuit, our team chose to solely use the SDR circuit in this testing stage. The outputs were compared, and improvements were discussed. These discussions helped us to decide which design to continue with.

7.3.1 Midsole I

Both walking and impact tests were performed on the midsole prototype and the results were discussed by the team. During the walking test, it was quickly evident that the rubber bands were not adequate in securing the midsole. The team predicted that rubber bands would not be a sustainable choice but a necessary one this early in the prototyping process. While walking, the TENG layers would slip out of the sides showing a need for a better securing method. The wearer stated the boot was still comfortable to wear and that there was not a noticeable difference between the altered and the unaltered shoe. During the automated testing, the camouflage fabric layer was secured to the top wood plate while the PTFE layer was placed on the unattached midsole as shown in Figure 121.



Figure 119: Midsole I Prototype Automated Testing

Though the separation between layers not in contact was significantly larger than would occur in an actual boot prototype, we deemed this initial test design to be appropriate as the frequency and impact was kept constant and accurate to that of a walking soldier. Each impact transferred 350 lbs of force on the TENG pair. We noticed the PTFE layer was secured poorly during this test. Due to the layer being lightweight, the PTFE would move slightly during and after each impact with the camouflage fabric layer. This caused certain areas of the TENGs to not come into full contact with the opposite layer of the pair. This had a detrimental effect on the output voltage, since the contact area directly correlates to power output. Though the interface was able to rectify positive output signals, the power output did not correlate with our intended output. Figure 122 below shows the voltage output of the midsole prototype.

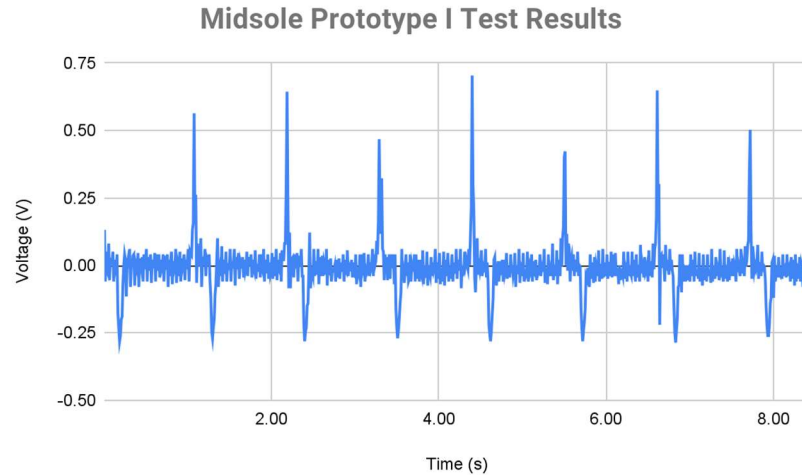


Figure 120: Midsole I Prototype Test Results

Ideally, this signal output would have linear behavior like the circuit when powered by the oscilloscope. Instead, the voltage would oscillate between values of 0V and around 300mV. The average peak-to-peak voltage output for this prototype was 0.109V. The circuit produced two negative voltage spikes with a magnitude similar to the positive peaks. These two points were filtered out of Figure 122 shown above. The prototype was tested for 17.4 seconds however we predicted no change in signal output would occur through a longer test time frame.

7.3.2 Sock I

Both walking and automated tests were conducted on the sock TENG prototype. During the walking test, the wearer stated that the prototype felt like he was wearing two thick socks otherwise felt the same as the regular sock. The test was not long enough to evaluate how moisture would impact the comfort or performance of the TENG pair. The set up for the automated test is shown in Figure 123. The sock was placed on the same bottom sole used for the midsole prototype to simulate actual conditions of a boot during walking.



Figure 121: Sock I Prototype Automated Testing

The evaluation of the initial sock prototype was run under the same circumstances as the midsole test. Each impact exerted 350lb of force, and the separation remained consistent throughout the test. Since both TENGs were sewn inside of the socks, the pair was unable to be shifted. This ultimately impacted the TENG pairs' contact. Though these constraints were set up for a fair evaluation of this prototype, the voltage output was the worst of the four prototypes tested. Figure 124 below illustrates the inconsistency of the voltage output.

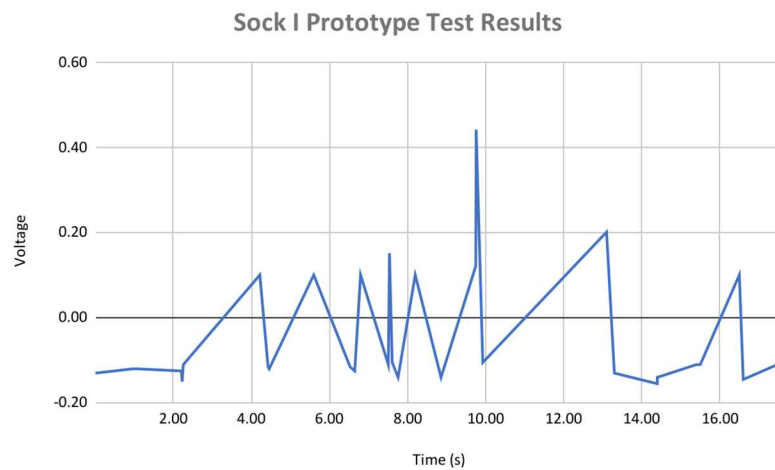


Figure 122: Sock I Prototype Test Results

The sock prototype output an average peak-to-peak voltage of 0.282V per impact, however at times the voltage would spike higher. Another issue was these spikes still did not match the voltage peaks or even the average voltage output of the midsole tester. Our group theorized that static electricity build-up was a factor that interfered with the voltage output. The wearer stated that the overall comfort of the sock prototype was quite uncomfortable as the TENG pairs would slide against each other often.

For these reasons, our team ranked this prototype the worst overall after comparing its performance to the other prototypes.

7.3.3 Sock-Insole I

Both tests were performed on the sock-sole pair and the results of each test were discussed. During the walking test, the user stated that the prototype boot felt the same as the unaltered boot. There was also no slippage between the layers during movement. While it was hypothesized that moisture would affect performance, the walking test was not long enough to notice whether sweat would impact the TENG's performance or comfort.

This prototype concept was evaluated by sewing the camouflage fabric TENG to a sock and then adhering that to the impact face of the pneumatic tester. The experimental setup is shown in Figure 125. The PTFE TENG was adhered to the boot sole cutout. This setup was modeled to mimic the TENG pair being between a soldier's sock and the insole of the boot. Aside from this test, a team member further evaluated this prototype by wearing the sock and putting on a soldier's boot with the PTFE covering the top layer of the insole. The recorded qualitative remarks were similar to those of the Midsole I prototype. The prototype did not alter the overall feel of walking aside from slippage at times. This was noticed more frequently while running with the prototype. Quantitatively, the sock-insole pair performed consistently. Figure 126 below plots the voltage output of the sock-insole prototype over a 12.5 second time frame.



Figure 123: Sock to Insole I Prototype Automated Testing

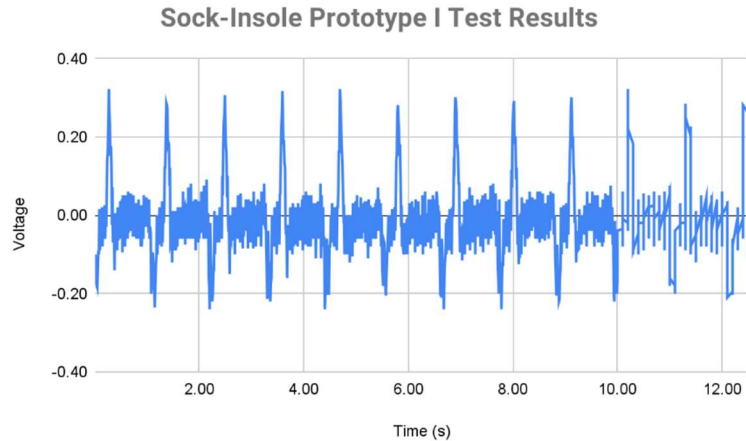


Figure 124: Sock to Insole I Prototype Test Results

The average peak-to-peak voltage for this prototype test was 0.367V. The signal output peaks were also consistent in structure, with the only major variation being the slight difference between peaks. This consistency was considered a positive, as symmetrical voltage peaks have a low chance of producing signal interference across rectification circuits. This ensures optimal voltage peaks across the resistor load substituting for an ideal rechargeable battery.

7.3.4 Insole I

The walking and automated testing were performed on the insole TENG and the results were discussed. During the walking test, there was some slippage during the steps. The slippage occurs between the TENG layers and between the wearer's sock and the acrylic tape. Other than that, the wearer reported no discomfort with wear. During the automated testing, the TENG layers were placed on the bottom wooden platform. This is pictured in Figure 127.

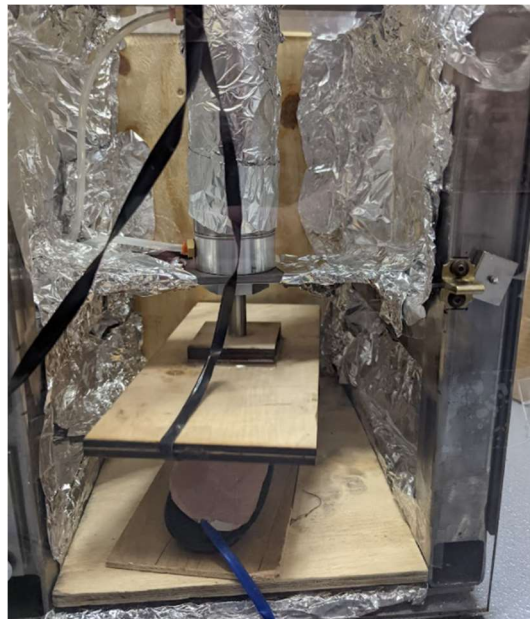


Figure 125: Insole I Prototype Automated Testing

The impact test for the insole prototype was performed under the same parameters as the previous three experiments. We theorized the impulse per step played a large factor in the power output of the TENG pair. Since the insole is a rubber material with elastic properties, we assumed a lower impulse magnitude compared to the midsole prototype since the two layers for the midsole prototype are more stiff and rigid. Figure 128 below shows the voltage output peaks per impact for this test.

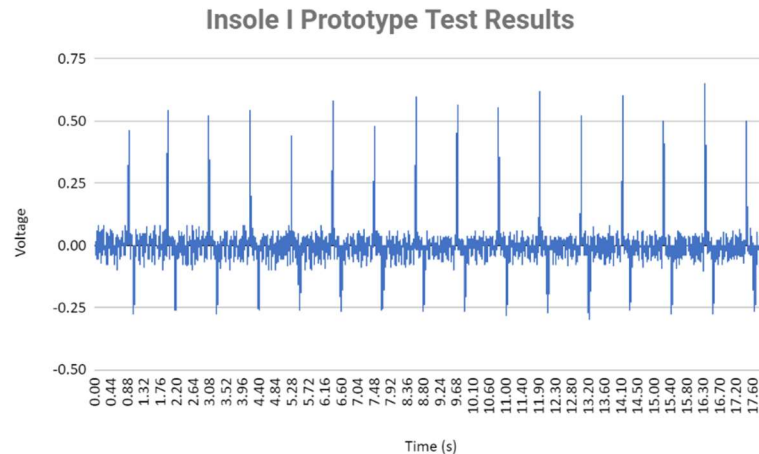
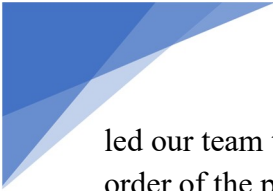


Figure 126: Insole I Prototype Test Results

Our team correctly predicted the relationship between the midsole and the insole prototype. Magnitude wise, the highest peak voltages were competitive with the midsole prototype. The average peak-to-peak voltage output for this trial was 0.553V. However, the midsole prototype peaks were more consistent. Referring back to Figure 122, the output consistently peaked around 400mV, while the insole prototype output would peak at 250mV occasionally. Despite the comparison to the midsole prototype, our team ranked the insole prototype's performance above the sock prototype's performance. This decision was made based on quantitative results as the insole prototype had more consistent peaks of a higher magnitude. The sock-insole prototype had more consistent and higher voltage outputs, so it was ranked above the insole prototype in quantitative data. Though with regards to qualitative data, the insole prototype was significantly more comfortable to wear than the sock-insole prototype.

7.4 Stage One Prototype Conclusions

With the completion of the first stage of prototype development/testing stage, the two prototypes were eliminated. The sock prototype was ranked at the bottom due to its signal inconsistency and low voltage output peaks. Though the sock-insole prototype was the highest performing from a quantitative standpoint, the user discomfort made it less preferable. Our team also predicted replacing this type of prototype would be tedious. Since a TENG pair was sewn to the sock, the process of replacing the sock with a new TENG would be quite time consuming. The alternative of replacing the sock-TENG with a brand new one would not be cost-efficient. Our team believed the replicability of the midsole and insole prototypes to be far simpler. Despite better quantitative data, other qualities of the sock-insole prototype



led our team to rank the midsole and insole prototypes above the sock-insole prototype. Our ranking order of the prototypes was midsole, insole, sock-insole, and sock. Being the highest ranking, the midsole and insole prototypes advanced to the next development testing stage. In this stage our team sought to further refine both prototypes to optimize their voltage outputs and use.

Prior to moving to the second stage of prototype development and testing our team discussed improvements. These improvements were made in hopes of the performed tests representing the forces and pace of a soldier walking while also generating the best possible data. While we intended to integrate and interface the TENG pairs with the rectification circuits we decided to exclude the rectification circuits from the second testing stage. This decision was made in order to best evaluate the magnitude peak-to-peak voltage output of the TENG pairs within the prototypes tested. Components within the circuit such as diodes had voltage drops due to their internal resistance. The circuits were not able to rectify a linear direct current like what was produced when utilizing the oscilloscope as the circuits' power source. Regardless of the exclusion of the circuits the peak-to-peak voltages produced by the prototypes would still provide insight on the overall power the prototypes would provide to an external load interface.

Chapter 8: Prototyping Stage II

During the second stage of prototyping the team explored further options for the insole and midsole designs. For testing, the prototypes were worn to test wearer comfort and then tested using the automated tester for numerical results.

8.1 Stage Two Prototype Construction

After the first round of prototyping and testing of various TENG configurations, our team decided to implement one TENG iteration to test both the insole II and the midsole II prototypes. The TENG was a larger version of the three-fold TENG built and tested in Chapter 6. As shown in Figure 129 and 130, the camouflage fabric layer was constructed to fold along the toe and heel while the PTFE layer was constructed to fold on the sides of the foot. These two layers folded together are pictured in Figure 131. Some flaws of the design include the size and the weight of this TENG. After construction, the TENG had excess material that resulted in issues fitting within the confines of both the midsole and the insole. After construction of the TENG, our team noticed that the amount of material seemed to weigh down the TENG layers and this caused concern for the gap between them.



Figure 127: Camouflage Fabric Layer Prototype II



Figure 128: PTFE Layer Prototype II

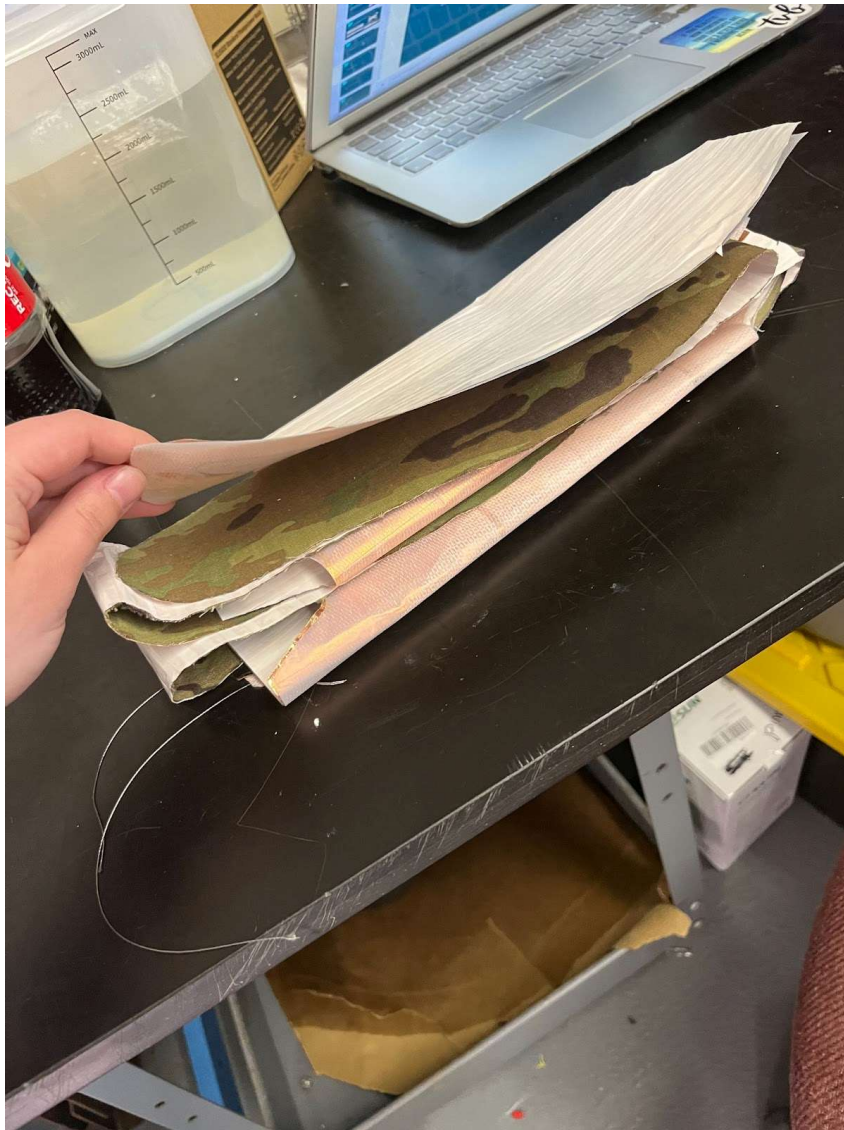


Figure 129: Prototype II TENG Layers

When constructing the insole prototype, the TENG proved to be too large for the boot. It was hard to insert and fit quite snugly when inside. There were no alterations to the boot itself for this prototype.

When constructing the second midsole prototype, adhesive was not used in this iteration due to supply and time constraints. The TENG size was too large for the midsole configuration as well. Our team milled a dent into the rubber midsole to create a gap for the TENG to rest. While carving, proper PPE needed to be worn and it took time due to the resistance of the rubber.

8.2 Stage Two Prototype Tests and Results

Before using the impact tester, both prototypes were implemented into a boot and worn to evaluate the overall comfort of each prototype. While wearing the boot, basic movements such as walking and jogging were performed. The midsole was deemed the most comfortable, as the user could not feel the slipping of the TENG. The TENG pairs used in the insole prototype were adhered to the top of the shoe insert and the bottom of the insole to prevent as much slippage as possible. Unfortunately, slippage between TENG layers still occurred, most likely due to the three-fold implementation within this prototype. The wearer noted that general movements with the basic insole prototype were uncomfortable and felt quite different than walking with an unmodified boot.



Figure 130: Midsole II Prototype Automated Testing

During the impact test, the midsole prototype was tested under the same conditions as the insole prototype. Impact force, time between impact, TENG pairs tested, and TENG materials remained consistent between experiments. The prototype was tested by adhering a shoe insert to the impact plate and the TENG pairs to the midsole cutout. Like the insole prototype, the midsole was also fully

assembled and worn by a team member. The wearer noted a significant improvement in the overall comfort of this prototype compared to the insole prototype. At times, slippage between TENG pairs would occur. However our team inferred that a better adhesive could be utilized to further minimize the slippage between these TENG layers.



Figure 131: Insole II Prototype Automated Testing

As stated before, our group decided to exclude the implementation of rectification circuits within this prototype testing stage due to the voltage drop and nonlinear signal outputs while using TENGs as a power source. After getting data from each prototype, we prioritized the peak-to-peak voltages produced per oscillation as the main evaluation criteria during experiments. Qualities such as consistency and each output signal's resemblance of a sinusoidal alternating current were also considered as factors for comparison. These factors were important for rectification circuits, which are designed to produce direct current voltages from the input of a signal with a consistent period, amplitude, and peaks.

8.2.1 Midsole II

Figure 134 below plots the voltage output of the TENG pair implemented within the midsole prototype for this stage of impact testing.

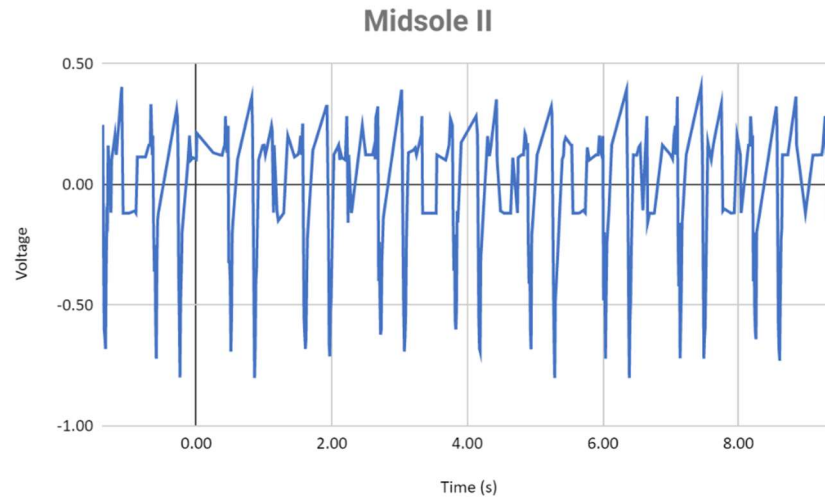


Figure 132: Midsole II Prototype Test Results

The midsole prototype produced an average peak-to-peak voltage of 0.54V per impact. Theoretically, this prototype would be capable of producing a similar DC voltage for an external electronic component such as a battery when rectified. The lowest peak-to-peak voltage produced by the prototype was approximately 900 mV. This value was still higher than the peak voltage produced by the top performing prototypes tested in the first prototype stage.

8.2.2 Insole II

Similar data was collected during the insole impact test for this prototype stage. The data acquired in this test can be seen in Figure 135 below.

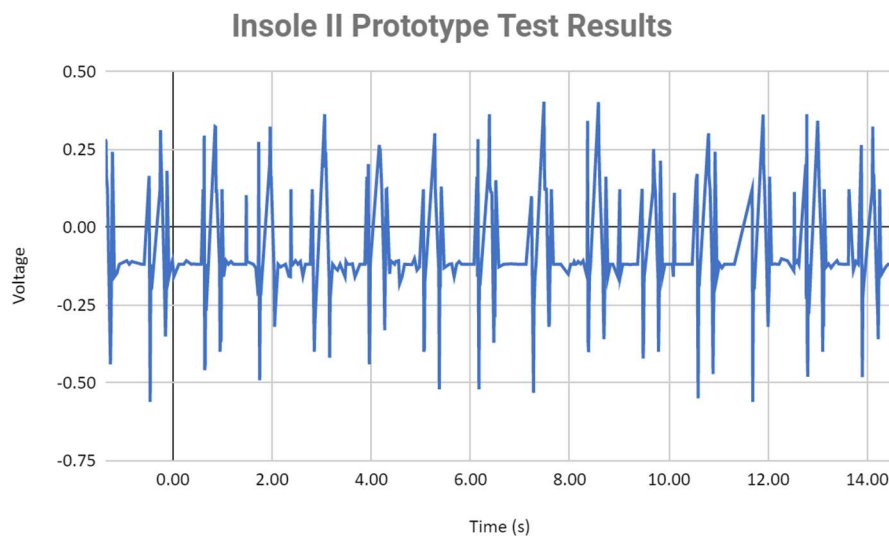
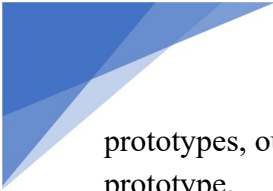


Figure 133: Insole II Prototype Test Results

Compared to the midsole prototype, the insole prototype had more inconsistent peak-to-peak voltage production which ranged from approximately 100mv to 900mv. The average peak-to-peak voltage for this prototype was 0.379V. When comparing the periods and amplitudes of the midsole and insole signal outputs, the midsole output is more ideal than the insole. In other words, out of the two



prototypes, our team concluded the midsole prototype is the most feasible for our intended final prototype.

8.3 Stage Two Prototype Conclusions

The midsole prototype was found to be the top-performing prototype at the completion of the second testing stage. With regards to overall use and comfort, the midsole prototype allowed the wearer to walk normally with minimal discomfort. On the other hand, the way the TENG pair was implemented within the insole prototype allowed the materials to slip together. This caused discomfort for the wearer. In quantitative data, the midsole once again trumped the insole prototype. The midsole prototype's largest peak-to-peak voltage was approximately 300mV higher than the insole prototype. Our group inferred that the overall stiffness of the rubber midsole played a large factor in creating a large impulse exerted on the TENG pair inserted between the two layers. This large impulse helped produce a larger voltage than the insole prototype. It was assumed that the resilience of the shoe insert in the insole prototype produced a low impulse which in return produced a low voltage output.

Following the completion of this stage our team identified key improvements necessary to further optimize our final prototype and the tests performed to evaluate its overall performance. Similar to last year's team, the voltage produced by the final prototype would be measured while a wearer used a treadmill to walk and run. This data was thought to be the most accurate to the voltage this prototype would produce when being in service.

Chapter 9: Final Prototyping Stage

The final prototype stage marked the culmination of all areas of research and development performed during this project. A hybrid TENG design was developed for this stage based on our iteration tests and evaluation. Along with the standard automated tester evaluation for this prototype, our team also recorded the voltage output of the prototype while the wearer was walking on a treadmill. The results and conclusions made from this stage allowed us to compare our results to the previous year's team and identify potential steps to take in efforts to further optimize this prototype.

9.1 Final Prototype Construction

Determining the optimal structure and features for the final design concept marked the beginning of the final prototyping stage of this project. As discussed above, we proceeded with the midsole design due to the performance and the wearer comfort. Prior to construction, design modifications that needed to be made to both the TENG and the boot were identified. To improve the overall wearability of the prototype, the midsole layers encasing the TENG pair would be adhered together. A gap was dremeled to improve the separation between the folded section of our TENG pair. A similar sized gap was dremeled to house a FPCB if implemented within this prototype. This would protect the FPCB from any environmental damage while the prototype is used.

The TENG used in this final prototype was a hybrid of a three-fold TENG and a regular TENG. Figure 136 illustrates this final iteration, and the CAD model is shown in Figure 137. The camouflage fabric layer was created in a long rectangle while the PTFE layer was created in the shape of an L. This was to create the same type of three-fold that was built and tested in TENG iterations. The small three-fold allows for a forced gap between the layers of the TENG without adding too much weight so the PTFE layer resists bending. The extra length of the three fold allows for more surface area contact to increase the current in the TENG. This design was constructed to have less surface area than the previous prototypes in order to increase the voltage.

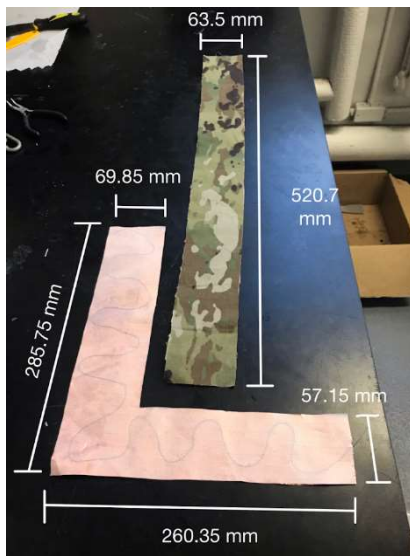


Figure 134: Final TENG Prototype

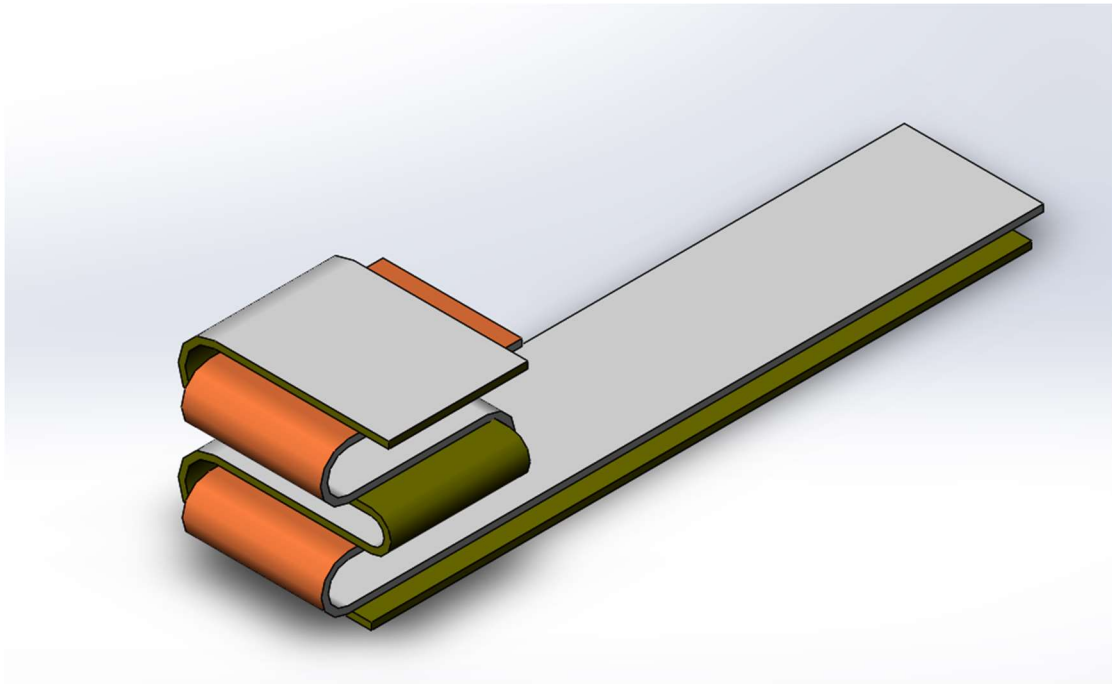


Figure 135: CAD Drawing of Final Prototype TENG

The TENG placement on the bottom cut of the midsole is shown in Figure 137. The folded section was placed near the front of the shoe, where the ball of the foot would be. We chose the bottom of the shoe because during walking it had significant flex and weight. During the walking cycle, the ball of the foot has some of the largest concentrations of force as seen in Figure 138. Looking at the chart, it is evident that the heel also has a great amount of force, but with the ball of the foot there is force for a longer time frame and it has a greater flex while walking. During the initial research, flex was reported to increase voltage due to friction and gappage. The thought process used in construction is that the three-fold should be placed in an area with the largest forces and in the largest area to fit the width of the TENG; the ball of the foot fits that criteria.



Figure 136: Final Prototype TENG Placement

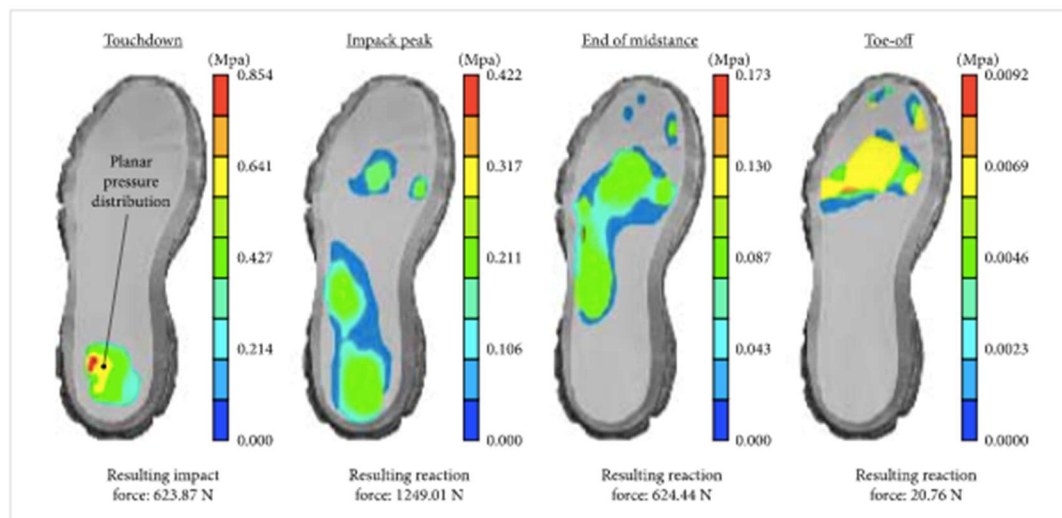


Figure 137: Force Exerted by Foot During Walking [74]

Based on the improvements discussed for the boot, several changes were made. To increase the gap, we further dremeled the cavity made in stage two prototyping. During the initial cut and the dremel/milling process, the team cut through the other material that is located between the midsole and the inside of the shoe. It is visible in Figure 140 as the white and black section of the shoe. That section of the shoe has the most gap as it will be the location of the folded section of the TENG. To house and protect the FPCB, a 55.12 mm by 55.7 mm cavity was dremeled in the heel. This is also pictured in Figure 140 along with the measurements of the midsole.

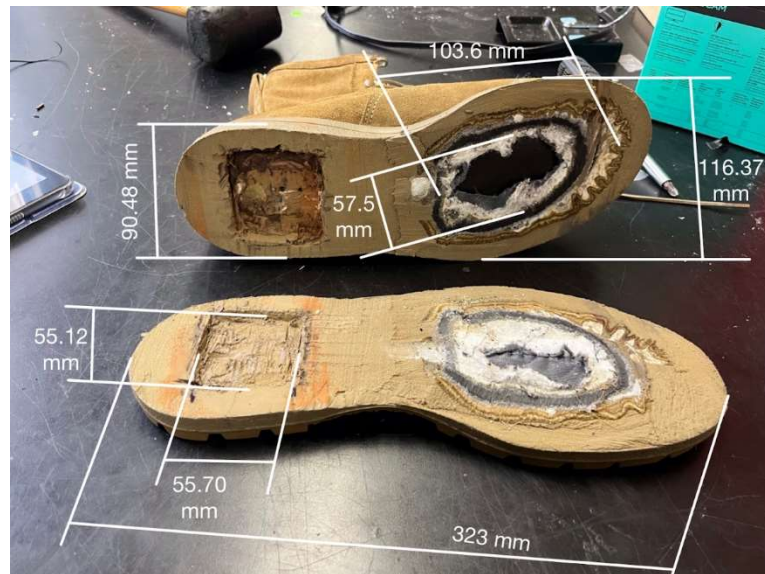


Figure 138: Final Prototype Midsole Measurements

There were several steps taken to combine the final TENG and the boot. First, the insulating tape side of the TENG layers was glued to the midsole. The team did this to aid in the gap and better secure the TENG within the midsole. Then our team needed to figure out a way to secure the midsole together. Initially, glue was to be used to hold the midsole layers together around the TENG. Potential issues with glue include the inability to reach the TENG or the FPCB after gluing and the risk of placing an element wrong without the ability to easily fix it. Due to these potential issues, our team decided to use screws to secure the midsole instead. The screws were easily removable and allowed the team to make last minute changes if needed. The placement of these screws is pictured in Figure 141.



Figure 139: Screw Placement on Final Prototype

9.2 Final Prototype Tests and Results

To compare the overall improvement of our STEP prototypes we tested the final prototype using the automated tester. The same input conditions were held for this final stage of testing as they were for the first two stages of prototype testing. Figure 142 below plots the voltage output of the final prototype.

Midsole III Prototype Test Results

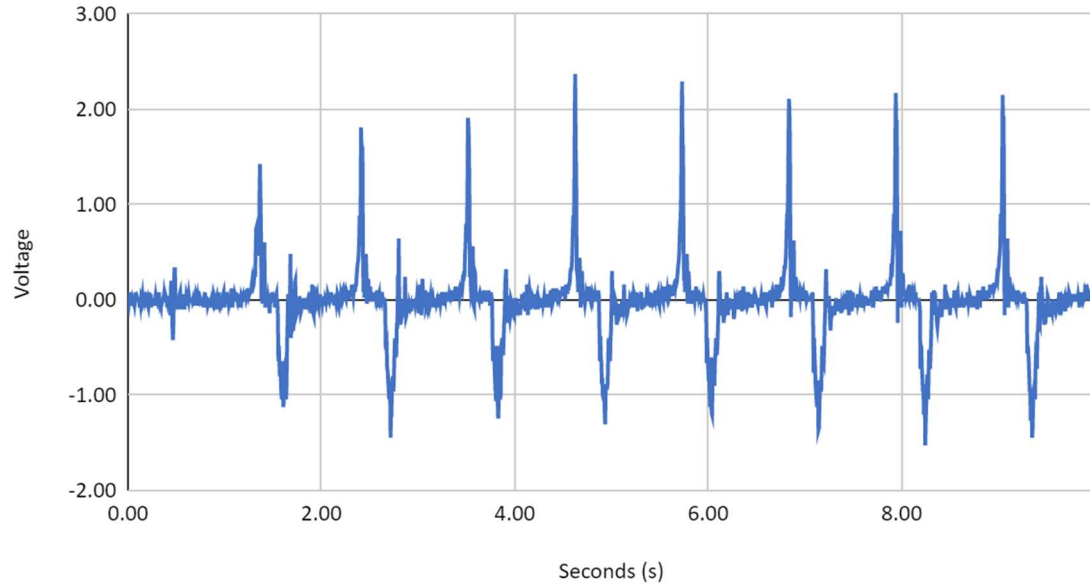


Figure 140: Final Prototype Test Results Automated Tester

This prototype produced a higher voltage than any other prototypes tested during this project. The average peak-to-peak output for this prototype test was 1.561V. The second highest voltage recorded was 1.2V which was produced by the second midsole prototype. This data attests that the midsole prototype was the best performing out of the for designed STEP applications tested in this project. The voltage output of the final prototype also behaved similar to an ideal AC current. Though the magnitude of the positive and negative peaks were never exactly the same, the period stayed consistent. This quality was considered to be beneficial as the rectification circuits utilized were designed to produce a direct current from the input of an ideal alternating current. Following the impact tests, the final step prototype was worn and tested while the wearer walked and ran on a treadmill.



Figure 141: Walking Test Performed on Final Prototype

The peak-to-peak voltage outputs measured in this experiment exceeded the peak-to-peak voltages measured when testing all other prototypes. Figure 144 below plots the voltage outputs of this experiment over a ten second interval during the walking test.

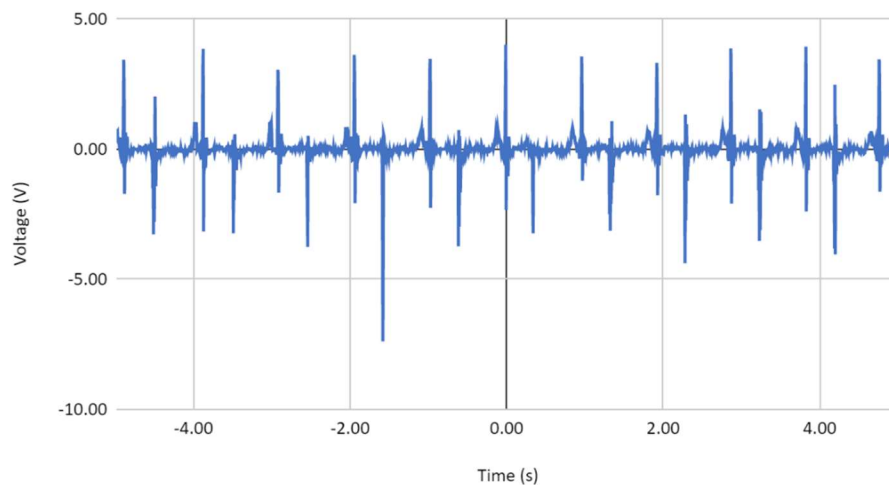



Figure 142: Final Prototype Walking Test Results

The largest peak-to-peak voltage measured during this experiment was 11.47V. This value was approximately 5V higher than the largest peak-to-peak voltage output measured when the final midsole prototype was tested with the automated tester. The average peak-to-peak voltage output for this prototype test was 6.50V. Our team hypothesized this to be a likely outcome. The TENG implemented within our final prototype was designed to undergo common force concentrations that are exerted when a person walks. Usually when a person takes a step, the ball of the foot experiences one of the largest



magnitudes of force concentrations throughout the step cycle. Therefore the three-fold section of the TENG was placed in the area of contact between the ball of the foot and the boot. In theory, the three-fold would be compressed under the one of the highest applied forces within a step cycle then decompress when no forces were exerted, and the foot was raised. Our hypothesis was deemed to be correct because of the measured voltage difference for both tests and the nature of forces applied by the automated tester and a foot during a walking cycle.

9.3 Final Prototype Stage Conclusions

The completion of the walking test for the final prototype marked the end of our development and testing stage of this project. Following this stage, team efforts were focused on further evaluating the final STEP prototype, identifying potential prototype and test improvements, and forming recommendations for teams continuing this project.

Chapter 10: Conclusion and Broader Impact

The completion of our final prototype marked the end of the prototype development stage for this year's project. The average peak-to-peak voltage produced by the final prototype was compared to the voltage output of last year's final STEP prototype. The average peak-to-peak voltage output of our team's final prototype was 6.5V. The final STEP prototype designed by last year's team averaged a peak-to-peak voltage output of 0.55V. Both of walking tests were governed by the same constants. The compared values were both obtained from a trial where the treadmill was set to 2.5 mph and a 0-degree incline. This marked an improvement of 1080% in voltage output. This improvement was derived from creating a reliable automated tester and testing the effect of multiple TENG iterations, which helped determine the best prototype concept designed at the beginning of the project. Upon reflection, our team was able to identify multiple recommendations for teams continuing this project to use as guidance towards our overall goals.

10.1 Automated Tester Modifications

In future testing, there may be a need to increase/decrease the frequency of the automated tester. This could be accomplished with a multi-position switch, which could be coded to change the delay that the automated tester uses between strikes. Another function to incorporate into the automated tester is a pause button, which would be used to temporarily stop the automated tester rather than triggering the door switch or turning off the entire circuit.

10.2 Bending Effects

The effect of bending on the TENGs voltage output could be tested next year. If the TENG is across the center of the shoe, it will experience some bending during walking. How this affects the TENG life and power output could be studied using automated or manual means.

10.3 Improved Midsole III TENG Accessibility

There were multiple issues regarding the method of detaching the midsole from the rest of the shoe. Initially, the rubber was extremely difficult to cut into, and a band saw needed to be used. The cut from a band saw is a vertical cut which limited the maneuvering that could be done to effectively remove the midsole. A shoe midsole is not usually attached in a strictly flat way due to the shape of the human foot and the supports put into footwear. The cut paired with a non-flat surface meant that the heel of the shoe had extra rubber above the cut and the ball of the shoe was cut through to the insole. We suggest researching and exploring ways to more effectively remove the midsole. Potential avenues include a handheld power tool to better control the cut and obtaining a shoe without a midsole and molding the rubber to the TENG specifications.

One of the drawbacks of the midsole design is the lack of accessibility after securing the TENG within the midsole. Our team used screws to make the prototype more accessible for alterations but that is not a long-term solution to the problem. We originally planned to use glue for the final prototype but then the TENG would have been completely inaccessible. We recommend researching and exploring ways to construct an easier access point to the midsole cut.

10.4 Improved Rectification Circuit Schematic

It was hypothesized that the rectification circuits required more components to be implemented within their design to operate as intended with the power input of a TENG. Multisim should be reevaluated to test and evaluate the implementation of components such as transistors and amplifiers for power output. This will allow the rectification circuits to take power input directly from a TENG and output a power supply suitable to charge or power an external device. Another key point to consider when designing these circuits is the dimensions of each circuit component. In other words, no component utilized should be large enough to reduce the mobility of the flexible printed circuit board. The capacitors utilized in our fabricated circuits were too large and often would snap off the substrate if bent too much. For future circuit iterations, smaller capacitors with similar electronic specs should be purchased to improve the mobility and reliance of these circuits.

10.5 Prototype Design Based on Biomechanics

Taking walking mechanics into consideration, there are certain loads that were not accounted for in the design of our final hybrid TENG. In other words, the forces exerted on the midsole of a boot are not all exerted in the same direction. Lateral-sliding TENGs could be implemented into the hybrid design iteration to allow the TENG to generate voltages from multi-axial forces. This would improve the voltage output of the midsole prototype.

10.6 TENG Current Output Measurements

The TENG iterations helped to increase the voltage for the final prototype, however, we were unable to see how the current was affected. To further this research, the next research team should research how to find the current. A simple ammeter cannot be used to read the currents because the peaks occur too fast for detection. Thus, one would need to find an ammeter that can read the quick peaks or use an oscilloscope with a circuit. This current reading along with voltage gives the power reading, allowing for better estimates of how long it will take for the battery to be charged. A successful TENG needs both a high voltage and current to charge the battery fast and effectively.

10.7 Triboelectric Material Spacing Improvements

From the equation for voltage output and our results in TENG iterations, we know that increasing the spacing increases the peak-to-peak voltage. Our group tried to increase the gap using sponges and foams. However, both methods yielded unsuccessful results. Other materials or methods should be researched to see if the gap between the two TENG materials can be increased. This could include testing TENGs that separate to different distances and comparing their voltages. Once the best distance is discovered, a material should be selected that will allow the TENG to be completely compressed and return to the set distance. This will allow the TENG to be even more effective.

10.8 Broader Impacts

10.8.1 Engineering Ethics

This project conformed to engineering ethics, as described by the code of ethics and model law of societies of professional engineering. Here, our obligation to the public was of the soldiers using the prototypes or result of this project, and our obligation to our client was of DEVCOM. We kept the health and safety of the public in mind by making sure our decision-making and design processes included injury prevention. We safeguarded the welfare of the public by focusing on cost-efficiency in our designs. Throughout this project, we have been transparent with our employer, DEVCOM. We have included all relevant information pertaining to the project and did not withhold/falsify information at any time. We had no conflict of interest during this project.

10.8.2 Societal and Global Impacts

With the delivery of a wearable prototype, mission constraints due to a soldier's electronic equipment would be loosened. Multiple sensors, communication devices, and other small devices rely on common AA and AAA batteries. If a soldier were able to charge batteries while walking, rucking, or running their overall dependence on resupplying the batteries would diminish. Beyond military applications, implementing TENGs into common footwear such as running shoes would be a breakthrough in clean energy. Portable devices such as phones could be charged while the wearer moved around through their daily routine. Further research, development, and design TENG applications could lead to an alternative clean energy option that is just as reliable as other energy sources.

10.8.3 Environmental Impacts


One of the overall goals for TENG research is to explore a potential sustainable energy source that converts mechanical forces into electrical forces. Other than the harvesting of the materials before we buy or obtain them, the building process has minimal to no waste. The implementation of a TENG within footwear would not affect any other processes or routines and therefore does not pose any immediately evident environmental detriments.

10.8.4 Economic Impacts

With our research, it is important to consider the economic costs for these TENGs. The goal of the project is to reduce the number of batteries that soldiers need to carry with them. The Army will also need to buy fewer batteries because the same ones will be able to be reused. Additionally, TENGs themselves are relatively cheap to build, meaning they can be replaced cheaply. The TENGs are made to be durable so they do not have to be exchanged often, saving costs on replacement. The way in which the TENG creates energy is free as it is harvested through the walking of a soldier.

10.9 Final Remarks

The delivery of the Midsole III prototype marked a significant step towards the production of an operational and reliable TENG-footwear application. The recommendations discussed in this final chapter can help guide future MQP teams to further expand their understanding of TENGs and appropriately within future design iterations. The application of TENGs broadens as further research and development related to TENGs is performed. Outside of military applications, TENG applications have



the potential to provide an effective alternative energy solution for problems reaching across countless areas of engineering.



Bibliography

1. Zi, Y., Wang, J., Wang, S., Li, S., Wen, Z., Guo, H., & Wang, Z. L. (2016). Effective energy storage from a triboelectric nanogenerator. *Nature Communications*, 7(1), 10987. <https://doi.org/10.1038/ncomms10987>
2. Fan, F. R., Tian, Z. Q., & Wang, Z. L. (2012). Flexible triboelectric generator. *Nano energy*, 1(2), 328-334. <https://doi.org/10.1016/j.nanoen.2012.01.004>
3. Introduction to Capacitors, Capacitance and Charge. (2013, July 26). *Basic Electronics Tutorials*. https://www.electronics-tutorials.ws/capacitor/cap_1.html
4. Lee, B. (n.d.). The Triboelectric Series—AlphaLab, Inc [The TriboElectric Series]. *AlphaLab, Inc*. Retrieved April 20, 2022, from <https://www.alphalabinc.com/triboelectric-series/>
5. Carlson, L., Cloutier, T., Patel, K., Pawlak, K., & Kalka-Riffel, A. (2019). *Harvesting Vibrational Energy*. : Worcester Polytechnic Institute. <https://digital.wpi.edu/show/707959105>
6. Liu, J., Gu, L., Cui, N., Xu, Q., Qin, Y., & Yang, R. (2019). Fabric-Based Triboelectric Nanogenerators. *Research*, 2019, 1–13. <https://doi.org/10.34133/2019/1091632>
7. Wang, J., Zhou, L., Zhang, C., & Wang, Z. L. (2020). Small-scale energy harvesting from environment by triboelectric nanogenerators. *A Guide to Small-Scale Energy Harvesting Techniques*. DOI: [10.5772/intechopen.83703](https://doi.org/10.5772/intechopen.83703)https://www.researchgate.net/publication/330948465_Small-Scale_Energy_Harvesting_from_Environment_by_Triboelectric_Nanogenerators
8. *Triboelectric nanogenerator based on vertical contact separation mode for energy harvesting*. (n.d.). Retrieved April 20, 2022, from <https://ieeexplore.ieee.org/document/8230037/>
9. Wu, C., Wang, A. C., Ding, W., Guo, H., & Wang, Z. L. (2019). Triboelectric Nanogenerator: A Foundation of the Energy for the New Era. *Advanced Energy Materials*, 9(1), 1802906. <https://doi.org/10.1002/aenm.201802906>
10. *Flexible Printed Circuits | Solution to Electronic Packaging Needs*. (n.d.). Retrieved April 20, 2022, from <https://www.allflexinc.com/flexible-circuits/>
11. *Temperature effects on resistance*. (n.d.). Learnabout Electronics. Retrieved April 20, 2022, from https://learnabout-electronics.org/Resistors/resistors_01a.php
12. Abramowitz, A. (1967). Principles, Current Practice, and Applications of Potentiometers Based on Poggendorff's Second Method. *Review of Scientific Instruments*, 38(7), 898–904. <https://doi.org/10.1063/1.1720918>
13. Gibbs, K. (2016). *The charge and discharge of a capacitor*. Schoolphysics. https://www.schoolphysics.co.uk/age16-19/Electricity%20and%20magnetism/Electrostatics/text/Capacitor_charge_and_discharge/index.html
14. *Capacitor Smoothing Circuits & Calculations » Electronics Notes*. (n.d.). Retrieved April 20, 2022, from https://www.electronics-notes.com/articles/analogue_circuits/power-supply-electronics/capacitor-smoothing-circuits.php

15. Plonus, M. (2020). 3—Diode Applications. In M. Plonus (Ed.), *Electronics and Communications for Scientists and Engineers (Second Edition)* (pp. 121–139). Butterworth-Heinemann. <https://doi.org/10.1016/B978-0-12-817008-3.00003-6>
16. Plonus, M. (2020). 3—Diode Applications. In M. Plonus (Ed.), *Electronics and Communications for Scientists and Engineers (Second Edition)* (pp. 121–139). Butterworth-Heinemann. <https://doi.org/10.1016/B978-0-12-817008-3.00003-6>
17. *Conformal Wearable Battery*. (2019). Combat Capabilities Development Command C5ISR Center. https://c5isr.ccdc.army.mil/news_and_media/Conformal_Wearable_Battery/
18. Editor, M. (n.d.). *4 Battery Companies Compete To build Conformal Wearable Battery – Defense TechConnect*. Retrieved April 20, 2022, from <https://defensetechconnect.com/2021/06/03/4-battery-companies-compete-to-build-conformal-wearable-battery/>
19. Lafontaine, D. (2021). *Army modernizes tactical power with battery interoperability*. DEVCOM C5ISR Center Public Affairs. https://www.army.mil/article/247141/army_modernizes_tactical_power_with_battery_interoperability
20. Marinoiu, A., Carcadea, E., Raceanu, M., Petreanu, I., Marin, E., & Teodorescu, C. (n.d.). *A Review Regarding A “Man-Portable” Lightweight Flexible Fuel Cell Concept Small Power Supply*.
21. *US Army OTC Testing Uses Fuel Cells Under Harsh Conditions*. (n.d.). Retrieved April 20, 2022, from [https://www.atec.army.mil/otc/pao/Archives%202012/OTCNews\(FuelCells6\).htm](https://www.atec.army.mil/otc/pao/Archives%202012/OTCNews(FuelCells6).htm)
22. Irwin, L. R., & Edward, M. (n.d.). *The Key to Cross-Domain Maneuver*. 2.
23. Bathmann, D. (n.d.). *Army deploys innovative battery-recharging kit*. Wwww.Army.Mil. Retrieved April 20, 2022, from https://www.army.mil/article/43176/army_deploys_innovative_battery_recharging_kit
24. *Power Platoon Generation W909MY-17-R-H007*. (2017). <https://govtribe.com/opportunity/federal-contract-opportunity/power-platoon-generation-w909my17rh007>
25. Howells, C. A. (2008). *Piezoelectric energy for soldier systems*. ARMY COMMUNICATIONS-ELECTRONICS RESEARCH DEVELOPMENT AND ENGINEERING CENTER FORT BELVOIR VA
26. Mishra, R., Jain, S., & Prasad, C. D. (2015). A review on piezoelectric material as a source of generating electricity and its possibility to fabricate devices for daily uses of army personnel. *International Journal of Systems, Control and Communications*, 6(3), 212-221
27. McCutcheon, A., Nguyen, N., Tess, S., Scholz, E., & Serven, R. (2021). *Triboelectric Energy Generation for the Army*. : Worcester Polytechnic Institute. <https://digital.wpi.edu/show/n296x207j>
28. http://www.nanoscience.gatech.edu/paper/2012/12_NE_04.pdf
29. Kim, Y., Wu, X., & Oh, J. H. (2020). Fabrication of triboelectric nanogenerators based on electrospun polyimide nanofibers membrane. *Scientific Reports*, 10(1), 2742. <https://doi.org/10.1038/s41598-020-59546-7>

30. Liu, C., Li, J., Che, L., Chen, S., Wang, Z., & Zhou, X. (2017). Toward large-scale fabrication of triboelectric nanogenerator (TENG) with silk-fibroin patches film via spray-coating process. *Nano Energy*, *41*, 359-366. [https://scholars.cityu.edu.hk/en/publications/publication\(3d7727ed-05b4-463b-ba23-22b806a5c3ce\).html](https://scholars.cityu.edu.hk/en/publications/publication(3d7727ed-05b4-463b-ba23-22b806a5c3ce).html)
31. Understand the basics of plasma treatment | What is Plasma? (n.d.). *Tantec*. Retrieved April 20, 2022, from <https://tantec.com/the-basics-of-plasma-treatment/>
32. Plasma Cleaning | What is Plasma | Plasma Cleaning Systems. (n.d.). *Tantec*. Retrieved April 20, 2022, from <https://tantec.com/what-is-plasma-cleaning-used-for/>
33. Vivekananthan, V., Chandrasekhar, A., Alluri, N. R., Purusothaman, Y., Khandelwal, G., & Kim, S. J. (2020). Triboelectric Nanogenerators: Design, Fabrication, Energy Harvesting, and Portable-Wearable Applications. In *Nanogenerators*. IntechOpen.
34. Osenga, G. (n.d.). *Dry Etching and Wet Etching*. Retrieved April 20, 2022, from <https://www.thierry-corp.com/plasma-knowledgebase/dry-etching-and-wet-etching>
35. Liu, Y., Mo, J., Fu, Q., Lu, Y., Zhang, N., Wang, S., & Nie, S. (2020). Enhancement of triboelectric charge density by chemical functionalization. *Advanced Functional Materials*, *30*(50), 2004714. <https://doi.org/10.1002/adfm.202004714>
36. Liu, C., Li, J., Che, L., Chen, S., Wang, Z., & Zhou, X. (2017). Toward large-scale fabrication of triboelectric nanogenerator (TENG) with silk-fibroin patches film via spray-coating process. *Nano Energy*, *41*, 359-366.
37. Cao, V. A., Lee, S., Kim, M., Alam, M. M., Park, P., & Nah, J. (2020). Output power density enhancement of triboelectric nanogenerators via ferroelectric polymer composite interfacial layers. *Nano Energy*, *67*, 104300. <https://doi.org/10.1016/j.nanoen.2019.104300>
38. Xia, W., Lu, J., Tan, S., Liu, J., & Zhang, Z. (2018). Manipulating Dielectric Properties by Modifying Molecular Structure of Polymers. In *Dielectric Polymer Materials for High-Density Energy Storage* (pp. 103-163). William Andrew Publishing.
39. Liu, Y., & Hu, C. (2020). Triboelectric nanogenerators based on elastic electrodes. *Nanoscale*, *12*(39), 20118–20130. <https://doi.org/10.1039/D0NR04868B>
40. Seol, M. L., Woo, J. H., Jeon, S. B., Kim, D., Park, S. J., Hur, J., & Choi, Y. K. (2015). Vertically stacked thin triboelectric nanogenerator for wind energy harvesting. *Nano Energy*, *14*, 201-208.
41. Zhu, J., Zhu, P., Yang, Q., Chen, T., Wang, J., & Li, J. (2020). A fully stretchable textile-based triboelectric nanogenerator for human motion monitoring. *Materials Letters*, *280*, 128568. <https://doi.org/10.1016/j.matlet.2020.128568>
42. Kim, Y., Lee, D., Seong, J., Bak, B., Choi, U. H., & Kim, J. (2021). Ionic liquid-based molecular design for transparent, flexible, and fire-retardant triboelectric nanogenerator (TENG) for wearable energy solutions. *Nano Energy*, *84*, 105925. <https://doi.org/10.1016/j.nanoen.2021.105925>
43. Zhou, J., Wang, S., Yuan, F., Zhang, J., Liu, S., Zhao, C., ... & Gong, X. (2021). Functional Kevlar-based triboelectric nanogenerator with impact energy-harvesting property for power source and personal safeguard. *ACS Applied Materials & Interfaces*, *13*(5), 6575-6584.
44. Liu, Y., & Hu, C. (2020). Triboelectric nanogenerators based on elastic electrodes. *Nanoscale*, *12*(39), 20118–20130. <https://doi.org/10.1039/D0NR04868B>

45. Cheng, L., Xu, Q., Zheng, Y., Jia, X., & Qin, Y. (2018). A self-improving triboelectric nanogenerator with improved charge density and increased charge accumulation speed. *Nature Communications*, 9(1), 3773. <https://doi.org/10.1038/s41467-018-06045-z>
46. Betz limit—*Energy Education*. (n.d.). Retrieved April 20, 2022, from https://energyeducation.ca/encyclopedia/Betz_limit
47. Sun, W., Ding, Z., Qin, Z., Chu, F., & Han, Q. (2020). Wind energy harvesting based on fluttering double-flag type triboelectric nanogenerators. *Nano Energy*, 70, 104526. <https://doi.org/10.1016/j.nanoen.2020.104526>
48. Wang, S., Mu, X., Wang, X., Gu, A. Y., Wang, Z. L., & Yang, Y. (2015). Elasto-aerodynamics-driven triboelectric nanogenerator for scavenging air-flow energy. *ACS nano*, 9(10), 9554-9563.
49. Chen, Y., Kuang, Y., Shi, D., Hou, M., Chen, X., Jiang, L., Gao, J., Zhang, L., He, Y., & Wong, C.-P. (2020). A triboelectric nanogenerator design for harvesting environmental mechanical energy from water mist. *Nano Energy*, 73, 104765. <https://doi.org/10.1016/j.nanoen.2020.104765>
50. Ahmed, A., Hassan, I., Jiang, T., Youssef, K., Liu, L., Hedaya, M., Yazid, T. A., Zu, J., & Wang, Z. L. (2017). Design guidelines of triboelectric nanogenerator for water wave energy harvesters. *Nanotechnology*, 28(18), 185403. <https://doi.org/10.1088/1361-6528/aa6612>
51. Gao, Q., Li, Y., Xie, Z., Yang, W., Wang, Z., Yin, M., ... & Wang, Z. L. (2020). Robust triboelectric nanogenerator with ratchet-like wheel-based design for harvesting of environmental energy. *Advanced Materials Technologies*, 5(1), 1900801. <https://doi.org/10.1002/admt.201900801>
52. Kim, T., Chung, J., Kim, D. Y., Moon, J. H., Lee, S., Cho, M., Lee, S. H., & Lee, S. (2016). Design and optimization of rotating triboelectric nanogenerator by water electrification and inertia. *Nano Energy*, 27, 340–351. <https://doi.org/10.1016/j.nanoen.2016.06.051>
53. Ryu, H., Lee, J. H., Khan, U., Kwak, S. S., Hinchet, R., & Kim, S.-W. (2018). Sustainable direct current powering a triboelectric nanogenerator via a novel asymmetrical design. *Energy & Environmental Science*, 11(8), 2057–2063. <https://doi.org/10.1039/C8EE00188J>
54. *Flexible Printed Circuits | Solution to Electronic Packaging Needs*. (n.d.). What Are Flexible Printed Circuits? Retrieved April 20, 2022, from <https://www.allflexinc.com/flexible-circuits/>
55. Macleod, P. (2002). *A review of flexible circuit technology and its applications* (pp. 1-59). Leicester: PRIME Faraday Partnership
56. Koncar, V. (2019). Smart textiles for monitoring and measurement applications. *Smart Textiles for In Situ Monitoring of Composites*, 1-151.
57. *Primary Material of Flexible PCB | PCBCart*. (n.d.). Retrieved April 20, 2022, from <https://www.pcbcart.com/article/content/primary-material-of-flexible-pcb.html>
58. Hou, Z., Lu, H., Li, Y., Yang, L., & Gao, Y. (2021). Direct ink writing of materials for electronics-related applications: a mini review. *Frontiers in Materials*, 8, 91. <https://www.frontiersin.org/articles/10.3389/fmats.2021.647229/full>
59. Dong, Y., Bao, C., & Kim, W. (n.d.). *Sustainable Additive Manufacturing of Printed Circuit Boards | Elsevier Enhanced Reader*. <https://doi.org/10.1016/j.joule.2018.03.015>

60. Abdulhameed, O., Al-Ahmari, A., Ameen, W., & Mian, S. H. (2019). Additive manufacturing: Challenges, trends, and applications. *Advances in Mechanical Engineering*, 11(2), 1687814018822880. <https://doi.org/10.1177/1687814018822880>
61. Zaman, S. U., Tao, X., Cochrane, C., & Koncar, V. (2021). Wash Analyses of Flexible and Wearable Printed Circuits for E-Textiles and Their Prediction of Damages. *Electronics*, 10(11), 1362. <https://doi.org/10.3390/electronics10111362>
62. Kawalec, J. (n.d.). *Mechanical testing of foot and ankle implants | Elsevier Enhanced Reader*. <https://doi.org/10.1016/B978-0-08-100286-5.00012-3>
63. Zi, Y., Niu, S., Wang, J., Wen, Z., Tang, W., & Wang, Z. L. (2015). Standards and figure-of-merits for quantifying the performance of triboelectric nanogenerators. *Nature Communications*, 6(1), 8376. <https://doi.org/10.1038/ncomms9376>
64. Zi, Y., Wang, J., Wang, S., Li, S., Wen, Z., Guo, H., & Wang, Z. L. (2016). Effective energy storage from a triboelectric nanogenerator. *Nature Communications*, 7(1), 10987. <https://doi.org/10.1038/ncomms10987>
65. Xu, L., Bu, T. Z., Yang, X. D., Zhang, C., & Wang, Z. L. (2018). Ultrahigh charge density realized by charge pumping at ambient conditions for triboelectric nanogenerators. *Nano Energy*, 49, 625-633.
66. Pu, X., Liu, M., Li, L., Zhang, C., Pang, Y., Jiang, C., Shao, L., Hu, W., & Wang, Z. L. (2016). Efficient Charging of Li-Ion Batteries with Pulsed Output Current of Triboelectric Nanogenerators. *Advanced Science*, 3(1), 1500255. <https://doi.org/10.1002/advs.201500255>
67. Zi, Y., Guo, H., Wang, J., Wen, Z., Li, S., Hu, C., & Wang, Z. L. (2017). An inductor-free auto-power-management design built-in triboelectric nanogenerators. *Nano Energy*, 31, 302-310.
68. Liu, W., Wang, Z., Wang, G., Zeng, Q., He, W., Liu, L., ... & Wang, Z. L. (2020). Switched-capacitor-convertors based on fractal design for output power management of triboelectric nanogenerator. *Nature communications*, 11(1), 1-10.
69. Fish, L., & Scharre, P. (n.d.). *The Soldier's Heavy Load*. Retrieved April 21, 2022, from <https://www.cnas.org/publications/reports/the-soldiers-heavy-load-1>
70. Colt M4 Carbine. (2013). *Army Technology*. <https://www.army-technology.com/projects/colt-m4-carbine-assault-rifle-us/>
71. Alamdari, A., & Krovi, V. N. (2017). A review of computational musculoskeletal analysis of human lower extremities. *Human Modelling for Bio-Inspired Robotics*, 37-73.
72. *Enhanced performance of triboelectric nanogenerator based on polyamide-silver antimony sulfide nanofibers for energy harvesting | Elsevier Enhanced Reader*. (n.d.). <https://doi.org/10.1016/j.renene.2021.07.118>
73. Kang, Y., Wang, B., Dai, S., Liu, G., Pu, Y., & Hu, C. (2015). Folded Elastic Strip-Based Triboelectric Nanogenerator for Harvesting Human Motion Energy for Multiple Applications. *ACS Applied Materials & Interfaces*, 7(36), 20469–20476. <https://doi.org/10.1021/acsami.5b06675>
74. Drougkas, D., Karatsis, E., Papagiannaki, M., Chatzimoisiadis, S., Arabatzi, F., Maropoulos, S., & Tsouknidas, A. (2018). Gait-specific optimization of composite footwear midsole systems facilitated through dynamic finite element modeling. *Applied Bionics and Biomechanics*, 2018.

Appendix

Appendix A: Pneumatic Gait Tester Design BOM

Part Name	Price	Quantity	Total Price	Link
A513 Steel Framing, 8ft	\$92.25	2	\$185.00	8ft framing
Quick Connect Adapter (1/4" quick connect to 1/4" NPT)	\$4.60	1	\$4.60	Quick Connect
Regulator (1/4" NPT)	\$30.15	1	\$30.15	Regulator
Filter (1/4" NPT)	\$27.00	1	\$27.00	Filter
Auto-shut off valve (1/4" push to connect)	\$82.84	1	\$82.84	Shut-Off Electric Valve
Air Tubing (1/4" PTC) - 10 ft	\$10.60	1	\$10.60	Tubing
Directional control valve, (1/4" PTC)	\$91.64	2	\$183.28	Directional control valve
Air Cylinder, 12" stroke	\$165.77	1	\$165.77	Long air cylinder
Air Cylinder, 6" stroke	\$106.18	1	\$106.18	Short air cylinder
Muffler (1/4" PTC)	\$11.98	1	\$11.98	Muffler (1/4)
Adapter - PTC to 1/4" NPT	\$2.26	6	\$13.56	1/4 NPT Adapter
Opaque PVC sheet, 12 x 24	\$25.63	1	\$25.63	Opaque Plastic

x 0.125"				
Clear polycarbonate sheet, 12 x 24 x 0.25"	\$54.98	2	\$109.96	Clear Plastic
Carbon steel sheet, 12 x 12 x 0.25"	\$86.49	1	\$86.49	Steel sheet
Clevis Rod end	\$12.29	2	\$24.58	Clevis Rod End
Hex bolt, ½-20" thread, 2.5" long, 10-pack	\$17.28	1	\$17.28	Hex bolt
Flange nuts, ½-20" thread, 10-pack	\$9.07	1	\$9.07	Flange Nuts
Large nut for pneumatic cylinder, 1.25-12" thread	\$3.93	2	\$7.86	Cylinder nut
Arduino Mega	\$40.30	1	\$40.30	Mega
INA219 Sensor breakout	\$9.95	1	\$9.95	INA219
SD card module	\$9.60	1	\$9.60	SD Card Adapter
PCF8523, real time clock	\$4.95	1	\$4.95	RTC
12-volt power supply	\$14.95	1	\$14.95	12V dual power
Relay, 200V maximum	\$5.45	3	\$16.35	Relay
Keyed E-	\$27.97	1	\$27.97	E-Stop

Stop Button				button
Reed Switch	\$2.05	2	\$4.10	Round Reed Switch
Total	-	-	\$1230.00	-

Appendix B: Weight-Based Tester Design BOM

Part Name	Price	Quantity	Total Price	Link
A513 Steel Framing, 8ft	\$92.25	2	\$185.00	8ft framing
AC Gearmotor, three- phase, 230 volts, 7 rpm @ 1730 in-lbs torque	\$976.13	1	\$976.13	AC Gearmotor
Keyed shaft	\$56.07	1	\$56.07	https://ww w.mcmaster.com/66 60N53/
Steel Sheet, 24 x 24 inches, 3/4 inch thick	\$496.58	1	\$496.58	High- strength steel sheet
Motor controller	\$39.24	1	\$39.24	Motor Switch
Opaque PVC sheet, 12 x 24 x 0.125"	\$25.63	1	\$25.63	Opaque Plastic
Clear polycarbonate sheet, 12 x 24 x 0.25"	\$54.98	1	\$54.98	Clear Plastic
Arduino Mega	\$40.30	1	\$40.30	Mega
INA219 Sensor breakout	\$9.95	1	\$9.95	INA219

SD card module	\$9.60	1	\$9.60	SD Card Adapter
PCF8523, real time clock	\$4.95	1	\$4.95	RTC
12-volt power supply	\$14.95	1	\$14.95	12V dual power
Relay, 200V maximum	\$5.45	1	\$5.45	Relay
Keyed E-Stop Button	\$27.97	1	\$27.97	E-Stop button
Reed Switch	\$2.05	2	\$4.10	Round Reed Switch
Total	-	-	\$1950.90	-

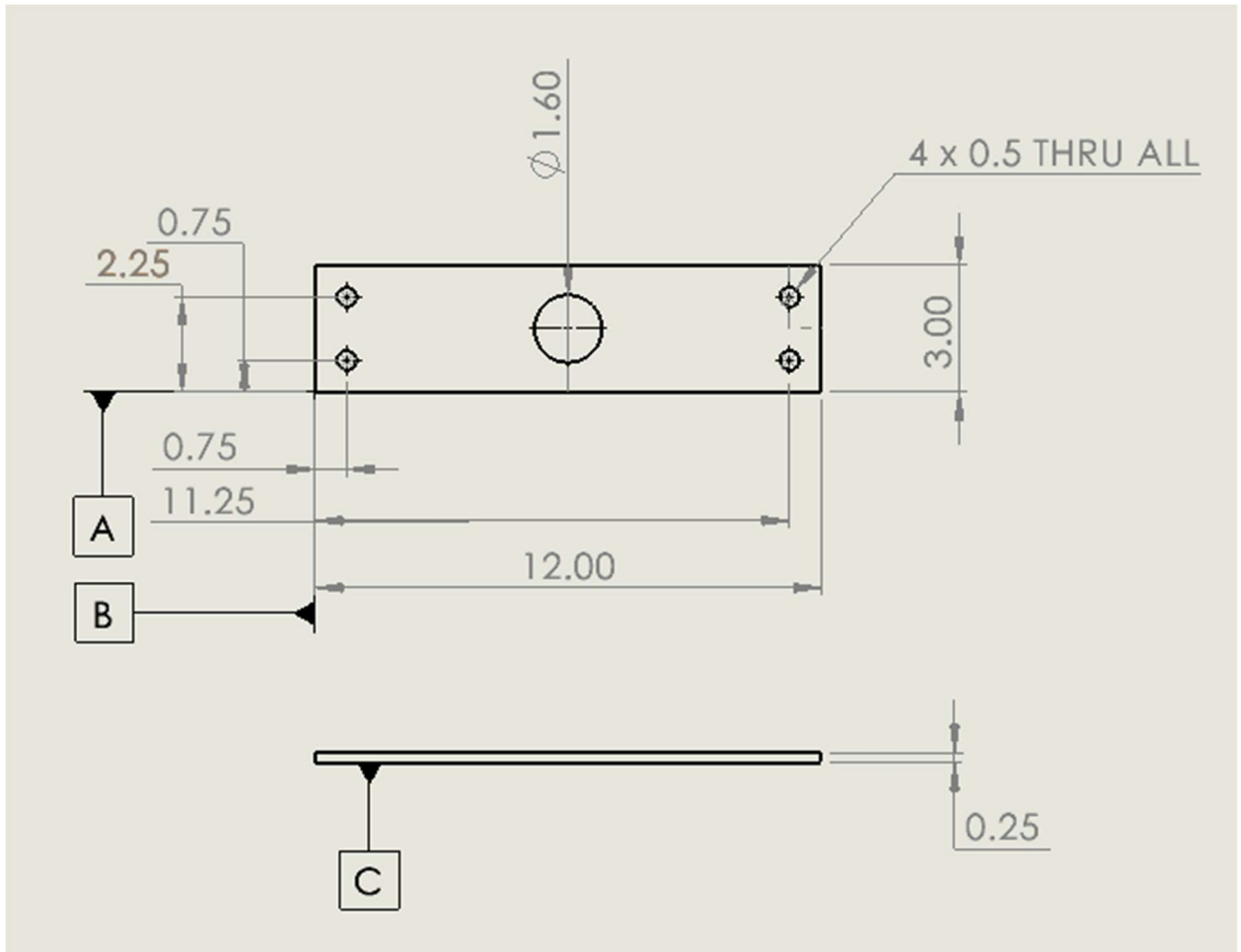
Appendix C: Final Straight Pneumatic Tester Design BOM

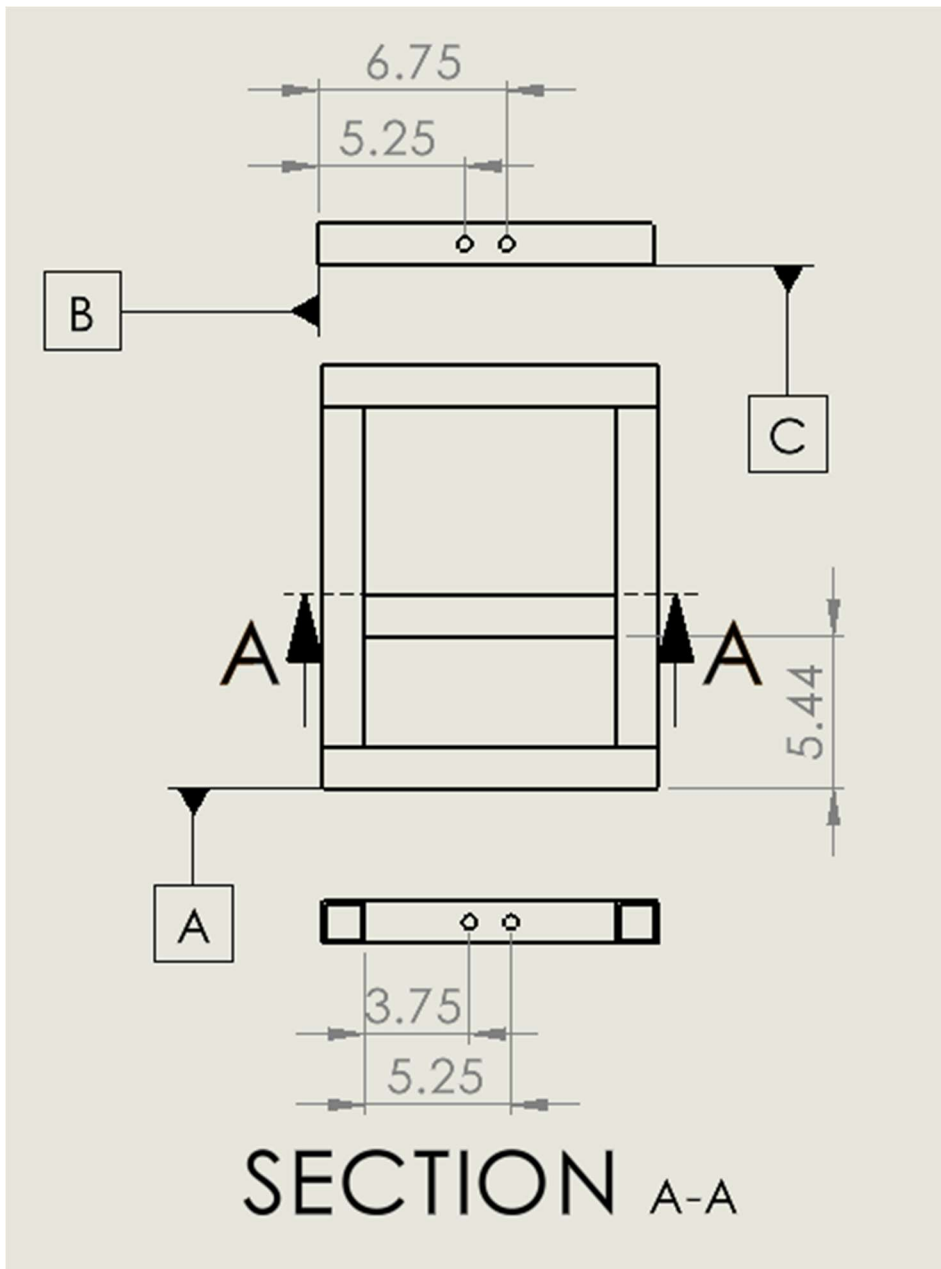
Part Name	Price	Quantity	Total Price	Link
A513 Steel Framing, 10ft	\$139.50	1	\$139.50	10ft frame
Quick Connect Adapter (1/4" QC to 1/4" NPT)	\$4.60	1	\$4.60	Quick Connect
Regulator (1/4" NPT)	\$30.15	1	\$30.15	Regulator
Filter (1/4" NPT)	\$27.00	1	\$27.00	Filter
Auto-shut off valve (1/4" push-to-connect)	\$82.84	1	\$82.84	Shut-Off Electric Valve
Air Tubing (1/4" PTC) - 10 ft	\$10.60	1	\$10.60	Tubing
Directional	\$91.64	1	\$91.64	Directional

control valve, (1/4" PTC)				control valve
Pneumatic Cylinder, 2.5" bore, 4" stroke length, 1/4" NPT connectors	\$132.08	1	\$132.08	Air Cylinder
Muffler (1/4" PTC)	\$11.98	1	\$11.98	Muffler (1/4)
Adapter - PTC to 1/4" NPT	\$2.26	4	\$9.04	1/4 NPT Adapter
Opaque PVC sheet, 12 x 24 x 0.125"	\$25.63	1	\$25.63	Opaque Plastic
Clear polycarbonate sheet, 12 x 24 x 0.25"	\$54.98	1	\$54.98	Clear Plastic
Carbon steel sheet, 12 x 12 x 0.25"	\$86.49	1	\$86.49	Steel sheet
Hex bolt, 1/2-20" thread, 2.5" long, 10-pack	\$17.28	1	\$17.28	Hex bolt
Flange nuts, 1/2-20" thread, 10-pack	\$9.07	1	\$9.07	Flange Nuts
Large nut for pneumatic cylinder, 1.25-12" thread	\$3.93	1	\$3.93	Cylinder nut
Arduino Mega	\$40.30	1	\$40.30	Mega
INA219 Sensor breakout	\$9.95	1	\$9.95	INA219

SD card module	\$9.60	1	\$9.60	SD Card Adapter
PCF8523, real time clock	\$4.95	1	\$4.95	RTC
12-volt power supply	\$14.95	1	\$14.95	12V dual power
Relay, 200V maximum	\$5.45	3	\$16.35	Relay
Keyed E-Stop Button	\$27.97	1	\$27.97	E-Stop button
Reed Switch	\$2.05	2	\$4.10	Round Reed Switch
Total	-	-	\$864.98	-

Appendix D: Additional Detail Drawings of A.T. Support





Appendix E: Structural Analysis of A.T. Support

Table YY: Properties of the metal bar for supporting the pneumatic cylinder from McMaster Carr.

Material Name	HSLA or AHSS (high-strength carbon steel)
Yield Strength	100,000 psi

Safety Factor (FOS)	8
Dimensions (LxWxH)	12 x 2.75 x 0.25 inches, with 1.6 inch cutout
Weakest point	Center of support

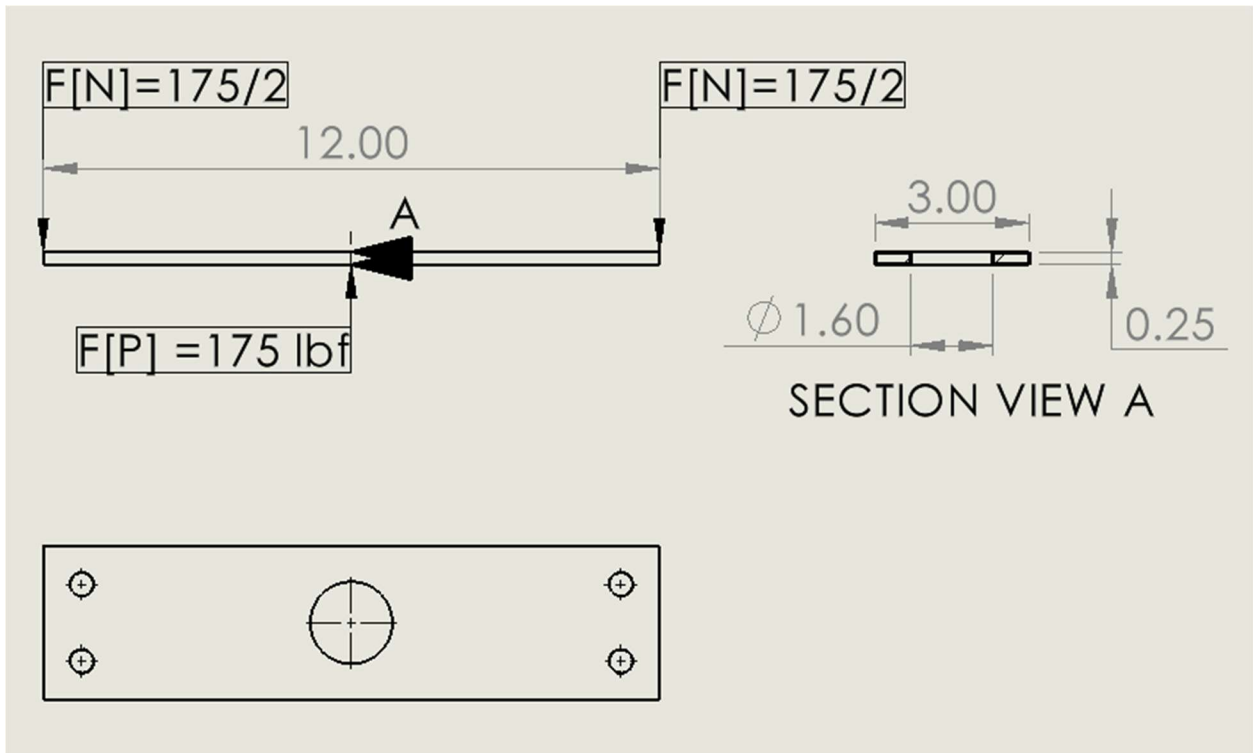


Figure ZX: Free body diagram of metal support for pneumatic cylinder.

Shear strength = Yield strength * shear multiplier = 100,000 psi * 0.577 = 57,700 psi

$$F_x = 0$$

$$F_y = 0 = +350\text{lbf} + [2*(-175\text{lbf})]$$

$$A_c = w * h = (2.75 - 1.6) \text{ in} * 0.25 \text{ in} = 0.2875 \text{ in}^2$$

$$= (F/A_c) * FOS = (175\text{lbf} + (-175/2 \text{ lbf})) / 0.2875 \text{ in}^2 * 8 = 2434.78 \text{ psi} = \mathbf{2430 \text{ psi}}$$

The shear stress for the metal bar is well below the shear strength of 57,700 psi (Table YY).

Appendix F: Structural Analysis of Vertical Frame

Table YZ: Properties of vertical framing rail from McMaster Carr.

Material Name	Carbon Steel
Yield Strength	72,000 psi
Safety Factor (FOS)	8
Dimensions	1.5 x 1.5 inch, with 1.25 x 1.25 inch cutout in center

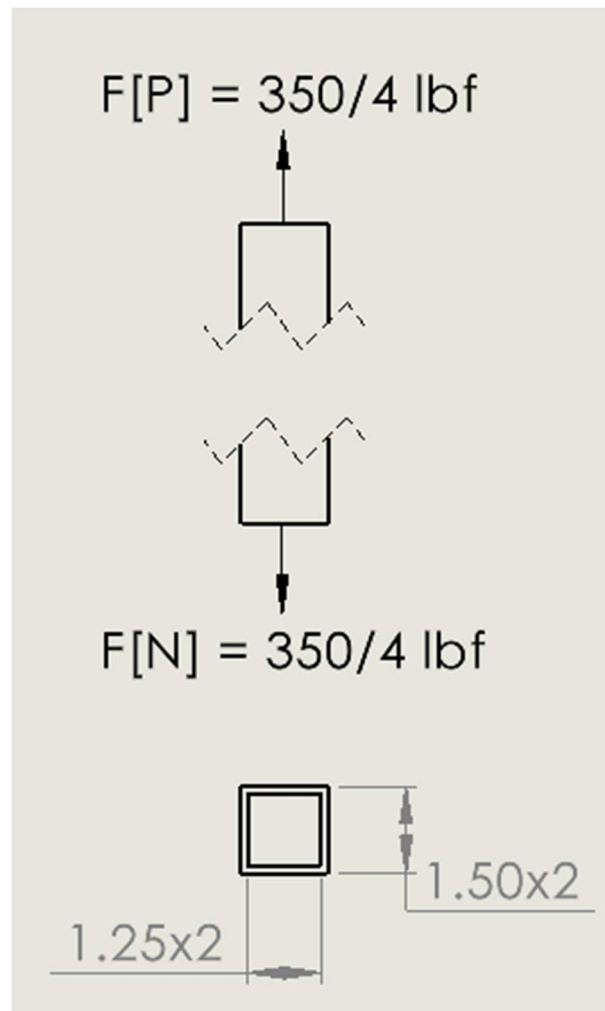


Figure ZY: Free body diagram for framing of the final design.

$$F_x = 0$$

$$F_y = 0 = +350\text{lbf} + (-350\text{lbf})$$

$$A_c = A_o - A_i = (1.5\text{in})^2 - (1.25\text{in})^2 = 0.6875\text{in}^2$$

$$\sigma = (F/A_c) * FOS = (350/4 \text{ lbf}) / 0.6875\text{in}^2 * 8 = 1018.18 \text{ psi} = 1020 \text{ psi}$$

The tensile stress for the framing is well below the yield strength of 72,000 psi (Table YZ).

Appendix G: Structural Analysis of Horizontal Frame

Table YZ: Properties of horizontal framing rail from McMaster Carr.

Material Name	Carbon Steel
Yield Strength	72,000 psi
Safety Factor (FOS)	8
Dimensions	12 inch long, 1.5 x 1.5 inch, with 1.25 x 1.25 inch cutout in center

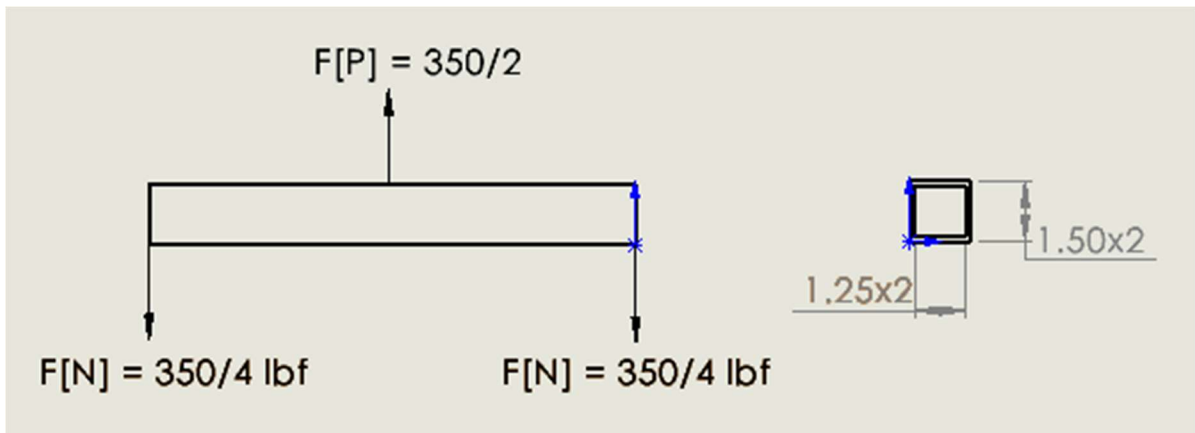


Figure ZY: Free body diagram for framing of final design.

$$\text{Shear strength} = \text{Yield strength} * \text{shear multiplier} = 72,000 \text{ psi} * 0.577 = 41,500 \text{ psi}$$

$$F_x = 0$$

$$F_y = 0 = +(350/2) \text{ lbf} + [2 * (-350/4) \text{ lbf}]$$

$$A_c = A_o - A_i = (1.5\text{in})^2 - (1.25\text{in})^2 = 0.6875\text{in}^2$$

$$= (F/A_c) * FOS = (350/2 \text{ lbf} + (-350/4 \text{ lbf})) / 0.6875\text{in}^2 * 8 = 1018.18 \text{ psi} = \mathbf{1020 \text{ psi}}$$

The shear stress for the metal bar is well below the shear strength of 41,500 psi (Table YY).

Appendix H: Automated Tester Code

```
#include <SPI.h>
#include <SD.h>
#include <Wire.h>
#include "RTClib.h"
#include <EasyButton.h>

RTC_PCF8523 rtc;

//constant integers
const int red_led = 3;
const int orange_led = 5;
const int green_led = 7;
const int prep_button = 2;
const int test_button = 4;
const int start_button = 6;
const int door_switch = 13;
const int extend_relay = 8;
const int safety_relay = 9;
const int chipSelect = 14;
const int prep_hold_time = 3500;

//Define state machine numbers
#define START 0
#define READY 1
```

```
#define EXTEND_TEST 2
#define RETRACT_TEST 3
#define CYCLE_START 4
#define EXTEND 5
#define RETRACT 6
#define RESET 7
#define STOP 8

//integers
int state;
int prep_count = 0;
int test_count;
int ready_reset_value;
int cycle_reset_value;
int test_confirmation_value;
unsigned long int future;
unsigned long int right_now;
unsigned long int extend_count;
bool cylinder;
int voltage;
int current;
int low_voltage_check;
int cyl_delay_time = 500; //delay between states

void setup() {
  Serial.begin(9600); //or 57600
  pinMode(red_led, OUTPUT);
  pinMode(orange_led, OUTPUT);
  pinMode(green_led, OUTPUT);
  Serial.println("LEDs initialized");
```

```
pinMode(prepare_button, INPUT_PULLUP);
pinMode(test_button, INPUT_PULLUP);
pinMode(start_button, INPUT_PULLUP);
pinMode(door_switch, INPUT);
Serial.println("Buttons initialized");
pinMode(extend_relay, OUTPUT);
pinMode(safety_relay, OUTPUT);
Serial.println("Relays initialized");
//-----RTC-----
if (! rtc.begin()){
  Serial.println("Couldn't find RTC");
  while(1);
}
rtc.adjust(DateTime(2014, 1, 21, 3, 0, 0));
if (! rtc.initialized()){
  Serial.println("RTC is not connected");
}

void state_machine(){
  switch(state){
    case START:
      digitalWrite(orange_led, LOW);
      Serial.println("State START");
      //DateTime now = rtc.now();
      right_now = millis();
      if (digitalRead(prepare_button) == LOW){ //if button is pressed
        Serial.println("PREP BUTTON ON");
        if (prep_count == 0){
          //initialize: first phase
          //checks current time
          Serial.println("Prep Count low");
        }
      }
    }
}
```

```
future = (right_now + prep_hold_time);
//must hold the button for 3.5 seconds in the future
prep_count++;
}
if (prep_count >= 1){
  //after initial: second phase
  if (right_now > future){
    future = (right_now + 60000);
    prep_count = 0;
    Serial.println("Moving into READY");
    state = READY;
    break;
  }
}
else if(digitalRead(prepare_button) == HIGH){//if button is not pressed
  //set count back to zero
  prep_count = 0;
  Serial.println("Prep button not on");
}
break;

case READY:
  //check which button (testing or start) is on
  //moves to corresponding starting state
  Serial.println("READY state");
  digitalWrite(orange_led, HIGH);
  digitalWrite(red_led, LOW);
  right_now = millis();
  if (ready_reset_value < 1){
    Serial.println("ready_reset_value < 1");
    if (right_now > future){
```

```
//if the prep phase happened greater than 60 seconds without any action, set back to start
state = START;
Serial.println("Moving back to START");
break;
}
}
if (digitalRead(test_button) == LOW){//if button is pressed
//if test_button is pressed, set to extend test
//now = rtc.now();
right_now = millis();
future = (right_now + 3000);
ready_reset_value++; //protects all outgoing code to ensure that it doesn't happen again
state = EXTEND_TEST;
Serial.println("Moving into EXTEND_TEST");
break;
}
//-----
if (digitalRead(start_button) == LOW){//if button is pressed
//if start_button is high, start program
ready_reset_value++; //protects all outgoing code to ensure that it doesn't happen again
digitalWrite(orange_led, LOW);
digitalWrite(green_led, HIGH);
state = CYCLE_START;
Serial.println("Moving into CYCLE_START");
break;
}
break;
case EXTEND_TEST:
//extends cylinder
//waits button to be pressed to retract
digitalWrite(extend_relay, HIGH);
//now = rtc.now();
```

```
right_now = millis();
//sets variable to use throughout states
if (right_now > future){
  //if the time is finished from the last state...
  if (digitalRead(test_button) == LOW){
    //if button is pressed
    future = (right_now + 5000); //sets future for the next state
    state = RETRACT_TEST;
    Serial.println("Moving into RETRACT_TEST");
    break;
  }
}
break;
case RETRACT_TEST:
  //retracts cylinder and delays
  //moves back to starting state
  digitalWrite(extend_relay, LOW);
  //now = rtc.now();
  right_now = millis();
  if (right_now > future){
    state = READY;
    Serial.println("Moving back to READY");
    break;
  }
  break;
case CYCLE_START:
  /*
  //read voltage, time, and continue to extend or retract
  //Write data? ***Will 15 ms be too costly?***
  //if voltage is low...keep count
  //if count is too high...stop
  //-----
```



```
if ((voltage > -0.5) and (voltage < 0.5)) {
  //both placeholder values for the normal voltage that will be in the circuit if it breaks
  low_voltage_check++;
}
else {
  //if everything's normal, set voltage check back to zero
  low_voltage_check = 0;
}
if (low_voltage_check > 10000) {
  state = STOP;
  Serial.println("Moving into next state");
  break;
}
*/
if (cycle_reset_value == 0) {
  //now = rtc.now();
  right_now = millis();
  future = (right_now + cyl_delay_time);
  cycle_reset_value = 1;
}
if (cylinder == HIGH) {
  state = EXTEND;
  Serial.println("Moving into EXTEND");
  break;
}
else if (cylinder == LOW) {
  state = RETRACT;
  Serial.println("Moving into RETRACT");
  break;
}
else {
  cylinder == HIGH;
```

```

}
break;

```

```

case EXTEND:

```

```

//extend cylinder and keep returning

```

```

//move back to CYCLE_START until *if* enough time to have fully extended

```

```

/*if so*, move to retract

```

```

digitalWrite(extend_relay, HIGH);

```

```

//now = rtc.now();

```

```

right_now = millis();

```

```

if (right_now > future){

```

```

    cylinder == LOW;

```

```

    future = (right_now + cyl_delay_time); //resets value for RETRACT

```

```

    state = RETRACT;

```

```

    Serial.println("Moving back to RETRACT");

```

```

    break;

```

```

}

```

/*the only other way I see of doing this is to create a system in CYCLE_START to count for either extend or retract

problem there being that I would have to be able to differentiate and switch between the two for each purpose*/

```

break;

```

```

case RETRACT:

```

```

//retract cylinder and keep returning

```

```

//move back to CYCLE_START *if* enough time to have fully retracted

```

```

/*if so*, move on to RESET

```

```

digitalWrite(extend_relay, LOW);

```

```

////now = rtc.now();

```

```

right_now = millis();

```

```

if (right_now > future){

```

```

    state = RESET;

```

```

    Serial.println("Moving to RESET");

```

```
        break;
    }
    break;
case RESET:
    //add to extend_value
    //set all values back to start
    extend_count++;
    Serial.println(extend_count);
    cycle_reset_value = 0;
    cylinder = HIGH;
    state = CYCLE_START;
    Serial.println("Moving into CYCLE_START");
    break;
case STOP:
    //write to SD card that it's stopped
    //put red LED on
    //set all values back to normal
    //send to START
    digitalWrite(red_led, HIGH);
    cycle_reset_value = 0;
    cylinder = HIGH;
    prep_count = 0;
    ready_reset_value = 0;
    extend_count = 0;
    state = START;
    Serial.println("Moving back to START");
    break;
}
}

void loop() {
```

```

/*cyl_delay_time = Serial.parseInt(); //added on 2_7
if (millis() > 4294967295){ //added on 2_7
  state = STOP;
  Serial.println("Integer has reached MAX value");
}*/
if (digitalRead(prepare_button) == LOW){ //added on 2_7
  if ((state == EXTEND_TEST) or (state == RETRACT_TEST) or (state == RESET) or (state
== CYCLE_START)){ //added Cycle start on 2_9
    state = READY;
    Serial.println("Paused");
  }
}
if (digitalRead(door_switch) == HIGH){ //2_7 changed from "else if" to "if"
  Serial.println("Door switch disconn");
  digitalWrite(green_led, LOW);
  digitalWrite(orange_led, LOW);
  digitalWrite(red_led, HIGH);
  state = READY;
}
if (digitalRead(door_switch) == LOW){ //if the door is closed
  //Serial.println("Door switch active, moved towards state machine");
  digitalWrite(red_led, LOW);
  Serial.println("Door switch conn");
  state_machine();
}
}

```

Appendix I: Procedure for Creating 2x2 Samples

Materials

- Conductive Copper Foil Electrical Tape
- Stainless Medium Conductive Thread - 3 ply

- PTFE Film with Coarse Texture
- Acrylic Tape
- MIL DTL 32429 Type 1 Class 8 Universal Camo Print Fabric
- Scissors
- Fabric Scissors
- Electrical Tape

Procedure

Create Negative Side of TENG

1. Cut out a 2x2 section of MIL DTL 32429 type 1 class 8 universal camo print Fabric from a roll of fabric with fabric scissors.
 - a. Cut one foot of stainless medium conductive thread-3 ply (wire)
 - b. Start on one corner of the 2x2 section and one end of the wire. Lay the wire on the backside of the fabric in a sinuous pattern, letting the extra wire hang out of the diagonal corner from where it started.
 - i. Makes sure to hold the wire so it does not move
 - c. While keeping one hand on the wire, apply the copper foil tape over the wire on the backside. Start from the top and apply the tape horizontally.
 - i. Make sure the tape is applied with little to no wrinkling and that no fabric is showing on the back
 - d. Apply acrylic tape over the copper tape in strips going the same direction as the copper wire
 - i. No copper should be showing
 - e. Cut off the excess copper tape around the TENG

Create Positive side of TENG

1. Cut out a 2x2 section of PTFE film.
 - a. Cut one foot of stainless medium conductive thread-3 ply (wire)
 - b. Start on one corner of the 2x2 section and one end of the wire. Lay the wire on one side of the PTFE in a sinuous pattern through the 2x2 sections, letting the extra wire hang out of the diagonal corner from where it started.
 - i. Makes sure to hold the wire so it does not move
 - c. While keeping one hand on the wire, apply the copper foil tape to the side of the PTFE to which the wire was applied. Start from the top and apply the tape horizontally.

- i. Make sure it is applied with little to no wrinkling and that no fabric is showing on the back
 - ii. Make sure to add pressure when applying because PTFE is harder to bond to
 - d. Cut off the excess copper tape around the TENG
2. Stack the TENGs together with the front side of the fabric and PTFE touching.
 3. Try to keep the wires from touching each other. Electrical tape can be applied to make sure the positive and negative ends are not in contact.

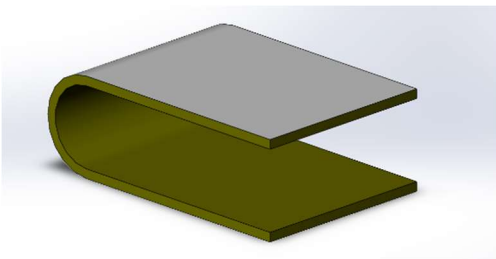
Appendix J: Procedure for Creating Folded TENGs

Materials

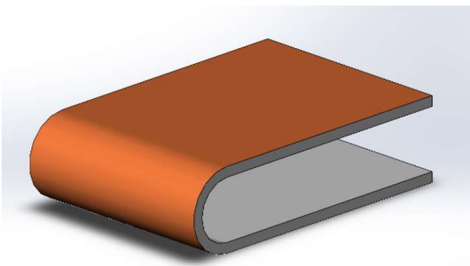
- 2x4 inch TENG Sample
- 2x6 inch TENG Sample
- 2x8 inch TENG Sample

Procedure

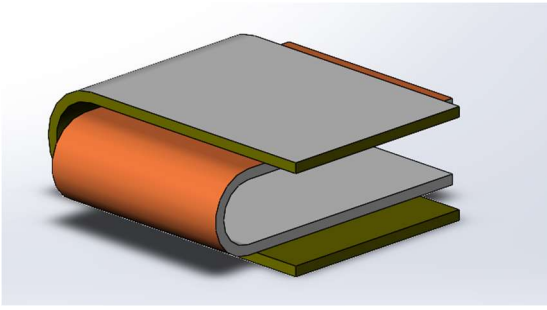
1. Using the procedure for creating a 2x2 TENG, create three samples of sizes: 2x4, 2x6, and 2x8 inches.
2. Make sure to refer to the previous procedure for TENG layers
3. Creating Folded 2x4 Sample
4. Fold the negative layer so that the fabric is on the inside and the acrylic tape is on the outside



5. Fold the positive layer so that the PTFE is on the outside of the fold and the acrylic tape is on the inside

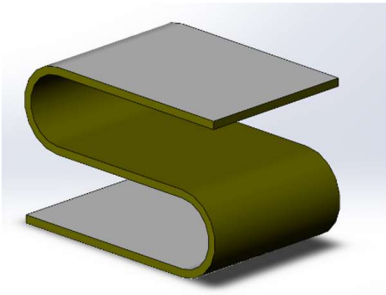


6. Insert the folded positive layer into the negative layer so that the fabric and PTFE are touching.

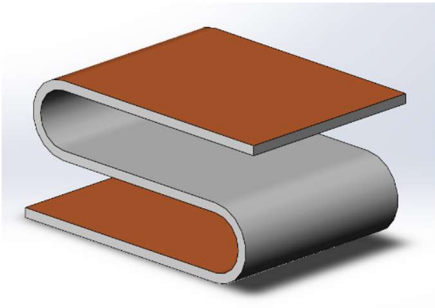


Creating Folded 2x6 Sample

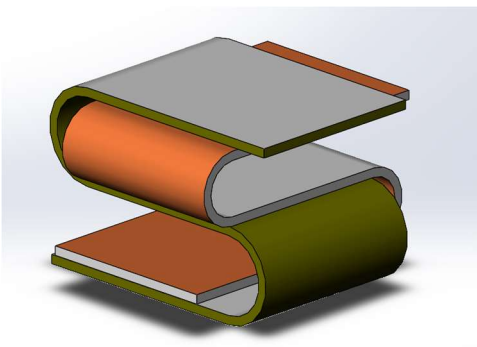
- a. Fold the negative layer into multiple 2x2 sections using an accordion style. The acrylic tape side should be shown on the top.



2. Fold the positive layer into multiple 2x2 sections using the accordion style. The PTFE side should be shown on the top.

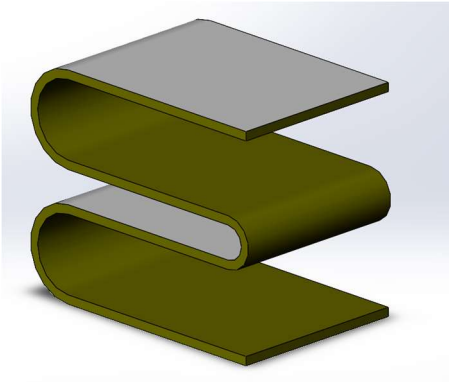


3. Turn the positive TENG 90 degrees and slide the positive and negative layers together so that the PTFE and the fabric are always touching each other.
 - a. An image of the fold is shown below.

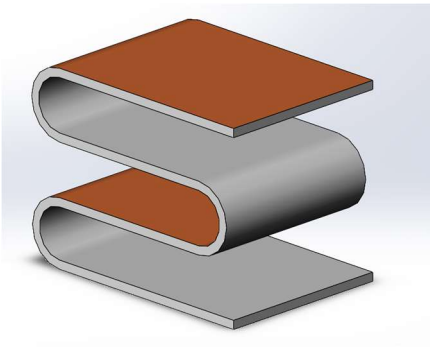


Creating Folded 2x8 Sample

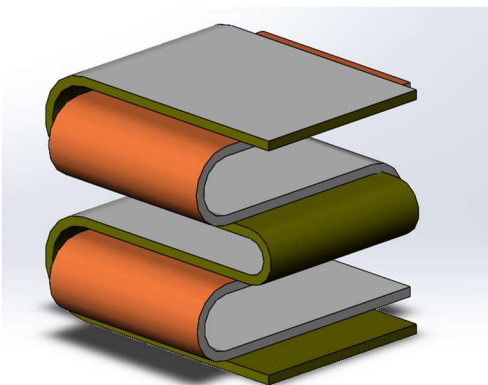
1. Fold the negative layer into multiple 2x2 samples using an accordion style. The acrylic tape side should be shown on the outside of the fold.



- 2.
3. Fold the positive layer into multiple 2x2 samples using the accordion style. The PTFE layer side should be shown on the outside of the fold.



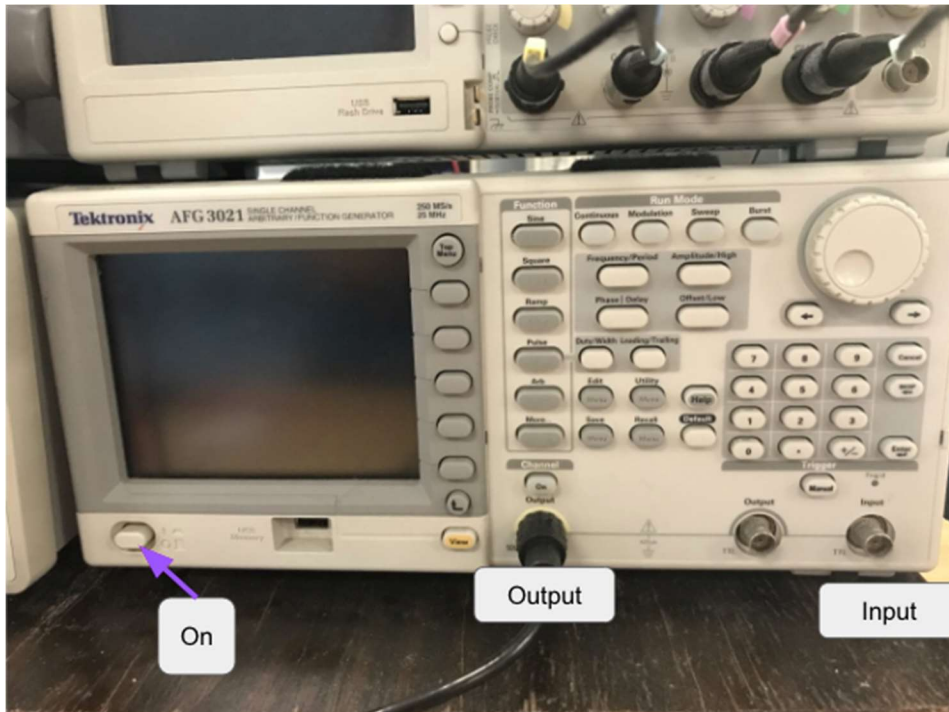
- 4.
5. Turn the positive TENG 90 degrees and slide the positive and negative layers together so that the PTFE and the fabric are always touching each other.
 - a. Images of the fold are shown below.



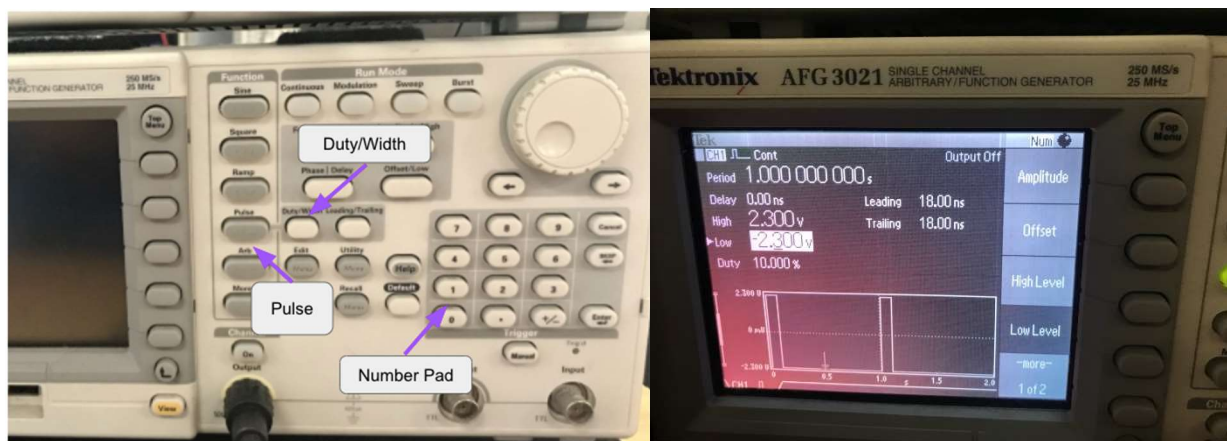
- 6.

Appendix K: Procedures for Oscilloscope Tests

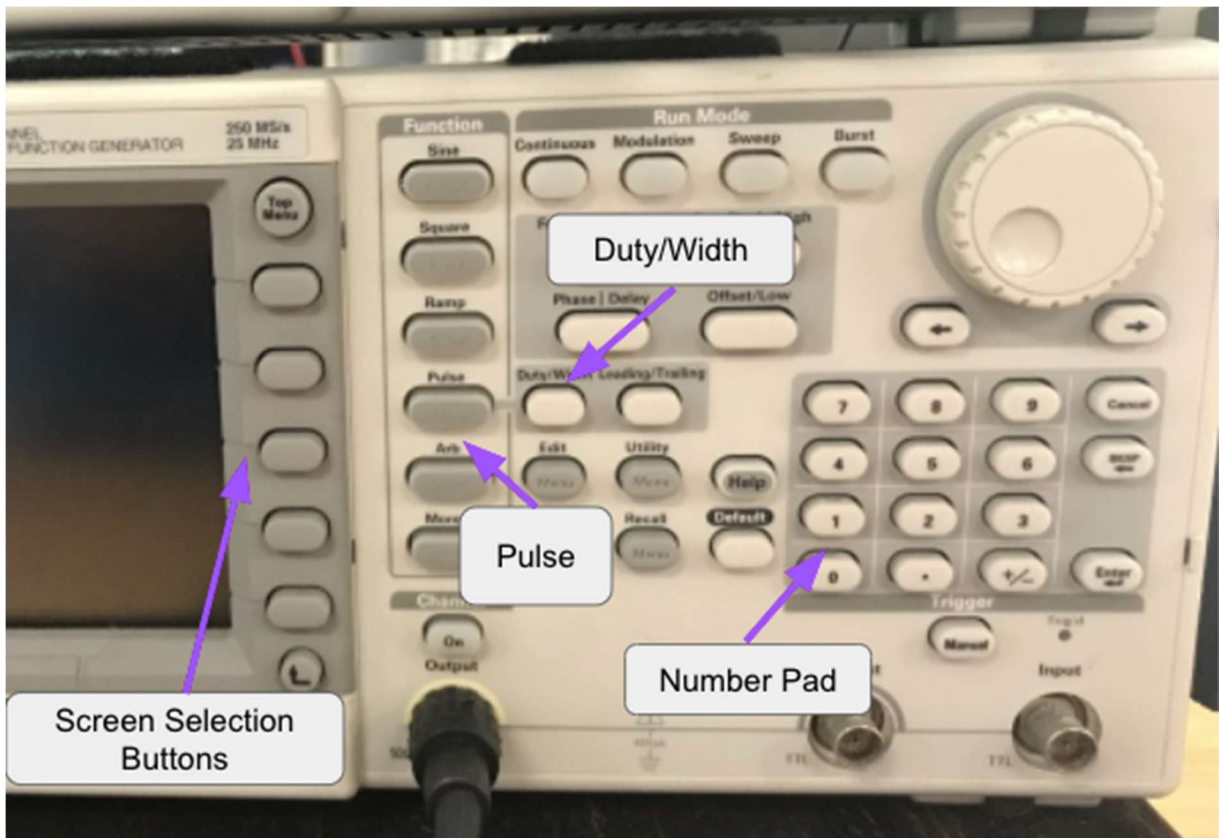
Turn on the oscilloscope and attach the output and input probes.



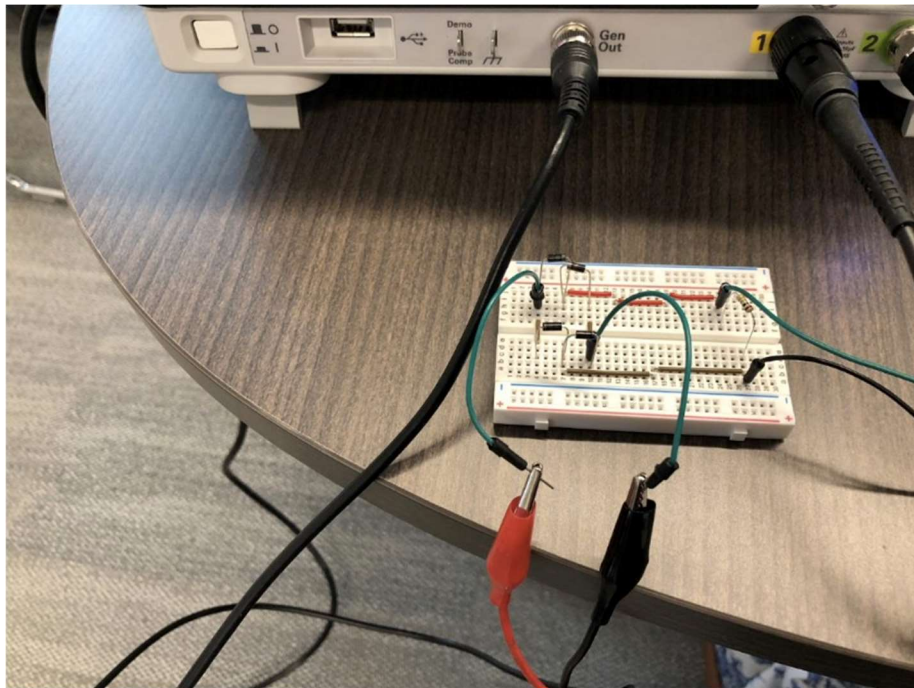
Press the “Pulse” button and then select the “Duty/Width” button and use the “number pad” and set the Duty Cycle as 10%



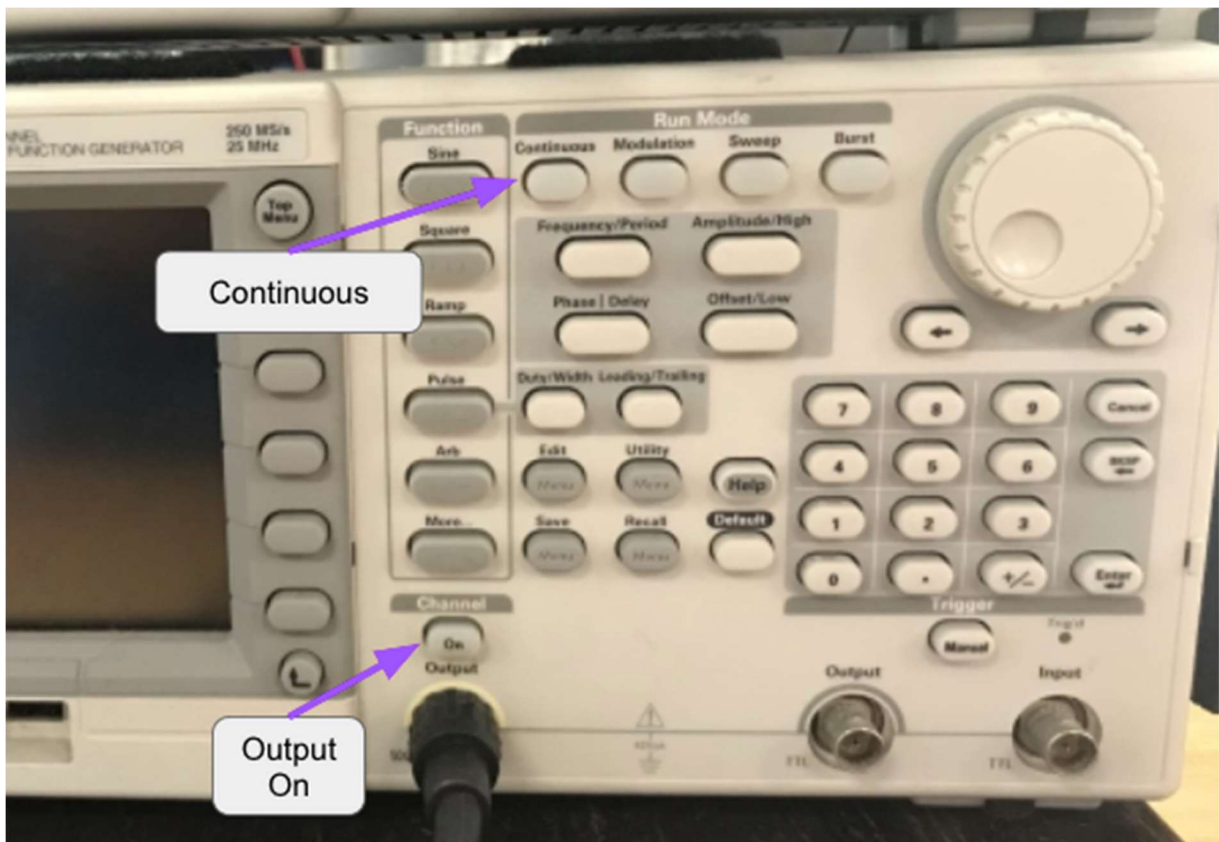
Use the “Screen Selection Buttons” and “Number Pad” to set the frequency as 10 Hz. Use the same buttons to change the peak voltages as +/- 2.3 volts.



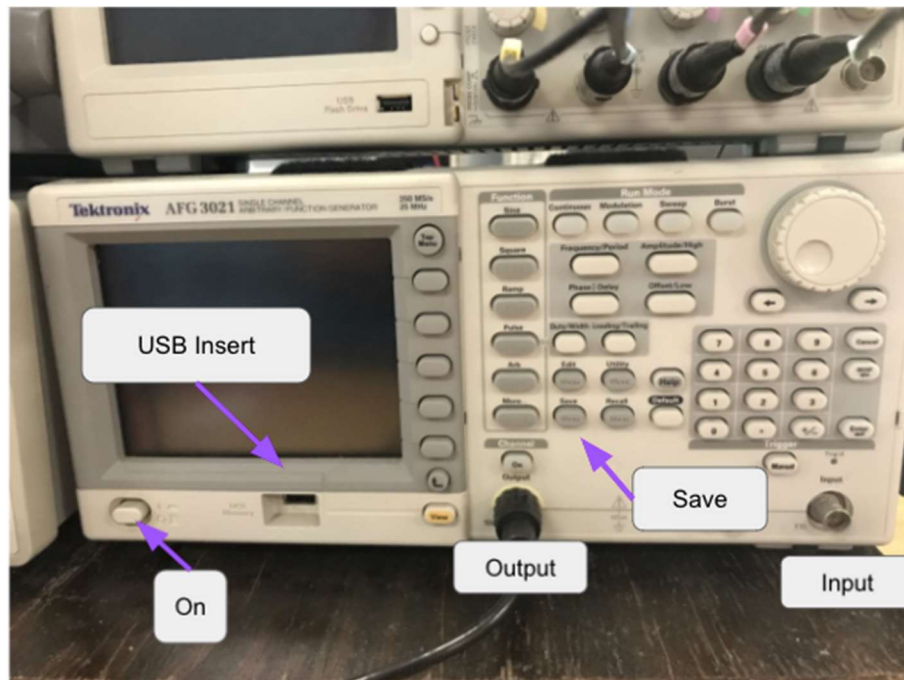
Attach the two clips at the end of the output wire to the respective power input wires of the circuit being tested.



Attach the two clips at the end of the input wire to the wires in parallel to the resistor representing the external charging device.




Press the “Continuous” button and then press the “Output On” button to start the test and view the results.



To save, insert a 2GB USB and let the circuit run for 30 second or more and then hit the “Save” button.

Appendix L: Voltera V-One Circuit Printer Procedure

1. Print designed circuit schematic file to a .gbr file
2. Connect the V-One USB cable to a personal computer
3. Make sure to have the Voltera software downloaded on the selected computer
4. Wait for the user interface to load and the software to connect with the V-One
5. Select the print option
6. Load the schematic planned to be printed
7. Connect the calibration probe to the cartridge port (U.I. will show the exact location to insert)
8. Place the used substrate (circuit board) on the ledges of the two clamps fastened to the board
9. Let the printer calibrate and trace the circuit with the probe
10. Assure the substrate is flat and there will be no collisions with the clamps
11. Replace the probe with the conductive ink cartridge
12. Make sure the cartridge is primed to dispense ink
13. Select “print” on the U.I. program
14. Closely monitor the printing process

- 
- i. Be ready to select stop on the U.I. in case abnormal prints or collisions occur
 15. Once the print is completed detach the conductive ink cartridge from the printer
 16. The printer surface then will heat the board for 30-50 minutes to cure the ink to the substrate
 17. Print a .gbr file that identifies solder paste dispense locations
 18. Select “print” on the U.I. and upload the solder paste file
 19. Probe the schematic and ensure the probe is touching the center of each solder paste area
 20. Prime the solder paste cartridge then attach it to the printer
 21. Select “print” on the U.I. program
 22. Closely monitor the printing process
 - i. Be ready to select stop on the U.I. in case abnormal prints or collisions occur
 23. Once the print is complete, attach all components to their respective position and orientation
 24. Firmly press all components onto the board to ensure the solder paste will adhere the components to the board
 25. Select the “reflow” process option on the U.I. main menu
 26. Select the reflow process required for the selected solder paste
 27. Certain pastes require certain temperatures and or heating times
 28. Begin reflow process
 29. Closely monitor all components when the paste liquifies to ensure they do not shift from their positioning
 30. Once the process is completed let the board sit for 10-20 minutes
 31. Traditional solder methods can be utilized to adhere input and output lead wires to the circuit board
-